ESA Climate Change Initiative CCI+

Product Validation and Intercomparison Report

snow cci

Issue 4 / Revision 0

20 May 2024

Deliverable No.:	D4.1
ESA Contract No.:	4000124098/18/I-NB
Science Lead & Prime:	Thomas Nagler, ENVEO IT GmbH, thomas.nagler@enveo.at
Technical Officer:	Anna-Maria Trofaier, ESA-ECSAT, anna.maria.trofaier@esa.int

To be cited as:

Barella, R., Notarnicola, C., C. Marin, V. Premier, N. Ciapponi, C. Mortimer, C. Derksen, and G. Schwaizer (2024) ESA CCI+ Snow ECV: Product Validation and Intercomparison Report, version 4.0, Mai 2024.

Checked by	Gabriele Schwaizer / ENVEO, Project Manager	29 / 04 / 2024
Authorized by	Thomas Nagler / ENVEO, Science Leader	29 / 04 / 2024
Accepted by	Anna Maria Trofaier / ECSAT, ESA Technical Officer	20 / 05 / 2024

This document is not signed. It is provided as electronic copy.

ESA STUDY CONTRACT REPORT

ESA CONTRACT NO:	Subject: ESA Climate Change Initiative CCI+ - SNOW		CONTRACTOR:
4000124098/18/I-NB	Product Validation and Intercomparison Report		ENVEO
ESA CR ( )NO:	**STAR CODE:**	**NO OF VOLUMES:** 5 **THIS IS VOLUME NO:** 4	**CONTRACTOR'S REF:** Deliverable D4.1

Abstract:

The European Space Agency (ESA) Climate Change Initiative aims to generate high quality Essential Climate Variables (ECVs) derived from long-term satellite data records to meet the needs of climate research and monitoring activities.

The product validation and intercomparison report (PVIR) for *snow_cci* ECVs snow cover fraction (SCF) and snow water equivalent (SWE) describes the validation results obtained by the application of the Product Validation Plan (PVP). The report provides all the insights to assess the *snow_cci* products in terms of: i) quantify the error ii) characterize the performance against seasonality, forest presence, local topography, and land cover type and iii) quantify the error of the provided *snow_cci* uncertainty. At the end of the report recommendations to further improve the overall product quality are provided.

The work described in this report was done under ESA Contract. Responsibility for the contents resides in the author or organisation that prepared it.

AUTHORS: RICCARDO BARELLA; CLAUDIA NOTARNICOLA; CARLO MARIN; VALENTINA PREMIER; NICOLA CIAPPONI; COLLEEN MORTIMER; CHRIS DERKSEN; GABRIELE SCHWAIZER

ESA STUDY MANAGER: ANNA MARIA TROFAIER / ECSAT	ESA BUDGET HEADING:

Document Change Record

Version	Date	Changes	Originator
1.0draft	21 / 10 / 2019	First version of the document	Notarnicola et al.
1.0	11/ / 11 / 2019	Fist version approved by ESA, including comments by ESA	Notarnicola et al.
2.0draft	02 / 11 / 2020	Second version of the document	Notarnicola et al.
2.0	25 / 11 / 2020	Second version approved by ESA	Notarnicola et al.
3.0draft	14 / 12 / 2021	Third version of the document	Notarnicola et al.
3.0	17 / 12 / 2021	Third version approved by ESA	Notarnicola et al.
4.0draft	25 / 04 / 2024	Fourth draft version of the document	Barella et al.
4.0	20 / 05 / 2024	Fourth version approved by ESA	Barella et al.

TABLE OF CONTENTS

This page is intentionally left blank.

1. INTRODUCTION

The Product Validation and Intercomparison Report (PVIR, D4.2 v4.0) is an updated version of the PVIR v3.0 [RD-1]. It describes the validation results obtained by the application of the Product Validation Plan (PVP v4.0) [RD-2]. The validation is performed by using snow cover products derived from high resolution optical satellite data, in-situ measurements and third-party products prepared following the instructions reported in the PVP [RD-2]. The algorithms used to obtain the *snow_cci* products are described in the Algorithm Theoretical Basis Document (ATDB) [RD-3]. The sources for the data to be used are compiled in the Data Access Requirement Document (DARD) [RD-4].

The quality assessments presented in this 4th version of the report are resulting from the validation and intercomparison of the snow cover fraction (SCF) and snow water equivalent (SWE) products of the *snow_cci* Climate Research Data Package (CRDP) v3.0, documented in [RD-5].

1.1. Purpose and Scope

The PVIR is provided as deliverable D4.1 to the ESA *snow_cci* project. This document is the fourth version of the PVIR. The report provides all the insights to assess the *snow_cci* products for: i) quantifying the error ii) characterizing the performance against seasonality, forest presence, local topography, and land cover type and iii) quantifying the error of the provided *snow_cci* uncertainty. At the end of the report recommendations to improve the overall product quality are provided.

1.2. Document Structure

Chapter 2 recalls the data used for the validation and intercomparison. Details for accessing these data are provided in the DARD [RD-4]. Chapter 3 presents the results of the analysis for the Snow Cover Extent (SCE) products whereas Chapter 4 presents the results of the analysis for the Snow Water Equivalent (SWE) products. Chapter 5 draws the main conclusions of the study and makes recommendations for improving the quality of the products. References are listed in Chapter 6.

1.3. Applicable and Reference Documents

[AD-1] Phase 1 of the ESA Climate Change Initiative CCI+ New ECVS (Snow). ESRIN Contract No: 4000124098/18/I-NB

[AD-2] Climate Change Initiative Extension (CCI+) Phase 1 – New Essential Climate Variables (Annex E: Snow ECV (Snow_cci), ESA-CCI-PRGM-EOPS-SW-17-0032

[AD-3] Technical Proposal (Part 3) in response to ESA Climate Change Initiative Phase 1 ESA ITT AO/1-9041/17/I-NB, ENVEO Innsbruck, Austria

[RD-1] Notarnicola, C., C. Marin, G. Schwaizer, T. Nagler, K. Luojus, C. Derksen, C. Mortimer, S. Wunderle, K. Naegeli (2019) ESA CCI+ Snow ECV: Product Validation and Intercomparison Report, version 3.0, November 2020.

[RD-2] Notarnicola, C., Marin, C., Schwaizer, G., Nagler, T., Luojus, K., Derksen, C., Mortimer, C., Wunderle, S., Naegeli, K. (2021) ESA CCI+ Snow ECV: Product Validation Plan, version 4.0, October 2021.

[RD-3] Schwaizer, G., S. Metsämäki, M. Moisander, K. Luojus, S. Wunderle, K. Naegeli, T. Nagler, J. Lemmetyinen, J. Pulliainen, M. Takala, R. Solberg, L. Keuris, P. Venäläinen, and N. Mölg (2021): ESA CCI+ Snow ECV: Algorithm Theoretical Basis Document, version 4.0, July 2023.

[RD-4] Wunderle, S., K. Naegeli, G. Schwaizer, T. Nagler, C. Marin, C. Notarnicola, C. Derksen, K. Luojus, S. Metsämäki, and R. Solberg (2021) ESA CCI+ Snow ECV: Data Access Requirements Document, version 3.1, February 2021.

[RD-5] Solberg, R., G. Schwaizer, T. Nagler, M. Hetzenecker, S. Wunderle, X. Xiao, C. Neuhaus, A. Wiesmann, K. Luojus, M. Takala, J. Pulliainen, J. Lemmetyinen, M. Moisander, and N. Mölg (2024) ESA CCI+ Snow ECV: Climate Research Data Package, version 4.0, April 2024.

[RD-6] Derksen, C., T. Nagler, and G. Schwaizer (2021) ESA CCI+ Snow ECV: User Requirements Document, version 3.0, January 2021.

[RD-7] Marin, C., R. Barella, C. Notarnicola, N. Mölg, G. Schwaizer and T. Nagler (2023) ESA CCI+ Snow ECV, Option 4 - High Resolution Snow Mapping from Sentinel-2 and Landsat data: Annex to Algorithm Theoretical Basis Document, version 1.0, July 2023.

[RD-8] Barella, R., Marin, C., Schwaizer, G., Mölg, N., and T. Nagler (2023) ESA CCI+ Snow ECV, Option 4 - High Resolution Snow Mapping from Sentinel-2 and Landsat data: Annex to Product Validation and Intercomparison Report, version 1.0, July 2023.

1.4. Acronyms

AATSR	Advanced Along Track Scanning Radiometer
AVHRR	Advanced Very High Resolution Radiometer
CCI	Climate Change Initiative
CDR	Climate Data Record
CP	Contractual Phase
CRDP	Climate Research Data Package
DARD	Data Access Requirement Document
DEM	Digital Elevation Model
ECV	Essential Climate Variable
ESA	European Space Agency

ESDR	Earth Science Data Record
FP	False Positive
FN	False Negative
FSC	Fractional Snow Cover
HR	High Resolution
LAMSU	Multi-Spectral Unmixing with Locally Adaptive end-member selection
MetOp	European Meteorological Operational Satellite
MODIS	Moderate resolution Imaging Spectroradiometer
NDSI	Normalized Difference Snow Index
NOAA	National Oceanic and Atmospheric Administration
PMW	Passive Microwave
PVIR	Product Validation and Intercomparison Report
PVP	Product Validation Plan
QA4EO	Quality Assurance framework for Earth Observation
RMSE	Root Mean Square Error
SCE	Snow Cover Extent
SCF	Snow Cover Fraction
SCFG	Snow Cover Fraction on Ground
SCFV	Snow Cover Fraction Viewable
SD	Snow Depth
SnowFLAKES	Snow extent applying a Flexible Learning Algorithm using KErnel-based Spectral unmixing
SnowPEx	Satellite Snow intercomparison and evaluation Experiment
SWE	Snow Water Equivalent
TP	True Positive
TN	True Negative
uRMSE	Unbiased Root Mean Square Error
USGS	U.S. Geological Survey

2. SUMMARY OF DATA FOR VALIDATION AND INTERCOMPARISON

An overview on the reference data available for the validation and inter-comparison is provided in the Data Access Requirement Document DARD v3.1 [RD-1], Sections 4 and 5. The used ancillary data are described in [RD-1], Section 6.

2.1. High resolution optical satellite imagery

The high resolution optical satellite data from Landsat satellites selected, downloaded and processed according to the Product Validation Plan (PVP) [RD-2] for the validation of *snow_cci* Snow Cover Fraction (SCF) products are described in the [RD-2].

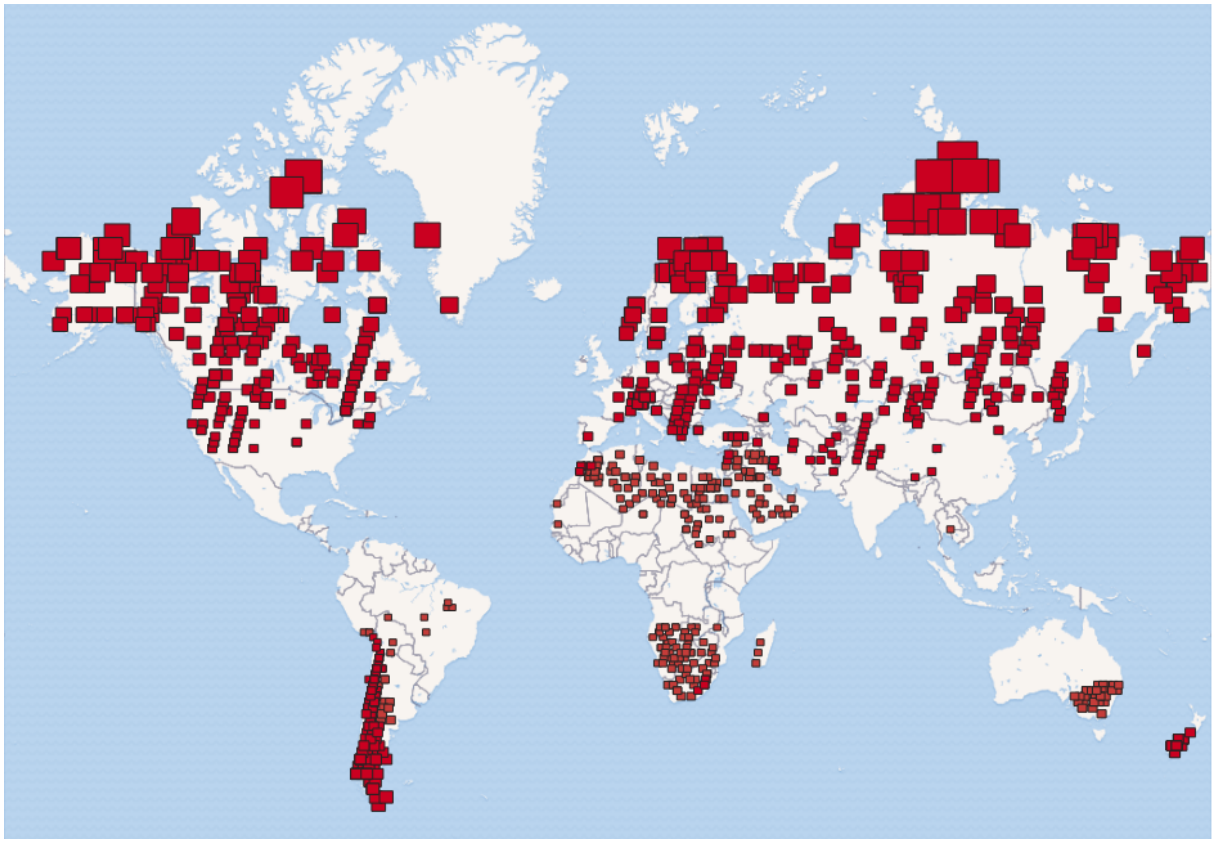

Figure 2.1: High-resolution images selected for *snow_cci* validation activities.

2.2. In-situ data

Measurements of snow depth, density, and SWE collected at multiple points along a designated transect used for the validation of *snow_cci* SCF and SWE products are described in the PVP [RD-2].

The in-situ data presented in the [RD-2] are complemented by a collection of homogenised snow depth (SD) measurements collected from seven different sources:

- ECMWF (North America and Eurasia, 07/1979-12/2018);
- RIHMI-WCD (Russia, 01/1979-12/2018);
- NDCD GHCN (North America, 01/1979-12/2018);
- NDCD GHCN (Eurasia, 01/1979-12/2018);
- US Dave Robinson (USA, 01/1978-12/2009);
- Met service of Canada (Canada, 01/1979-09/2010);
- Canadian data from ECCC (Ross Brown) (Canada, 01/2004-07/2018).

An overview on the spatial distribution of these datasets is shown in Figure 2.2.

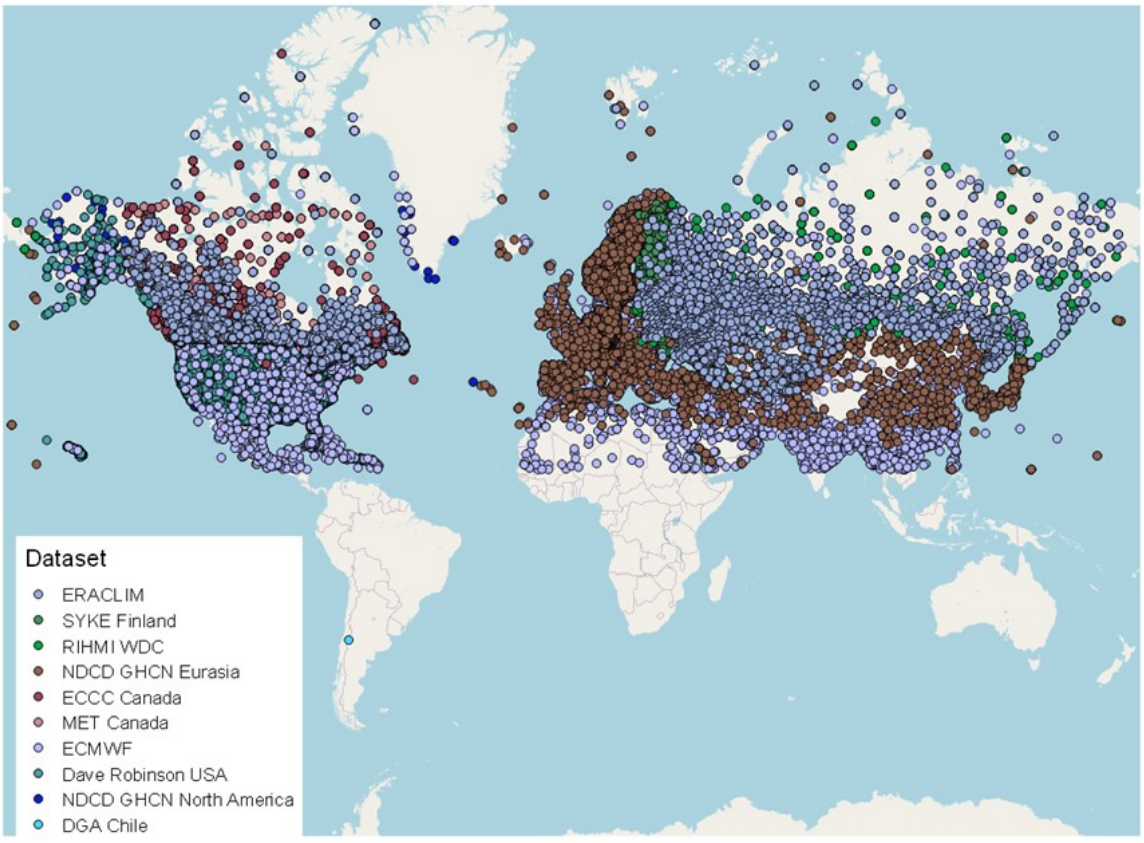

Figure 2.2: In-situ snow depth observations selected for *snow_cci* validation activities.

3. VALIDATION RESULTS FOR SNOW COVER EXTENT PRODUCTS

The snow cover fraction (SCF) products derived from MODIS (CRDP v3.0), AVHRR (CRDP v3.0) and AATSR (CRDP v1.0) are assessed using the validation plan documented in the PVP [RD-2]. The SCF products provide information on both i) *snow on ground* (SCFG) and ii) *viewable snow* (SCFV). In detail, the results of the comparison with in-situ measurements, high-resolution snow maps and other medium resolution snow products are reported in the following three sections. The evaluation of the estimated uncertainty is discussed in Section 3.4.

3.1. Comparison with in-situ measurements

This chapter presents the validation results for the *snow_cci* time series produced from 570 MODIS, 168 AATSR and 735 AVHRR SCF maps using the snow depth data described in [RD-2] available all around the globe for that time. The *snow_cci* time series considered for this comparison spans the time from 2000 to 2018 for the MODIS-based products of CRDP v3.0, from 2002 to 2007 for AATSR-based products from CRDP v1.0 and from 1982 to 2018 for the AVHRR-based products from CRDP v3.0. It is worth noting that, even though not all the *snow_cci* products and in-situ data have been used, the number of validation samples is statistically significant i.e., about 2.5M samples for MODIS-based, about 250K samples for AASTR-based and 3.3M samples for AVHRR-based *snow_cci* products. As described in the PVP [RD-2], three different thresholds were implemented for the in-situ snow depth measurements to determine if the associated pixel is covered by snow: SD≥0 m, SD≥0.02 m and SD≥0.15 m. A second set of thresholds was applied on the SCF maps to transfer the fractional to a binary snow information: SCF≥25% and SCF≥50%.

Contingency matrices and binary metrics were calculated considering all the available data. Validation results for the 570 MODIS based SCFV and SCFG products using about 2.5M in-situ measurements applying the different combinations of thresholds are reported in Table 3.1. The equivalent for the 735 AVHRR based SCFV and SCFG products validated with about 3.6M in-situ measurements are presented in Table 3.2. In all following tables, the colour scale represents the best (green) and the worst (red) results obtained for each metric. The total number of snow and snow-free pixels used for the computation of the statics are reported on the right side of each contingency matrix in the following tables.

The accuracy (hit rate and F-score) is high for both products, SCFG and SCFV, from both sensors, MODIS and AVHRR, with maximum values of 98%. As expected by increasing the threshold on SCF from 25% to 50% we are losing in sensitivity i.e., the recall decreases. Whereas, by increasing the threshold on the SD, the recall increases at the expenses of the other metrics. This means that the *snow_cci* products identify shallow snowpack or patchy situations well. The same patterns as observed for the global statistics are valid when only mountainous and plain areas are considered (see Table 3.4 and Table 3.5 for MODIS, Table 3.6 and Table 3.7 for AATSR, and Table 3.8 and Table 3.9 for AVHRR).

3.1.1. Overall

Table 3.1: Statistics obtained for **MODIS** based SCF products. a) and c) binary metrics for SCFV and SCFG. b) and d) contingency matrix in % for SCFV and SCFG. S and NS stand for Snow and No Snow, respectively.

a) SCFV

	0m-25%	0m-50%	0.02m-25%	0.02m-50%	0.15m-25%	0.15m-50%
Recall	0.75	0.453	0.785	0.481	0.866	0.538
Precision	0.953	0.96	0.921	0.935	0.627	0.621
False Alarm Rate	0.004	0.002	0.006	0.003	0.028	0.016
Hit Rate (Accuracy)	0.974	0.951	0.976	0.956	0.966	0.963
Critical Success Index	0.724	0.444	0.736	0.466	0.572	0.405
F-score	0.84	0.615	0.848	0.635	0.728	0.577

b) SCFV

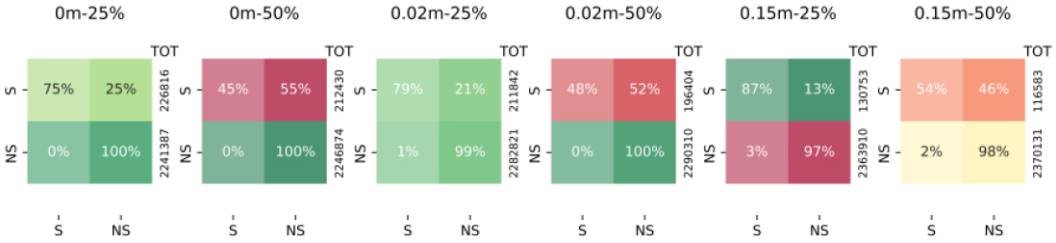

c) SCFG

	0m-25%	0m-50%	0.02m-25%	0.02m-50%	0.15m-25%	0.15m-50%
Recall	0.871	0.815	0.901	0.855	0.968	0.952
Precision	0.947	0.961	0.914	0.94	0.633	0.687
False Alarm Rate	0.005	0.003	0.009	0.005	0.037	0.026
Hit Rate (Accuracy)	0.982	0.98	0.983	0.983	0.964	0.973
Critical Success Index	0.831	0.789	0.831	0.811	0.619	0.664
F-score	0.907	0.882	0.908	0.895	0.765	0.798

d) SCFG

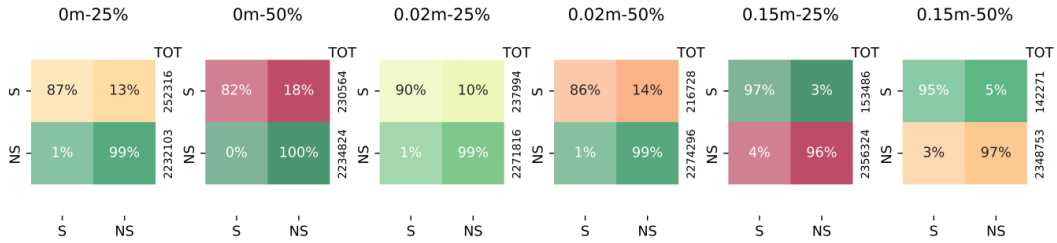

Table 3.2: Same as Table 3.1 for **AATSR** based SCF products.

a) SCFV

	0m-25%	0m-50%	0.02m-25%	0.02m-50%	0.15m-25%	0.15m-50%
Recall	0.771	0.509	0.793	0.529	0.847	0.583
Precision	0.819	0.811	0.769	0.761	0.498	0.494
False Alarm Rate	0.02	0.013	0.026	0.017	0.054	0.034
Hit Rate (Accuracy)	0.958	0.939	0.956	0.942	0.94	0.945
Critical Success Index	0.659	0.455	0.64	0.454	0.456	0.365
F-score	0.795	0.625	0.781	0.624	0.627	0.535

b) SCFV

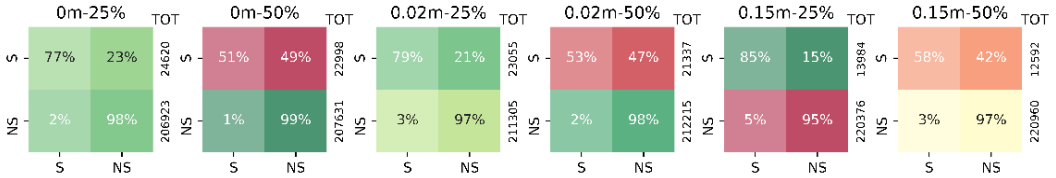

c) SCFG

	0m-25%	0m-50%	0.02m-25%	0.02m-50%	0.15m-25%	0.15m-50%
Recall	0.872	0.815	0.891	0.843	0.93	0.911
Precision	0.828	0.849	0.78	0.809	0.506	0.561
False Alarm Rate	0.024	0.017	0.031	0.021	0.066	0.047
Hit Rate (Accuracy)	0.964	0.966	0.96	0.966	0.934	0.95
Critical Success Index	0.738	0.711	0.712	0.703	0.488	0.532
F-score	0.849	0.831	0.832	0.826	0.656	0.695

d) SCFG

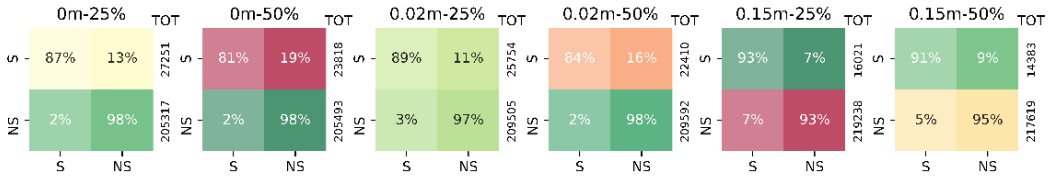

Table 3.3: Same as Table 3.1 for **AVHRR** based SCF products.

a) SCFV

	0m-25%	0m-50%	0.02m-25%	0.02m-50%	0.15m-25%	0.15m-50%
Recall	0.81	0.678	0.832	0.705	0.872	0.753
Precision	0.944	0.947	0.912	0.92	0.574	0.565
False Alarm Rate	0.006	0.004	0.009	0.006	0.041	0.031
Hit Rate (Accuracy)	0.975	0.966	0.975	0.968	0.954	0.958
Critical Success Index	0.773	0.654	0.77	0.665	0.529	0.477
F-score	0.872	0.791	0.87	0.798	0.692	0.646

b) SCFV

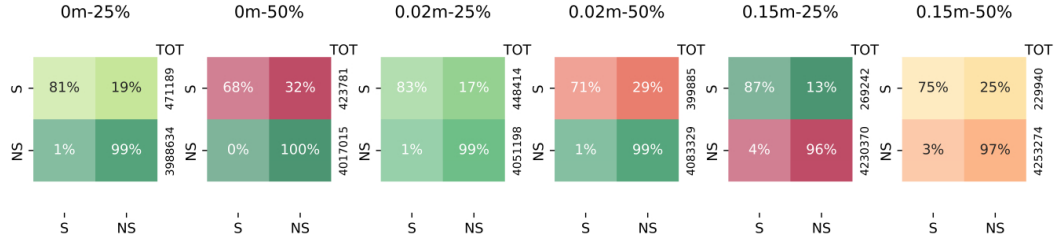

c) SCFG

	0m-25%	0m-50%	0.02m-25%	0.02m-50%	0.15m-25%	0.15m-50%
Recall	0.848	0.832	0.867	0.855	0.899	0.895
Precision	0.944	0.951	0.911	0.926	0.579	0.601
False Alarm Rate	0.006	0.005	0.01	0.008	0.046	0.04
Hit Rate (Accuracy)	0.977	0.977	0.977	0.978	0.951	0.955
Critical Success Index	0.807	0.798	0.8	0.8	0.544	0.562
F-score	0.893	0.888	0.889	0.889	0.705	0.719

d) SCFG

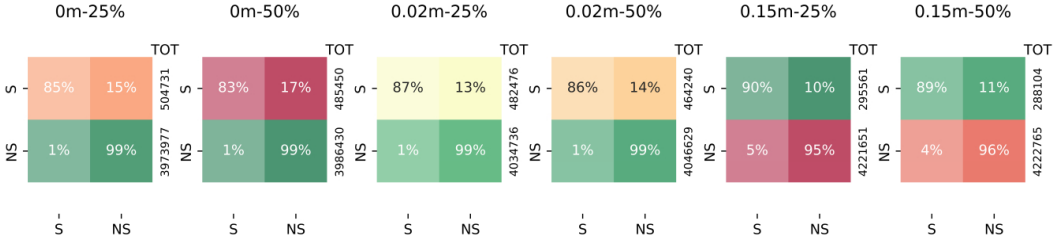

3.1.2. Mountains and plains

Table 3.4: Same as Table 3.1 for **MODIS** based SCF products in **mountainous areas.**

a) SCFV

	0m-25%	0m-50%	0.02m-25%	0.02m-50%	0.15m-25%	0.15m-50%
Recall	0.65	0.285	0.671	0.296	0.766	0.354
Precision	0.954	0.964	0.934	0.948	0.741	0.759
False Alarm Rate	0.004	0.001	0.006	0.002	0.024	0.009
Hit Rate (Accuracy)	0.953	0.911	0.956	0.917	0.959	0.942
Critical Success Index	0.63	0.282	0.64	0.291	0.605	0.318
F-score	0.773	0.44	0.781	0.451	0.754	0.483

b) SCFV

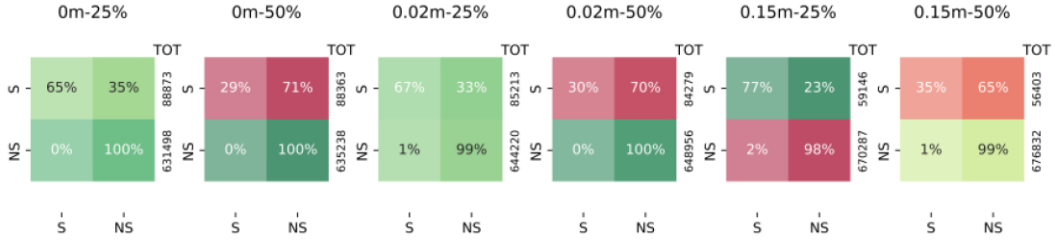

c) SCFG

	0m-25%	0m-50%	0.02m-25%	0.02m-50%	0.15m-25%	0.15m-50%
Recall	0.871	0.812	0.889	0.835	0.953	0.932
Precision	0.945	0.961	0.923	0.946	0.725	0.783
False Alarm Rate	0.009	0.005	0.012	0.007	0.041	0.027
Hit Rate (Accuracy)	0.974	0.971	0.974	0.973	0.959	0.97
Critical Success Index	0.829	0.786	0.827	0.798	0.7	0.741
F-score	0.906	0.88	0.905	0.887	0.823	0.851

d) SCFG

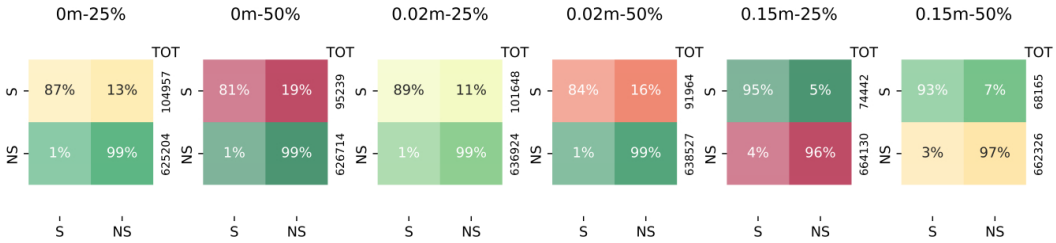

Table 3.5: Same as Table 3.1 for **MODIS** based SCF products for **plain areas**.

a) SCFV

	0m-25%	0m-50%	0.02m-25%	0.02m-50%	0.15m-25%	0.15m-50%
Recall	0.815	0.572	0.863	0.62	0.949	0.711
Precision	0.953	0.958	0.914	0.93	0.569	0.572
False Alarm Rate	0.003	0.002	0.006	0.003	0.03	0.019
Hit Rate (Accuracy)	0.982	0.968	0.984	0.973	0.969	0.972
Critical Success Index	0.783	0.558	0.798	0.593	0.552	0.464
F-score	0.879	0.717	0.888	0.744	0.711	0.634

b) SCFV

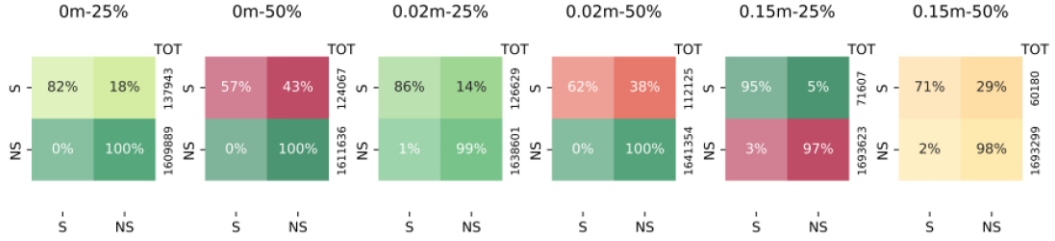

c) SCFG

	0m-25%	0m-50%	0.02m-25%	0.02m-50%	0.15m-25%	0.15m-50%
Recall	0.871	0.817	0.911	0.869	0.981	0.971
Precision	0.949	0.962	0.907	0.935	0.567	0.62
False Alarm Rate	0.004	0.003	0.008	0.005	0.035	0.026
Hit Rate (Accuracy)	0.985	0.983	0.986	0.986	0.966	0.974
Critical Success Index	0.832	0.792	0.833	0.82	0.561	0.609
F-score	0.908	0.884	0.909	0.901	0.719	0.757

d) SCFG

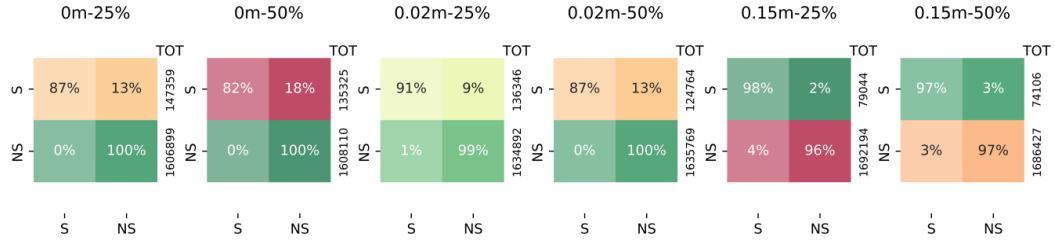

Table 3.6: Same as Table 3.1 for **AATSR** based SCF products in **mountainous areas.**

a) SCFV

	0m-25%	0m-50%	0.02m-25%	0.02m-50%	0.15m-25%	0.15m-50%
Recall	0.616	0.309	0.627	0.316	0.691	0.36
Precision	0.84	0.823	0.815	0.8	0.608	0.604
False Alarm Rate	0.018	0.01	0.021	0.011	0.042	0.021
Hit Rate (Accuracy)	0.933	0.9	0.934	0.905	0.935	0.927
Critical Success Index	0.551	0.29	0.549	0.293	0.478	0.291
F-score	0.71	0.45	0.709	0.453	0.647	0.451

b) SCFV

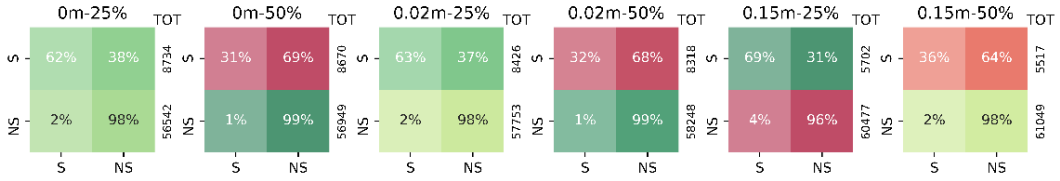

c) SCFG

	0m-25%	0m-50%	0.02m-25%	0.02m-50%	0.15m-25%	0.15m-50%
Recall	0.798	0.747	0.807	0.763	0.858	0.836
Precision	0.848	0.869	0.823	0.849	0.612	0.668
False Alarm Rate	0.026	0.018	0.03	0.021	0.063	0.044
Hit Rate (Accuracy)	0.947	0.949	0.946	0.95	0.929	0.945
Critical Success Index	0.698	0.672	0.688	0.672	0.556	0.59
F-score	0.822	0.804	0.815	0.804	0.714	0.742

d) SCFG

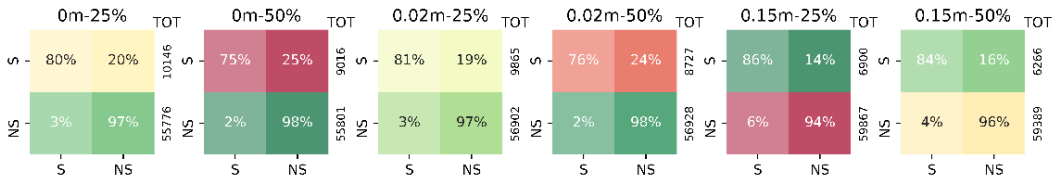

Table 3.7: Same as Table 3.1 for **AATSR** based SCF products in **plain areas.**

a) SCFV

	0m-25%	0m-50%	0.02m-25%	0.02m-50%	0.15m-25%	0.15m-50%
Recall	0.857	0.63	0.889	0.666	0.954	0.756
Precision	0.812	0.807	0.751	0.75	0.456	0.463
False Alarm Rate	0.021	0.014	0.028	0.019	0.059	0.039
Hit Rate (Accuracy)	0.967	0.955	0.965	0.957	0.942	0.953
Critical Success Index	0.715	0.548	0.686	0.545	0.447	0.403
F-score	0.834	0.708	0.814	0.705	0.617	0.574

b) SCFV

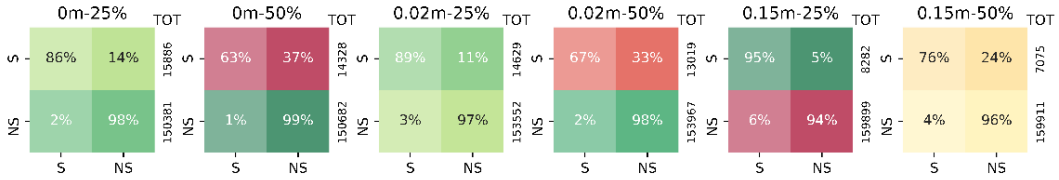

c) SCFG

	0m-25%	0m-50%	0.02m-25%	0.02m-50%	0.15m-25%	0.15m-50%
Recall	0.916	0.856	0.943	0.895	0.985	0.97
Precision	0.818	0.839	0.758	0.789	0.455	0.507
False Alarm Rate	0.023	0.016	0.031	0.021	0.068	0.048
Hit Rate (Accuracy)	0.97	0.972	0.966	0.972	0.935	0.953
Critical Success Index	0.761	0.735	0.725	0.722	0.452	0.499
F-score	0.864	0.847	0.841	0.838	0.622	0.666

d) SCFG

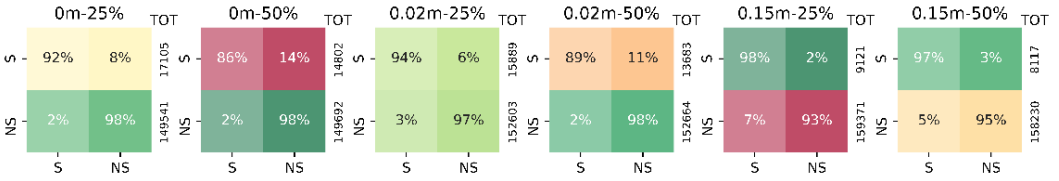

Table 3.8: Same as Table 3.1 for **AVHRR** based SCF products in **mountainous areas.**

a) SCFV

	0m-25%	0m-50%	0.02m-25%	0.02m-50%	0.15m-25%	0.15m-50%
Recall	0.708	0.498	0.72	0.512	0.766	0.567
Precision	0.946	0.948	0.917	0.921	0.66	0.662
False Alarm Rate	0.006	0.003	0.009	0.005	0.034	0.021
Hit Rate (Accuracy)	0.959	0.941	0.959	0.944	0.95	0.951
Critical Success Index	0.68	0.484	0.676	0.49	0.549	0.44
F-score	0.81	0.653	0.807	0.658	0.709	0.611

b) SCFV

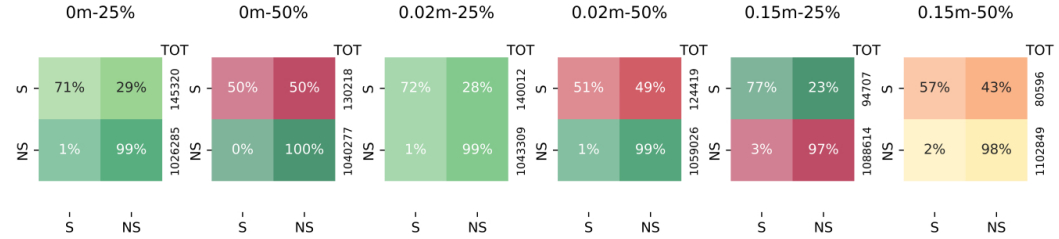

c) SCFG

	0m-25%	0m-50%	0.02m-25%	0.02m-50%	0.15m-25%	0.15m-50%
Recall	0.787	0.767	0.797	0.78	0.829	0.82
Precision	0.944	0.951	0.915	0.927	0.659	0.683
False Alarm Rate	0.008	0.006	0.011	0.009	0.043	0.037
Hit Rate (Accuracy)	0.964	0.964	0.963	0.964	0.945	0.95
Critical Success Index	0.751	0.738	0.742	0.735	0.58	0.594
F-score	0.858	0.849	0.852	0.847	0.734	0.745

d) SCFG

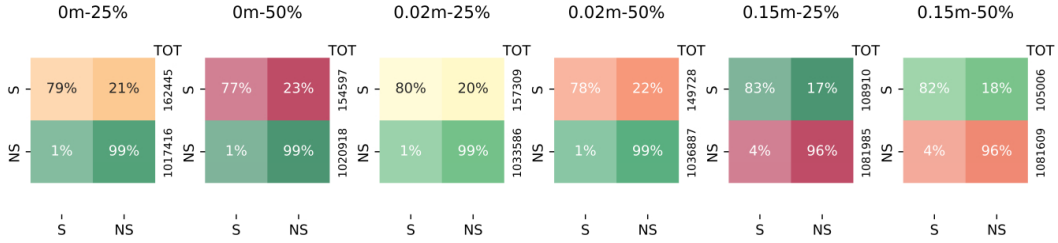

Table 3.9: Same as Table 3.1 for **AVHRR** based SCF products for **plain areas**.

a) SCFV

	0m-25%	0m-50%	0.02m-25%	0.02m-50%	0.15m-25%	0.15m-50%
Recall	0.855	0.758	0.882	0.793	0.929	0.853
Precision	0.943	0.947	0.911	0.92	0.542	0.537
False Alarm Rate	0.006	0.004	0.009	0.006	0.044	0.035
Hit Rate (Accuracy)	0.981	0.975	0.981	0.977	0.955	0.96
Critical Success Index	0.813	0.728	0.812	0.741	0.521	0.491
F-score	0.897	0.842	0.896	0.852	0.685	0.659

b) SCFV

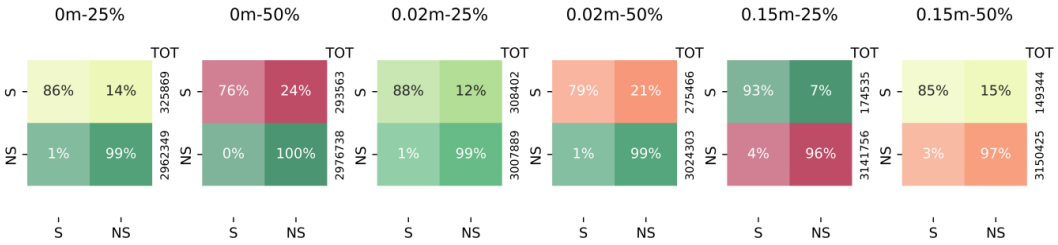

c) SCFG

	0m-25%	0m-50%	0.02m-25%	0.02m-50%	0.15m-25%	0.15m-50%
Recall	0.878	0.863	0.901	0.891	0.941	0.938
Precision	0.944	0.952	0.91	0.925	0.545	0.567
False Alarm Rate	0.006	0.005	0.01	0.008	0.047	0.042
Hit Rate (Accuracy)	0.982	0.982	0.982	0.983	0.953	0.957
Critical Success Index	0.834	0.826	0.828	0.831	0.527	0.547
F-score	0.909	0.905	0.906	0.908	0.69	0.707

d) SCFG

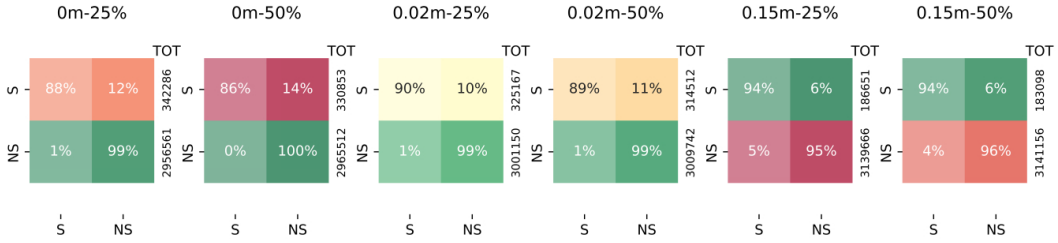

3.1.3. Forested and non-forested areas

Table 3.10: Same as Table 3.1 for **MODIS** based SCF products for **forested areas**.

a) SCFV

	0m-25%	0m-50%	0.02m-25%	0.02m-50%	0.15m-25%	0.15m-50%
Recall	0.71	0.316	0.737	0.334	0.836	0.412
Precision	0.964	0.974	0.941	0.961	0.73	0.771
False Alarm Rate	0.004	0.001	0.006	0.002	0.026	0.009
Hit Rate (Accuracy)	0.962	0.922	0.965	0.929	0.963	0.951
Critical Success Index	0.692	0.314	0.705	0.329	0.639	0.367
F-score	0.818	0.478	0.827	0.496	0.78	0.537

b) SCFV

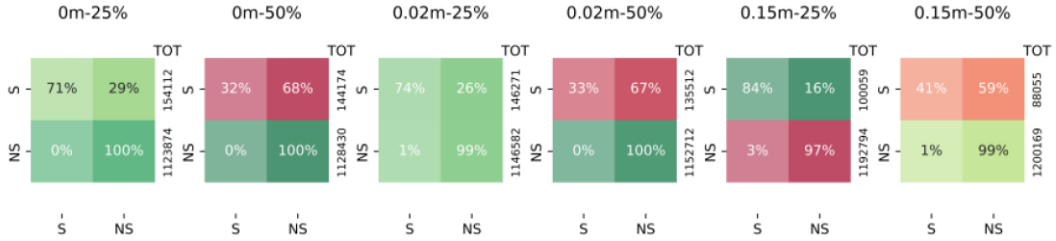

c) SCFG

	0m-25%	0m-50%	0.02m-25%	0.02m-50%	0.15m-25%	0.15m-50%
Recall	0.883	0.837	0.903	0.864	0.968	0.954
Precision	0.952	0.967	0.925	0.951	0.706	0.764
False Alarm Rate	0.007	0.004	0.011	0.006	0.042	0.028
Hit Rate (Accuracy)	0.978	0.976	0.978	0.978	0.959	0.97
Critical Success Index	0.846	0.813	0.841	0.827	0.689	0.737
F-score	0.916	0.897	0.914	0.905	0.816	0.848

d) SCFG

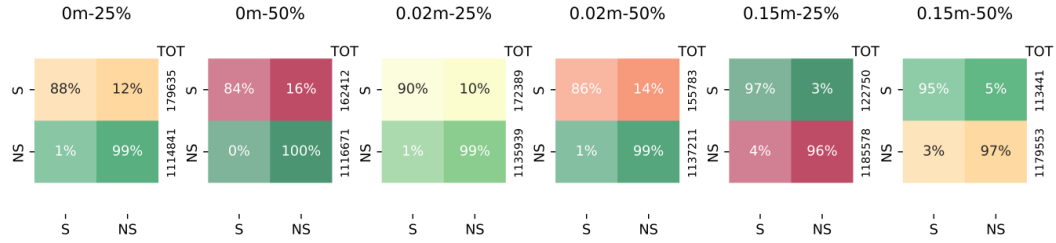

Table 3.11: Same as Table 3.1 for **MODIS** based SCF products for **open areas (non-forested)**.

a) SCFV

	0m-25%	0m-50%	0.02m-25%	0.02m-50%	0.15m-25%	0.15m-50%
Recall	0.836	0.741	0.893	0.809	0.965	0.928
Precision	0.935	0.947	0.886	0.912	0.448	0.49
False Alarm Rate	0.004	0.003	0.007	0.004	0.031	0.024
Hit Rate (Accuracy)	0.986	0.983	0.988	0.986	0.969	0.975
Critical Success Index	0.79	0.711	0.801	0.751	0.441	0.472
F-score	0.883	0.831	0.89	0.858	0.612	0.641

b) SCFV

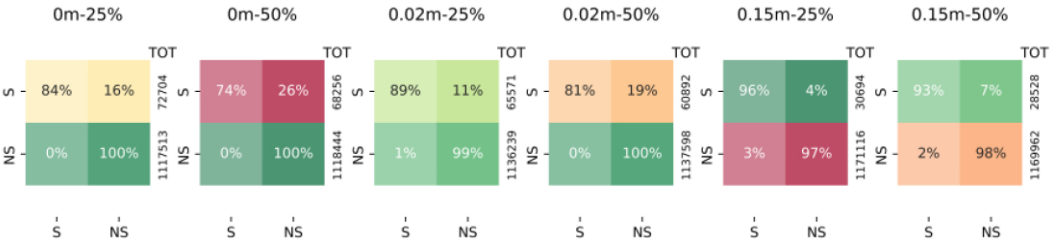

c) SCFG

	0m-25%	0m-50%	0.02m-25%	0.02m-50%	0.15m-25%	0.15m-50%
Recall	0.84	0.764	0.896	0.833	0.967	0.947
Precision	0.935	0.948	0.886	0.912	0.448	0.491
False Alarm Rate	0.004	0.003	0.007	0.004	0.031	0.024
Hit Rate (Accuracy)	0.987	0.984	0.988	0.987	0.969	0.975
Critical Success Index	0.794	0.733	0.803	0.771	0.441	0.478
F-score	0.885	0.846	0.891	0.871	0.612	0.647

d) SCFG

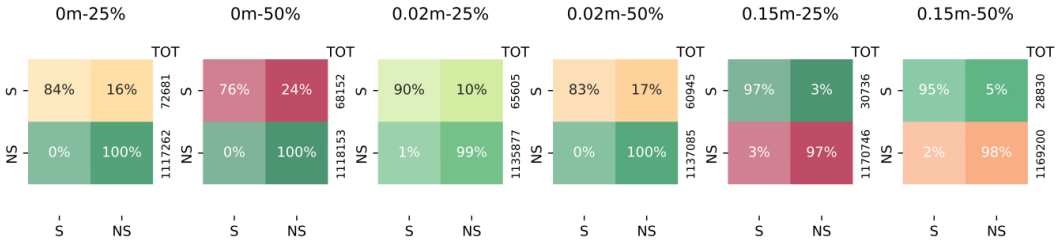

Table 3.12: Same as Table 3.1 for **AATSR** based SCF products in **forested areas.**

a) SCFV

	0m-25%	0m-50%	0.02m-25%	0.02m-50%	0.15m-25%	0.15m-50%
Recall	0.72	0.382	0.738	0.395	0.806	0.462
Precision	0.848	0.81	0.813	0.776	0.586	0.574
False Alarm Rate	0.02	0.013	0.025	0.015	0.053	0.028
Hit Rate (Accuracy)	0.944	0.909	0.945	0.914	0.935	0.933
Critical Success Index	0.637	0.35	0.631	0.354	0.513	0.344
F-score	0.779	0.519	0.774	0.523	0.679	0.512

b) SCFV

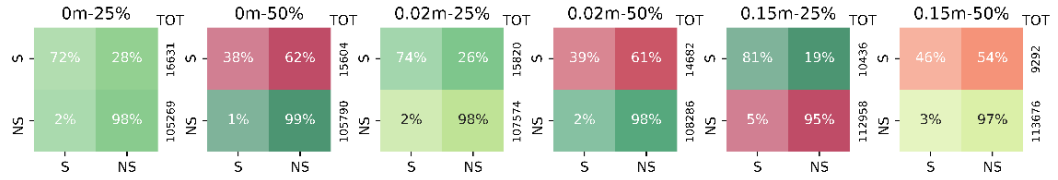

c) SCFG

	0m-25%	0m-50%	0.02m-25%	0.02m-50%	0.15m-25%	0.15m-50%
Recall	0.867	0.822	0.88	0.842	0.919	0.902
Precision	0.853	0.865	0.817	0.837	0.575	0.631
False Alarm Rate	0.028	0.02	0.034	0.024	0.076	0.053
Hit Rate (Accuracy)	0.956	0.958	0.953	0.958	0.924	0.943
Critical Success Index	0.754	0.729	0.735	0.723	0.548	0.591
F-score	0.86	0.843	0.848	0.839	0.708	0.743

d) SCFG

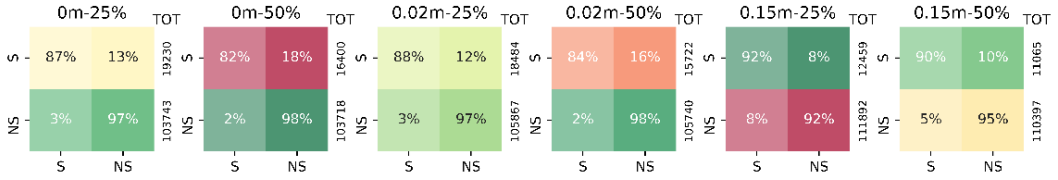

Table 3.13: Same as Table 3.1 for **AATSR** based SCF products in **open areas.**

a) SCFV

	0m-25%	0m-50%	0.02m-25%	0.02m-50%	0.15m-25%	0.15m-50%
Recall	0.879	0.778	0.914	0.826	0.967	0.923
Precision	0.775	0.811	0.7	0.746	0.363	0.413
False Alarm Rate	0.02	0.013	0.027	0.018	0.056	0.04
Hit Rate (Accuracy)	0.973	0.973	0.969	0.973	0.945	0.959
Critical Success Index	0.7	0.659	0.657	0.645	0.359	0.399
F-score	0.824	0.794	0.793	0.784	0.528	0.571

b) SCFV

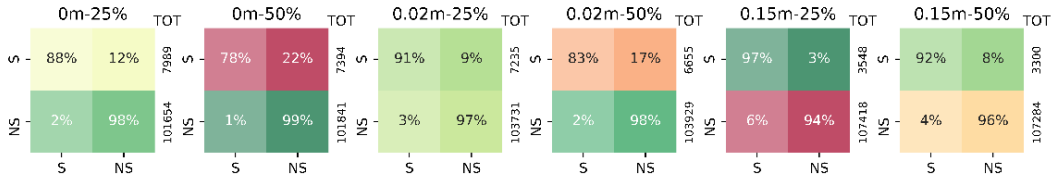

c) SCFG

	0m-25%	0m-50%	0.02m-25%	0.02m-50%	0.15m-25%	0.15m-50%
Recall	0.883	0.798	0.917	0.846	0.968	0.941
Precision	0.776	0.815	0.701	0.75	0.362	0.414
False Alarm Rate	0.02	0.013	0.027	0.018	0.056	0.041
Hit Rate (Accuracy)	0.973	0.974	0.969	0.974	0.944	0.958
Critical Success Index	0.703	0.675	0.66	0.66	0.358	0.403
F-score	0.826	0.806	0.795	0.795	0.527	0.575

d) SCFG

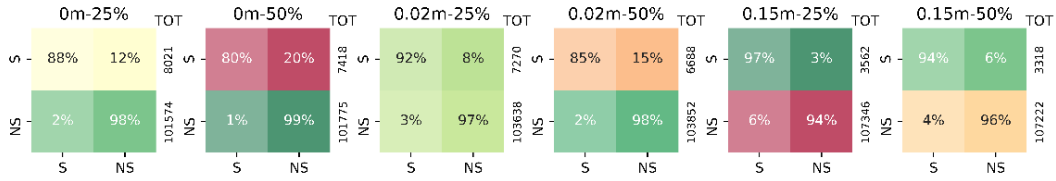

Table 3.14: Same as Table 3.1 for **AVHRR** based SCF products for **forested areas.**

a) SCFV

	0m-25%	0m-50%	0.02m-25%	0.02m-50%	0.15m-25%	0.15m-50%
Recall	0.79	0.627	0.812	0.654	0.862	0.721
Precision	0.954	0.958	0.928	0.937	0.634	0.635
False Alarm Rate	0.005	0.003	0.008	0.005	0.037	0.025
Hit Rate (Accuracy)	0.972	0.96	0.973	0.963	0.956	0.96
Critical Success Index	0.761	0.61	0.764	0.627	0.575	0.51
F-score	0.864	0.758	0.866	0.77	0.73	0.676

b) SCFV

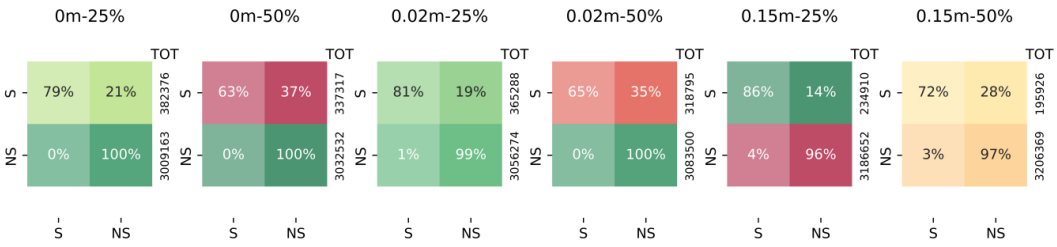

c) SCFG

	0m-25%	0m-50%	0.02m-25%	0.02m-50%	0.15m-25%	0.15m-50%
Recall	0.838	0.822	0.857	0.844	0.895	0.89
Precision	0.952	0.959	0.925	0.938	0.632	0.656
False Alarm Rate	0.006	0.005	0.009	0.007	0.043	0.037
Hit Rate (Accuracy)	0.975	0.975	0.975	0.976	0.952	0.957
Critical Success Index	0.805	0.794	0.801	0.799	0.588	0.607
F-score	0.892	0.885	0.89	0.889	0.741	0.755

d) SCFG

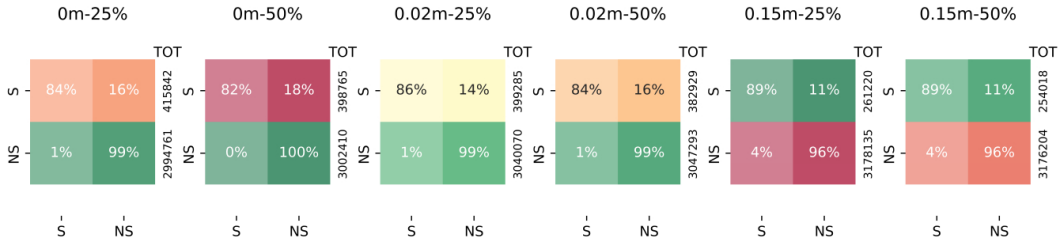

Table 3.15: Same as Table 3.1 for **AVHRR** based SCF products for **open areas (non-forested)**.

a) SCFV

	0m-25%	0m-50%	0.02m-25%	0.02m-50%	0.15m-25%	0.15m-50%
Recall	0.895	0.88	0.918	0.907	0.937	0.935
Precision	0.907	0.919	0.855	0.875	0.361	0.378
False Alarm Rate	0.008	0.007	0.013	0.011	0.055	0.05
Hit Rate (Accuracy)	0.984	0.984	0.982	0.983	0.945	0.95
Critical Success Index	0.82	0.816	0.794	0.802	0.352	0.369
F-score	0.901	0.899	0.885	0.89	0.521	0.539

b) SCFV

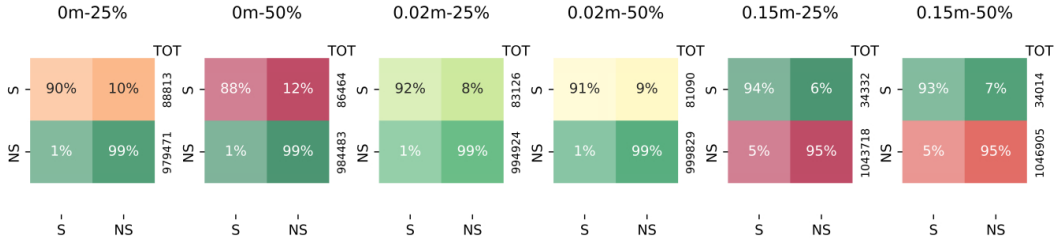

c) SCFG

	0m-25%	0m-50%	0.02m-25%	0.02m-50%	0.15m-25%	0.15m-50%
Recall	0.896	0.881	0.918	0.908	0.937	0.935
Precision	0.907	0.919	0.855	0.874	0.36	0.378
False Alarm Rate	0.008	0.007	0.013	0.011	0.055	0.05
Hit Rate (Accuracy)	0.984	0.984	0.982	0.983	0.945	0.949
Critical Success Index	0.82	0.817	0.794	0.803	0.352	0.368
F-score	0.901	0.899	0.885	0.891	0.52	0.538

d) SCFG

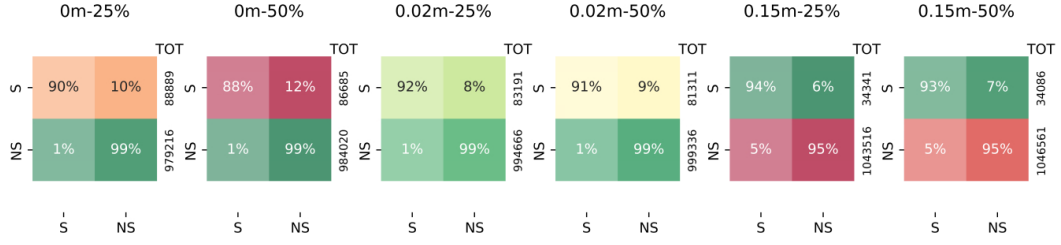

Finally, we checked the accuracy considering the stations surrounded by forest or in open areas, i.e. for non-forested areas. As one can notice from Table 3.10 to Table 3.15, the accuracy in forested areas decreases about 2% in terms of hit rate and F-score for both the sensors when SCFV is considered. This is an expected result given the well-known issues of identifying snow in forested areas using optical remote sensing data. However, the SCFG provide a consistent accuracy for both forested and non-forested areas indicating the robustness of the *snow_cci* products. It is worth noting that the performance of the algorithms retrieving SCFG and SCFV are very similar in non-forested areas. This indicates a good consistency between the *snow_cci* algorithms.

Figure 3.1, Figure 3.2, and Figure 3.3 show the accuracy and false alarm rates considering all the threshold combinations from 2000 to 2018 for MODIS-based *snow_cci* products, from 2002 to 2007 for AATSR, and from 1986 to 2018 for the AVHRR-based products, respectively. In general, we can observe that the accuracy remains above 97% and the false alarm rate remains below 3% for MODIS-based products whereas the accuracy is above 95% and the false alarms below 5% for AVHRR-based products. This indicates a good temporal stability of the *snow_cci* SCF products. Finally, it is worth noting that the higher accuracy of the SCFG products indicate a robustness in detecting snow in forested areas.

Compared to *snow_cci* products of CRDP v2.0 derived from MODIS and AVHRR, the general good performance is confirmed also for CRDP v3.0 products from these sensors with a slight overall improvement of the accuracy in the order of 1%.

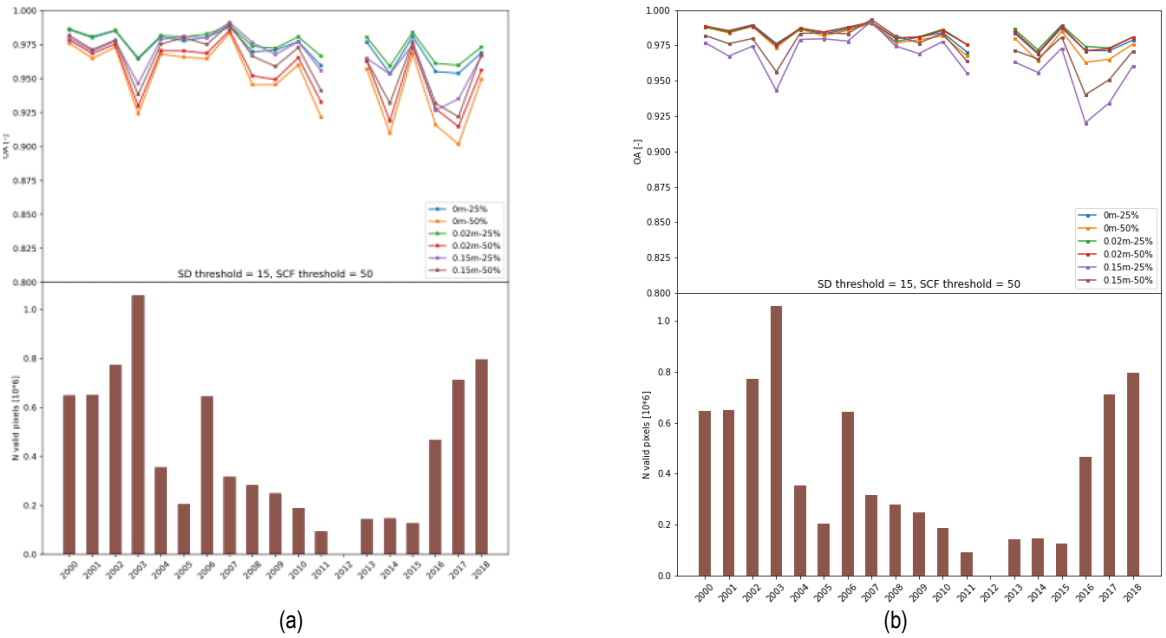

Figure 3.1: Annual time series of accuracy considering all the threshold combinations from 2000 to 2018 for MODIS-based *snow_cci* products. (a) SCFV and (b) SCFG.

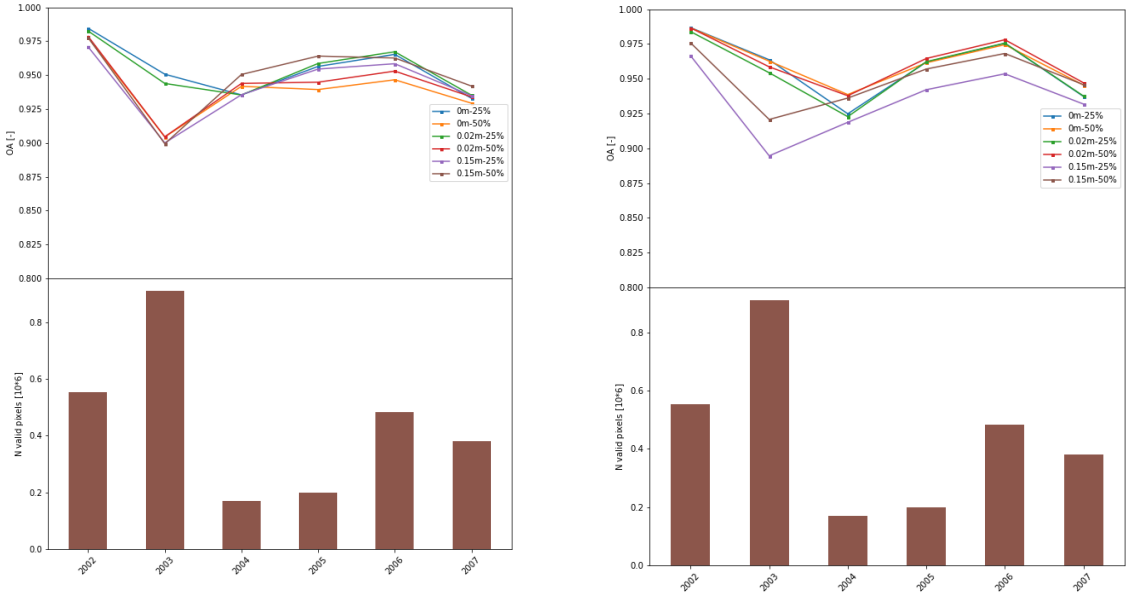

(a) (b)

Figure 3.2: Annual time series of accuracy considering all the threshold combinations from 2000 to 2018 for AATSR-based *snow_cci* products. (a) SCFV and (b) SCFG.

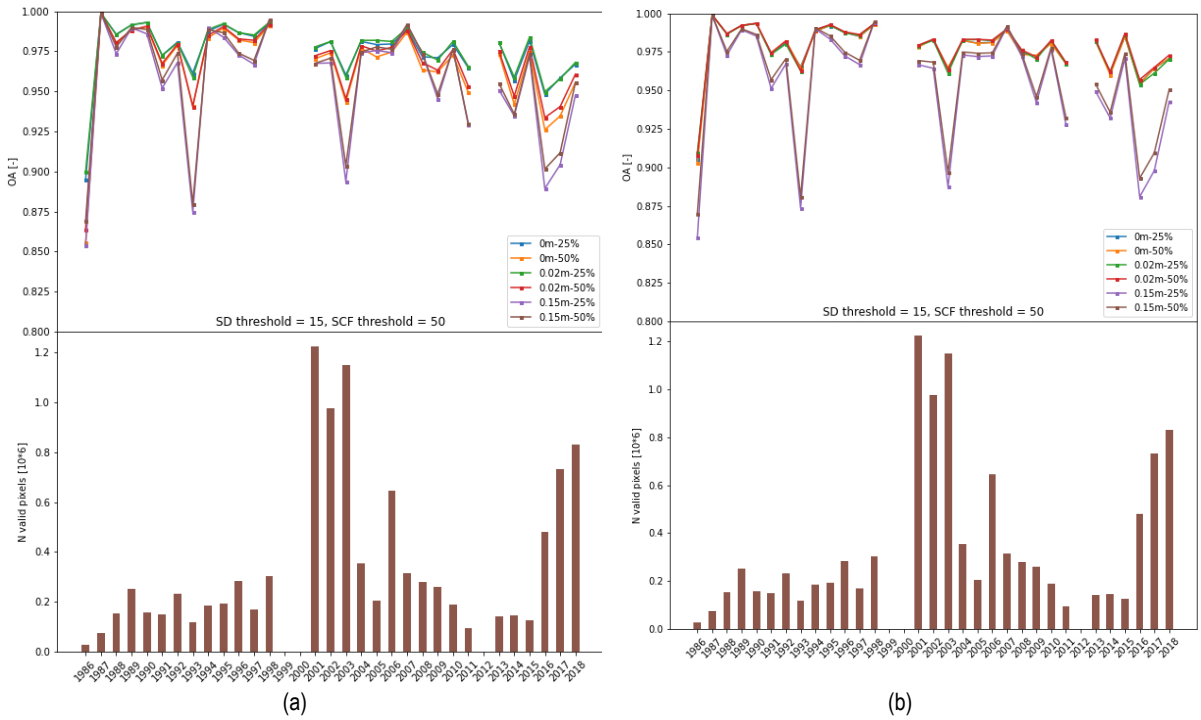

(a) (b)

Figure 3.3: Annual time series of accuracy considering all the threshold combinations from 1986 to 2018 for AVHRR-based *snow_cci* products. (a) SCFV and (b) SCFG.

3.2. Comparison with high resolution snow maps

In this section, the detailed validation results derived from the pixel-by-pixel comparison of the SCF products with snow maps derived from high-resolution (HR) optical satellite data are presented.

All reference snow maps are re-projected in the geographic map projection on WGS84 ellipsoid and aggregated to a fractional snow cover extent at the resolution of the *snow_cci* SCE products (i.e., 0.01 degrees and 0.05 degrees). For describing the results of the pixel-by-pixel inter-comparison, the statistical measures Bias, Root Mean Square Error (RMSE), Unbiased RMSE, and cross-correlation are used. All the metrics are described in detail in the PVP [RD-2], Chapter 4.4.1. In detail, 1050, 192 and 714 HR snow maps have been identified for the comparison with AVHRR, AATSR and MODIS-based products, respectively. These HR reference scenes are acquired all around the globe since 1986. Among the reference images, 271 and 16 scenes are completely snow free for evaluating the detection of snow free areas from AVHRR and MODIS, respectively. These reference images are acquired also in areas with very low probability of having snow e.g., the Sahara Desert or in the Amazon rainforest.

Table 3.16, Table 3.17 and Table 3.18 report the results obtained for MODIS, AATSR and AVHRR-based products, respectively, considering all the reference datasets.

Table 3.16: Summary of the validation of the *snow_cci* products derived from **MODIS** considering the total areas of the 714 Landsat images of the validation dataset.

a) SCFV	*Salomonson*	*Klein*	*Dozier*
RMSE	22.35	28.62	24.50
Unbiased RMSE	19.17	24.53	21.36
Bias	-11.49	-14.74	-12.01
Correlation Coefficient	0.90	0.85	0.89

b) SCFG	*Salomonson*	*Klein*	*Dozier*
RMSE	14.79	13.90	15.42
Unbiased RMSE	14.70	13.80	15.39
Bias	1.59	-1.65	1.08
Correlation Coefficient	0.95	0.96	0.95

Table 3.17: Summary of the validation of the *snow_cci* products derived from **AATSR** considering the total areas of the 192 Landsat images of the validation dataset.

a) SCFV	*Salomonson*	*Klein*	*Dozier*
RMSE	26.58	32.74	28.26
Unbiased RMSE	22.24	27.14	23.97
Bias	-14.56	-18.30	-14.96
Correlation Coefficient	0.86	0.81	0.86

b) SCFG	Salomonson	Klein	Dozier
RMSE	16.61	16.85	17.38
Unbiased RMSE	16.61	16.51	17.38
Bias	0.37	-3.37	-0.036
Correlation Coefficient	0.94	0.94	0.93

Table 3.18: Summary of the validation of the *snow_cci* products derived from **AVHRR** considering the total areas of the 1050 Landsat images of the validation dataset.

a) SCFV	Salomonson	Klein	Dozier
RMSE	24.256	28.55	25.36
Unbiased RMSE	23.12	26.49	23.91
Bias	-7.33	-10.65	-8.44
Correlation Coefficient	0.87	0.84	0.86

b) SCFG	Salomonson	Klein	Dozier
RMSE	23.65	25.13	24.09
Unbiased RMSE	23.56	24.56	23.89
Bias	-1.99	-5.30	-3.10
Correlation Coefficient	0.88	0.87	0.88

From the results reported in the tables, one can observed a general improvement of the performance compared to the *snow_cci* products of the CRDP v2.0 derived from MODIS and AVHRR. As described in the ATBD [RD-3], the *snow_cci* algorithm provide in forested areas two different information about the snow: the snow on ground (SCFG) i.e., canopy corrected snow information, and the viewable snow (SCFV) i.e., the snow that is visible from the satellite and that was intercepted by the stem of the trees. Since forested areas are very challenging for mapping the snow from remote sensing images, the validation of the *snow_cci* SCF products has also been separately analysed for “forested” and “non-forested” areas. The layer identifying the forested areas around the globe is described in the DARD [RD-1]. It is worth noting that the validation of the SCFG in forested areas required that also the state-of-the-art algorithms used for the snow classification from high resolution images can perform a canopy correction. In particular, after the aggregation at the low resolution, the algorithm proposed by Salomonson and Appel (2006) provides SCFV, whereas the algorithms proposed by Klein et al. (1998) and Dozier and Painter (2004) provide SCFG. Thus, in forested areas, the *snow_cci* SCFV is compared only with the Salomonson algorithm, whereas the *snow_cci* SCFG is compared with the Dozier and Klein algorithms.

In Table 3.19, Table 3.20 and Table 3.21, the comparison results for the SCFV and SCFG in forested and open areas from MODIS, AATSR and AVHRR, respectively, are summarized.

Table 3.19: Summary of the validation of the *snow_cci* products derived from **MODIS** considering 705 Landsat images separating forest from open areas. Results obtained for: a) SCFV and b) SCFG.

a) SCFV	*Salomonson forested*	*Salomonson open areas*	*Dozier open areas*	*Klein open areas*
RMSE	28.55	10.88	11.05	11.46
Unbiased RMSE	21.38	10.58	10.78	11.15
Bias	-18.92	-2.5	-2.44	-2.61
Correlation Coefficient	0.85	0.97	0.97	0.97

b) SCFG	*Salomonson open areas*	*Dozier forested*	*Dozier open areas*	*Klein forested*	*Klein open areas*
RMSE	10.88	18.27	11.05	15.63	11.46
Unbiased RMSE	10.58	17.82	10.78	15.60	11.15
Bias	-2.53	4.00	-2.44	-0.85	-2.61
Correlation Coefficient	0.97	0.92	0.97	0.94	0.97

Table 3.20: Summary of the validation of the *snow_cci* products derived from **AATSR** considering 192 Landsat images separating forest from open areas. Results obtained for: a) SCFV and b) SCFG.

a) SCFV	*Salomonson forested*	*Salomonson open areas*	*Dozier open areas*	*Klein open areas*
RMSE	35.04	11.16	11.09	11.16
Unbiased RMSE	23.68	10.98	10.81	10.87
Bias	-25.83	-1.97	-2.47	-2.51
Correlation Coefficient	0.79	0.97	0.97	0.97

b) SCFG	*Salomonson open areas*	*Dozier forested*	*Dozier open areas*	*Klein forested*	*Klein open areas*
RMSE	11.16	21.49	11.09	20.65	11.16
Unbiased RMSE	10.98	21.38	10.81	20.23	10.87
Bias	-1.97	2.15	-2.47	-4.14	-2.51
Correlation Coefficient	0.97	0.88	0.97	0.89	0.97

Table 3.21: Summary of the validation of the *snow_cci* products derived from **AVHRR** considering 1050 Landsat images separating forest from open areas. Results obtained for: a) SCFV and b) SCFG.

a) SCFV	*Salomonson forested*	*Salomonson open areas*	*Dozier open areas*	*Klein open areas*
RMSE	30.53	12.48	12.47	12.50
Unbiased RMSE	27.64	12.47	12.47	12.50
Bias	-12.97	-0.25	-0.27	-0.32
Correlation Coefficient	0.79	0.96	0.96	0.95

b) SCFG	Salomonson open areas	Dozier forested	Dozier open areas	Klein forested	Klein open areas
RMSE	12.48	30.30	12.47	31.77	12.50
Unbiased RMSE	12.48	29.82	12.47	30.39	12.50
Bias	-0.24	-5.33	-0.27	-9.27	-0.31
Correlation Coefficient	0.96	0.80	0.96	0.79	0.96

As expected, the performance of the *snow_cci* SCFV and SCFG in open areas are identical. This indicates that the SCFV and SCFG products are consistent.

As one can notice, the performance in forested areas is degraded compared to the one in open areas in terms of correlation coefficient and RMSE. However, the results seem contrasting for the bias. This may indicate that some residual errors on how the HR snow maps are calculated in forested areas are present. By examining the problem in detail, it is difficult to validate the accuracy of the high-resolution snow maps in forest since what is visible at 20 to 30 meters resolution is not the snow on ground but the mixed pixels of snow and trees canopy. In such complex situations, methods based to the Normalized Difference Snow Index (NDSI) tend to provide similar results for both high- and low-resolution detection. This may therefore be the main reason why the bias is reduced in forested areas. Among these results, the main information is given by the comparison in open areas, since under the canopy the high resolution is still not able to provide reliable information for validation.

To avoid any bias in the evaluation the remaining results reported in this document will consider only unforested areas without distinction between SCFG and SCFV, which provide identical results in open areas.

With respect to the *snow_cci* CRDP v2.0, a great improvement is noticeable for the MODIS-based SCF maps of the CRDP v3.0 in open areas.

To better understand the results presented up to now, we analyse the results obtained considering each Landsat scene independently. This will allow us to derive useful information on the local behaviour of the products. We start by analysing how the validation metrics spread out in the data set. Box plots for bias and unbiased RMSE for *snow_cci* products in different situations i.e., mountainous and plain areas and forest and open field, for the northern and the southern hemisphere are presented in Figure 3.4, Figure 3.5 and Figure 3.6, respectively.

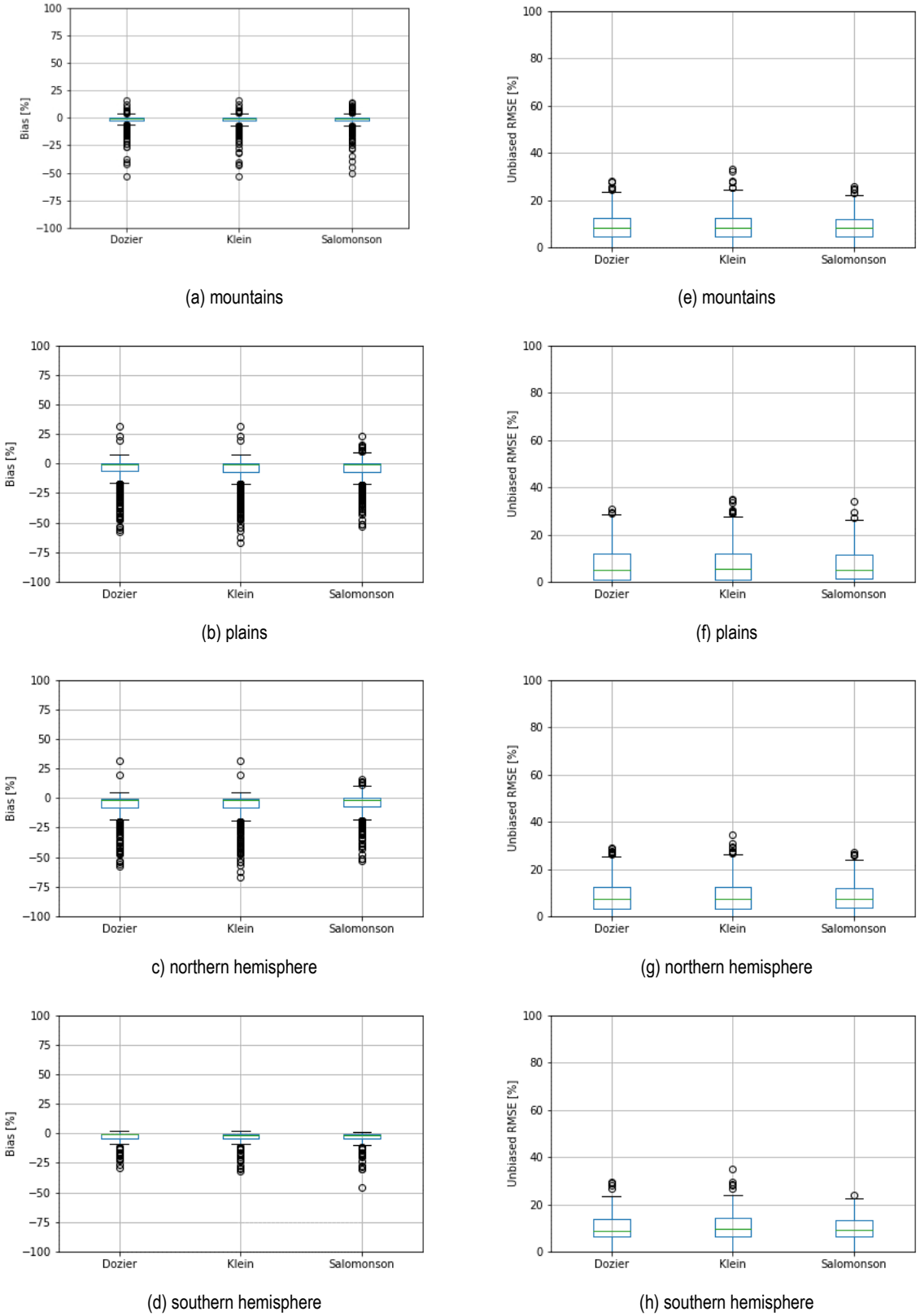

Figure 3.4: Boxplots of bias and unbiased RMSE resulting from the validation of the *snow_cci* SCF product derived from **MODIS** with snow maps generated by Dozier, Klein and Salomonson for different regions. (a)-(d) **bias** and (e)-(h) **unbiased RMSE**.

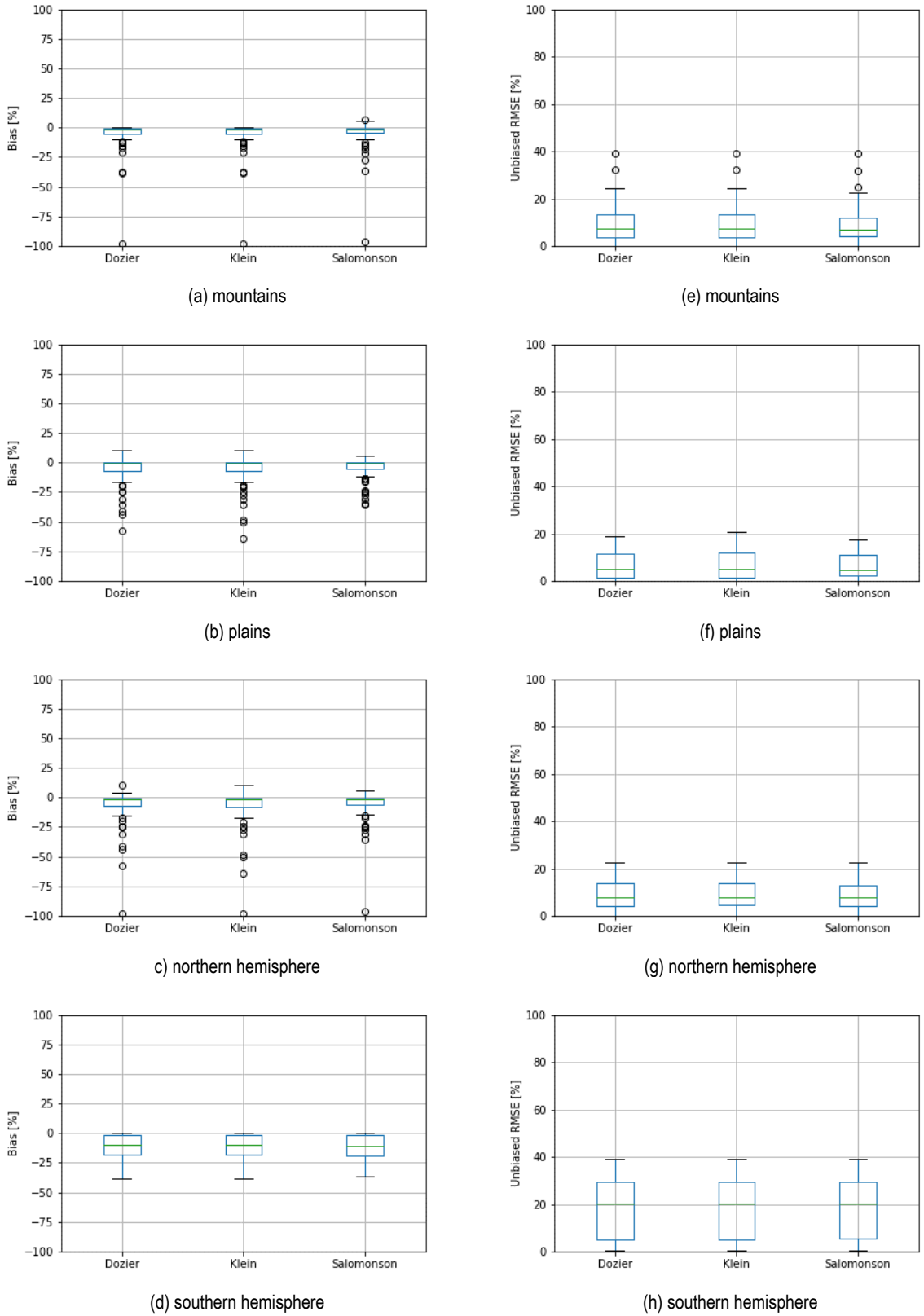

(a) mountains (e) mountains

(b) plains (f) plains

c) northern hemisphere (g) northern hemisphere

(d) southern hemisphere (h) southern hemisphere

Figure 3.5: Boxplots of bias and unbiased RMSE resulting from the validation of the *snow_cci* SCF product derived from **AATSR** with snow maps generated by Dozier, Klein and Salomonson for different regions. (a)-(d) **bias** and (e)-(h) **unbiased RMSE**.

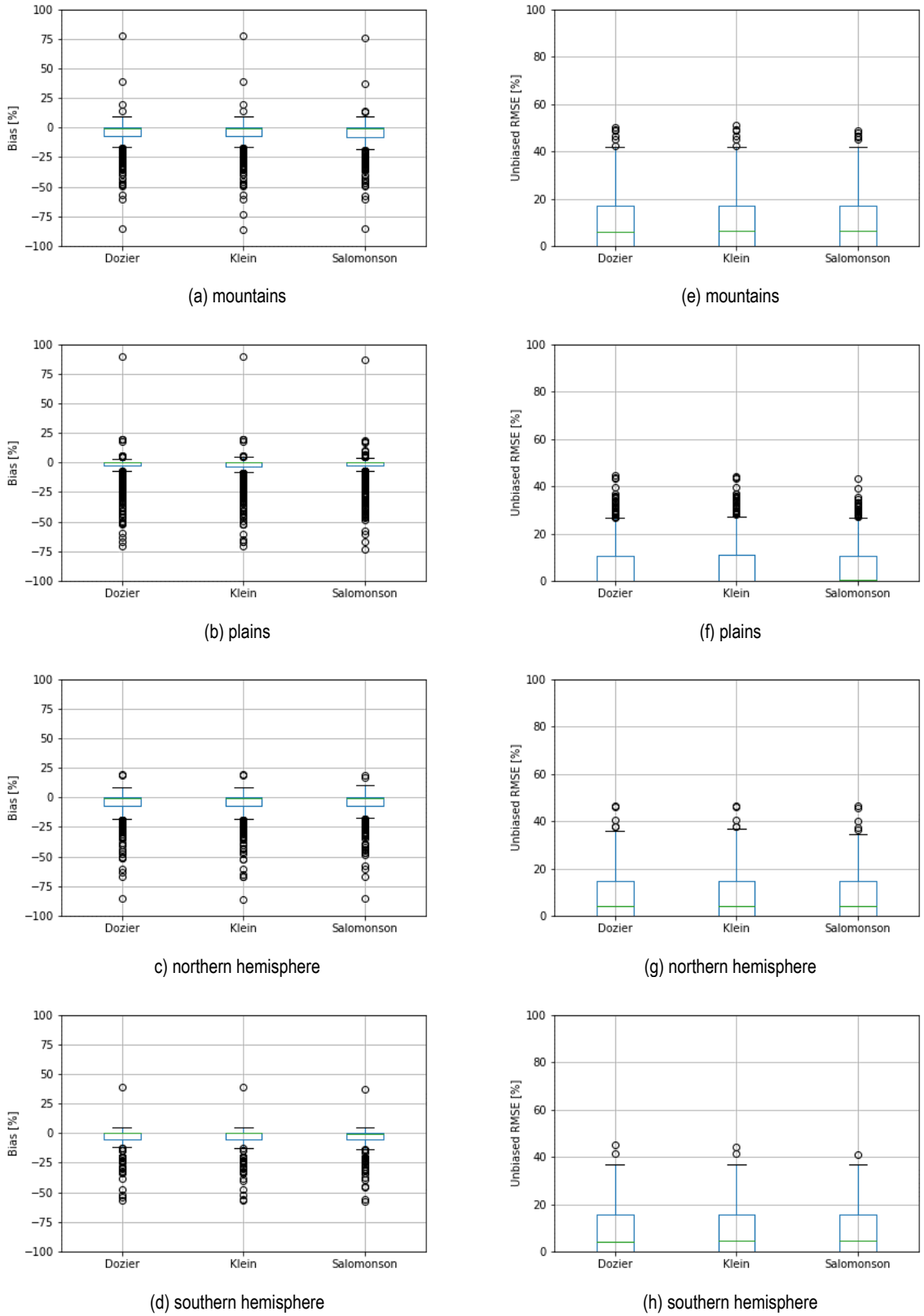

Figure 3.6: Boxplots of bias and unbiased RMSE resulting from the validation of the *snow_cci* SCF product derived from **AVHRR** with snow maps generated by Dozier, Klein and Salomonson for different regions. (a)-(d) **bias** and (e)-(h) **unbiased RMSE**.

The statistical measures unbiased RMSE and bias as function of the time resulting from the validation of the *snow_cci* SCF products with snow maps generated by Dozier, Klein and Salomonson approaches from Landsat scenes are illustrated in the plots of Figure 3.7, Figure 3.8, and Figure 3.9 for MODIS, AATSR, and AVHRR, respectively. These figures show the temporal consistency of the SCF products.

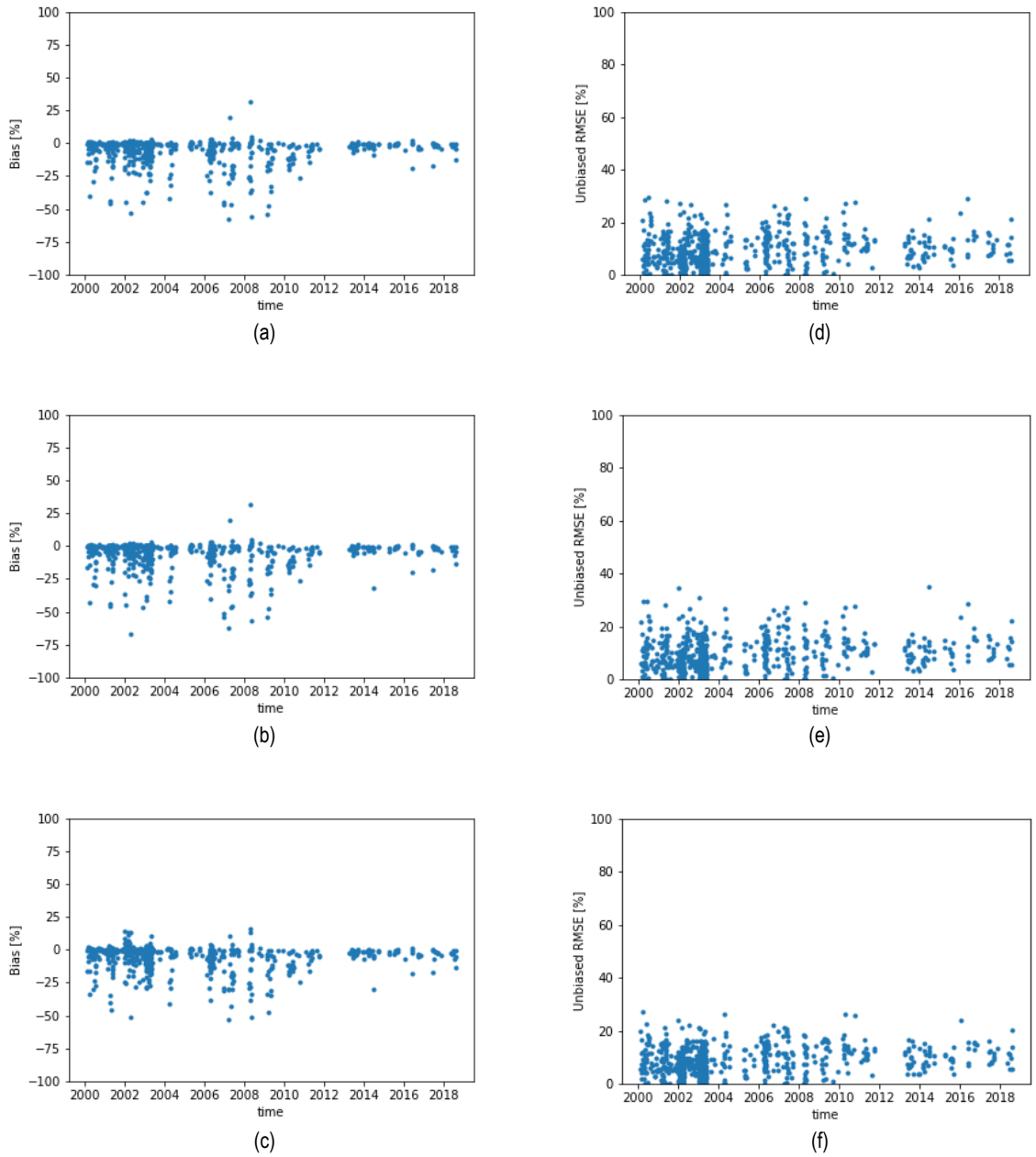

Figure 3.7: (a)-(c) Bias and (d)-(f) unbiased RMSE resulting from the validation of the *snow_cci* SCF products from **MODIS** data for the period 2000 – 2018 with reference snow maps from Landsat data generated by Dozier, Klein and Salomonson.

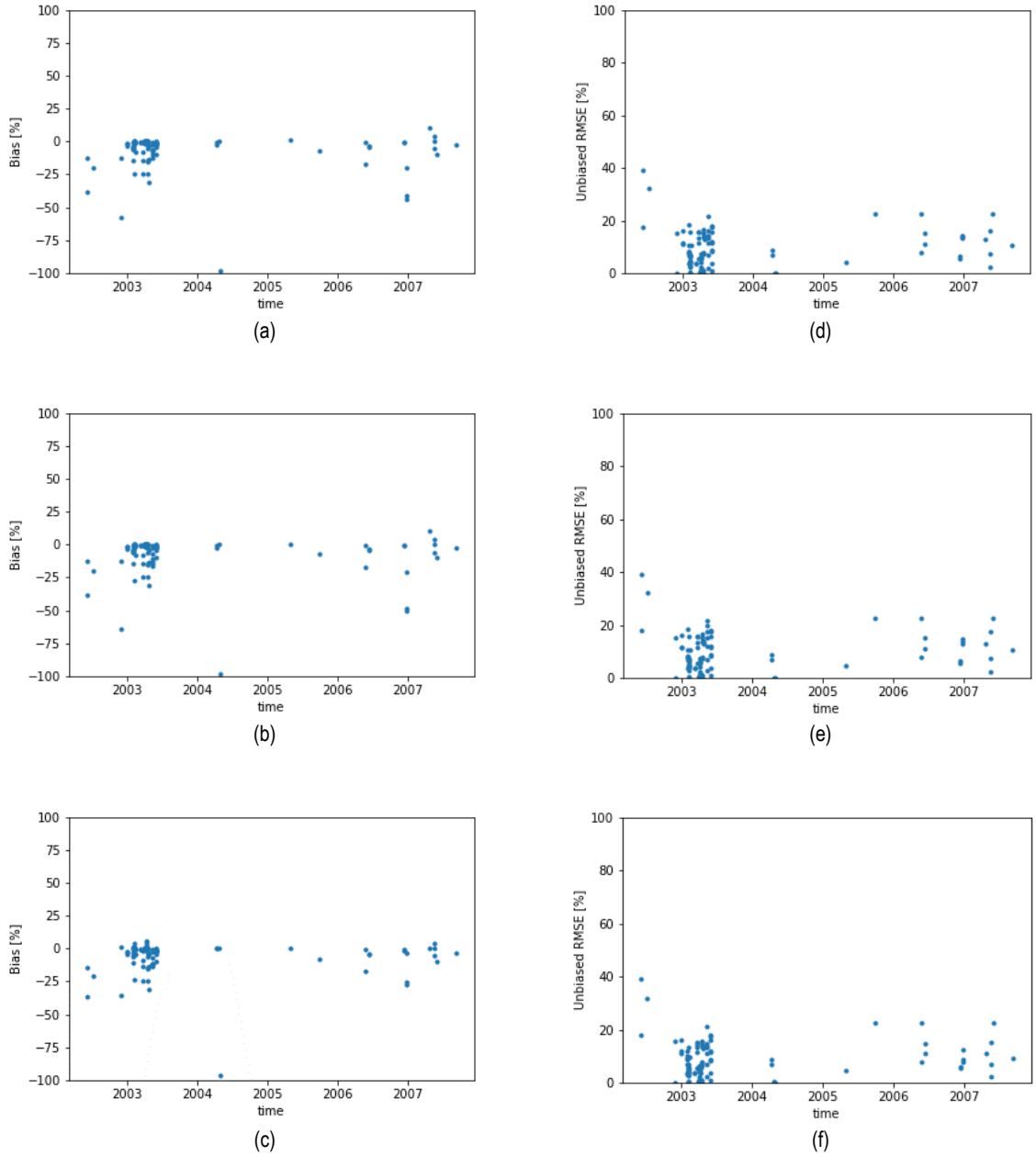

Figure 3.8: (a)-(c) Bias and (d)-(f) unbiased RMSE resulting from the validation of the *snow_cci* SCF products from **AATSR** data for the period 2000 – 2018 with reference snow maps from Landsat data generated by Dozier, Klein and Salomonson.

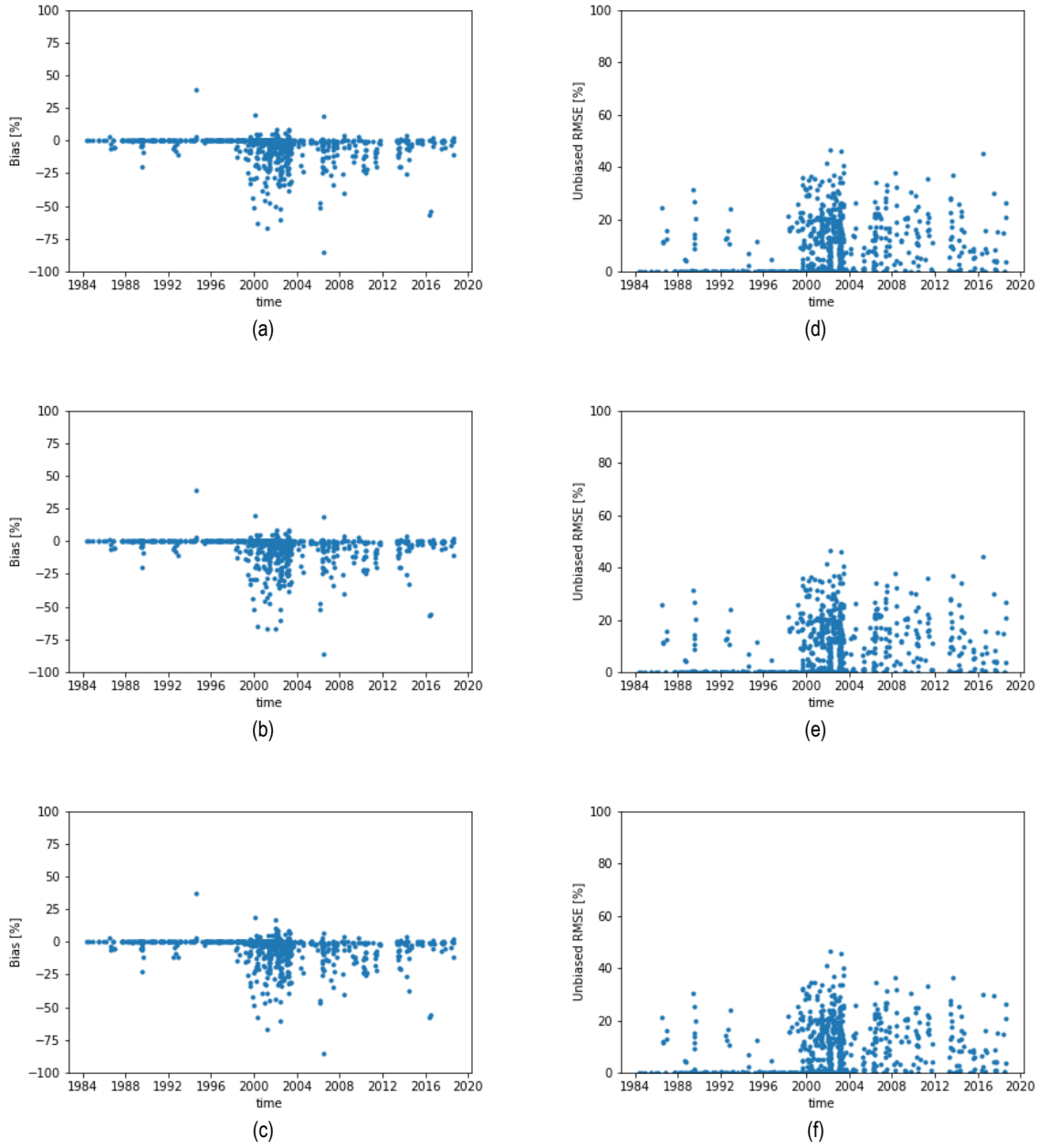

Figure 3.9: (a)-(c) Bias and (d)-(f) unbiased RMSE resulting from the validation of the *snow_cci* SCF products from **AVHRR** data for the period 1986 – 2018 with reference snow maps from Landsat data generated by Dozier, Klein and Salomonson.

From these plots is visible that the *snow_cci* CRDP v3 products are performing well on average with some extremes. These are situations in which the detection tends to be difficult e.g., presence of atmospheric disturbances that represent outliers to the accuracy assessment. But, this allows also to better understand the global performance of the products, taking the large number of samples used for the calculation of the statistical measures into account.

The validation of the SCE products was performed also considering the different SCF aggregated in steps of 10%. The unbiased RMSE and the Bias resulting from this validation considering all non-

forested, open land pixels from all the selected Landsat scenes are illustrated in the box-plots of Figure 3.10, Figure 3.11 and Figure 3.12 and for AVHRR, AATSR and MODIS, respectively. The box plots show a tendency to underestimate the SCF particularly in the range from 40% to 60%. The unbiased RMSE is showing a similar trend indicating a greater error spread in the values from 40% to 50%.

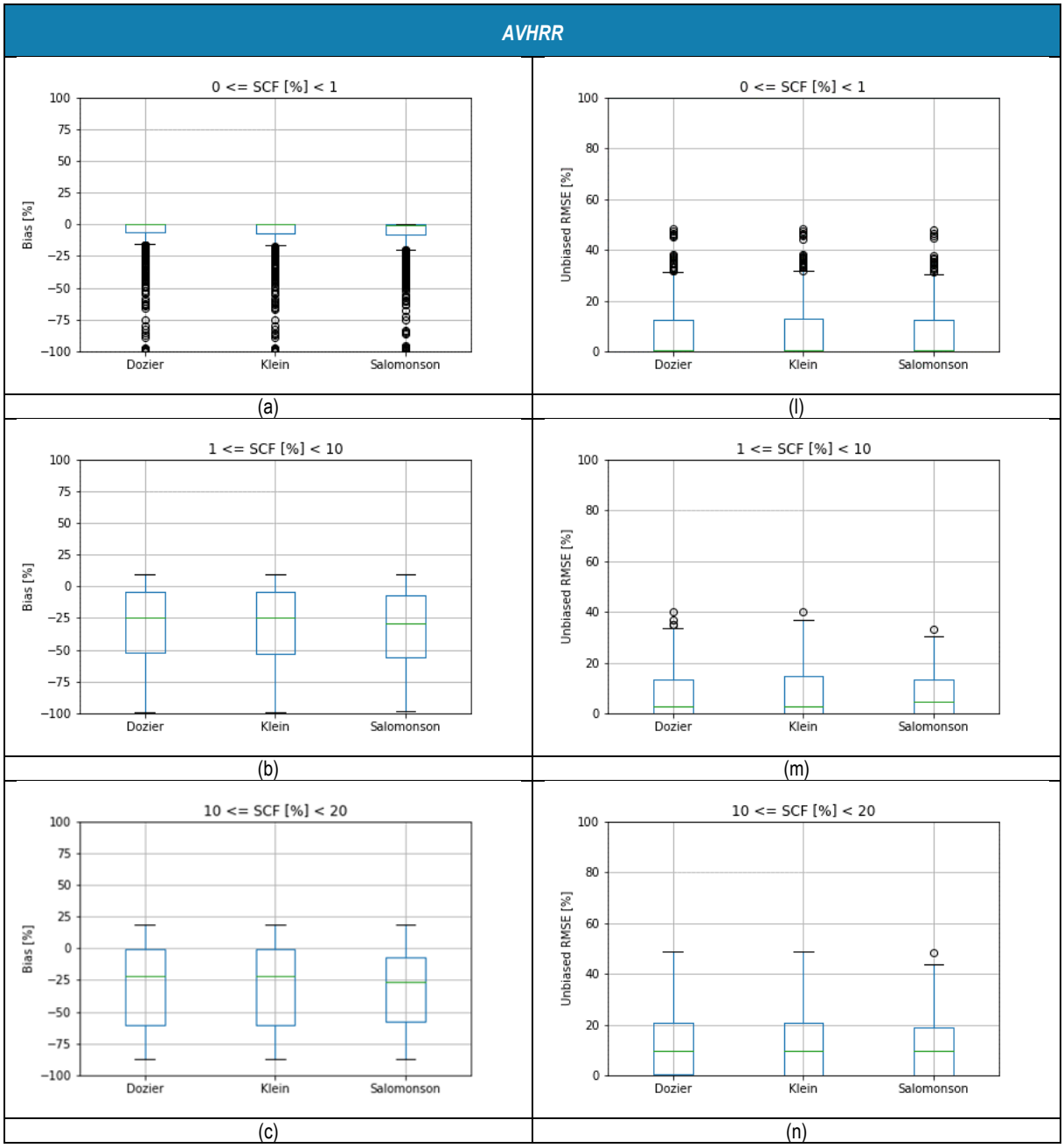

AVHRR	
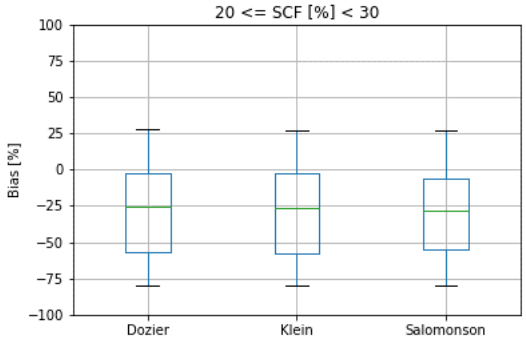	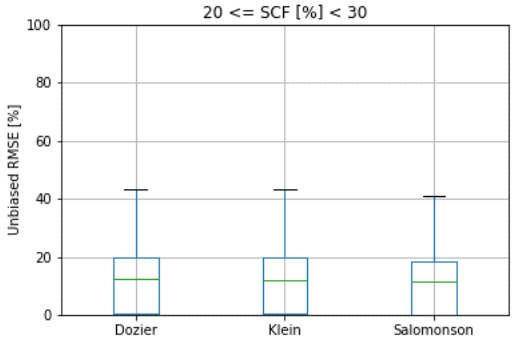
(d)	(o)
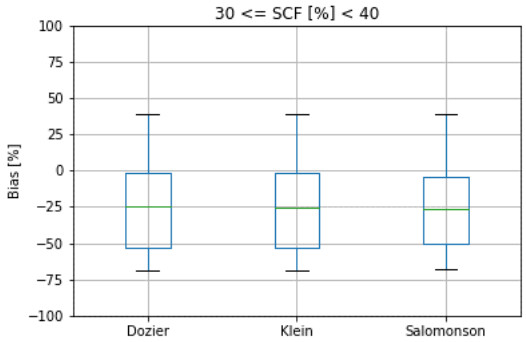	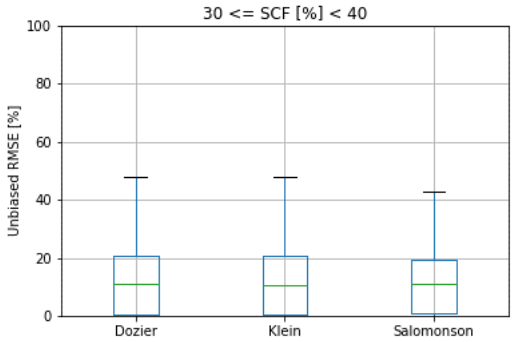
(e)	(p)
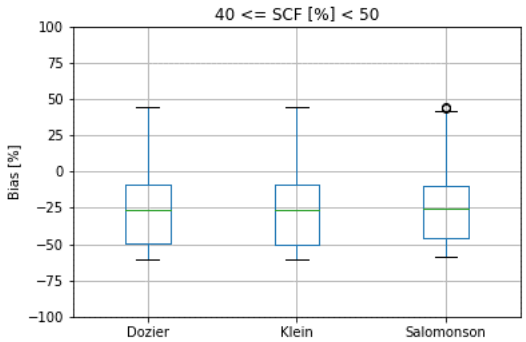	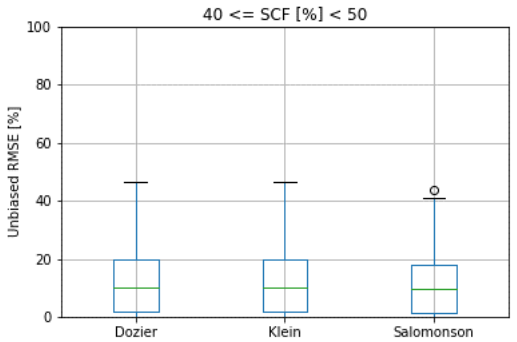
(f)	(q)
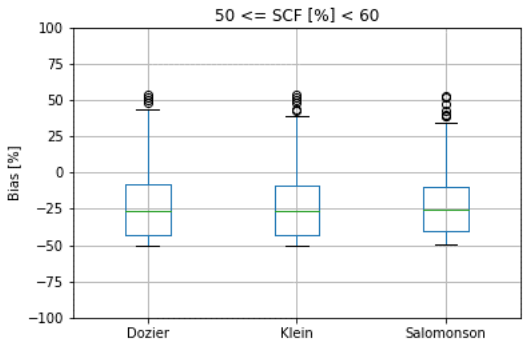	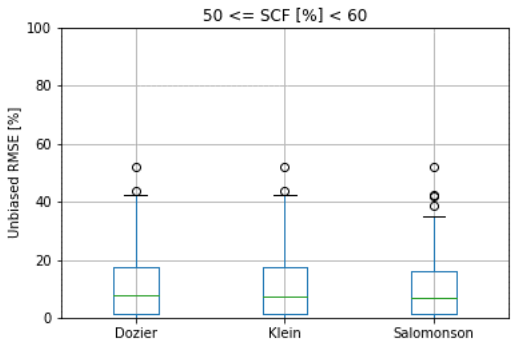
(g)	(r)

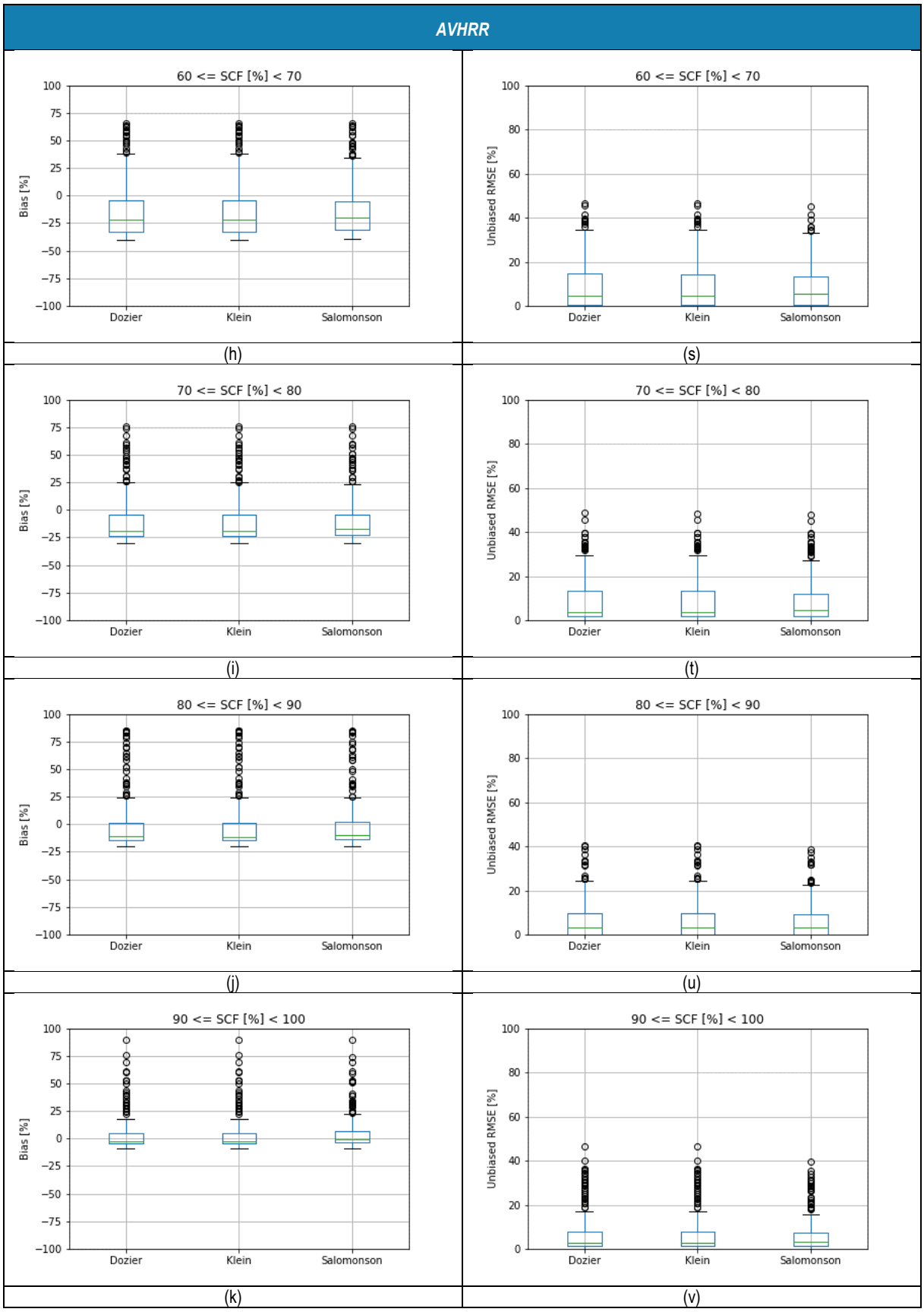

Figure 3.10: Bias (a)-(k) and unbiased RMSE (l)-(v) resulting from the validation of the **AVHRR** based SCF products with SCF step of 10% in non-forested areas.

AATSR	
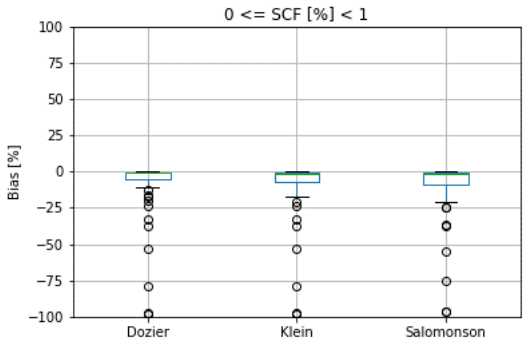	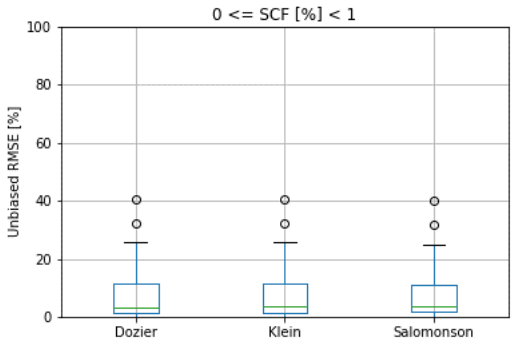
(a)	(l)
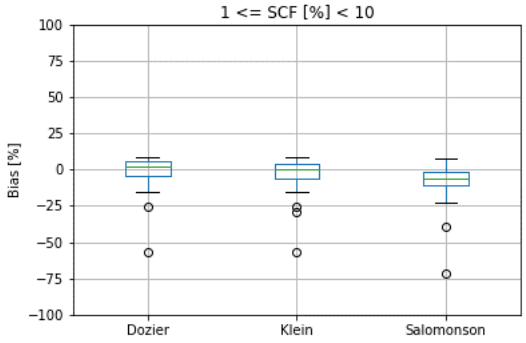	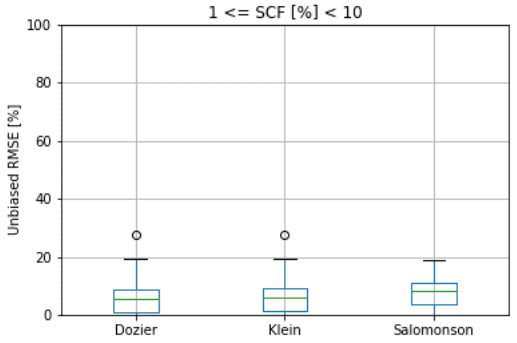
(b)	(m)
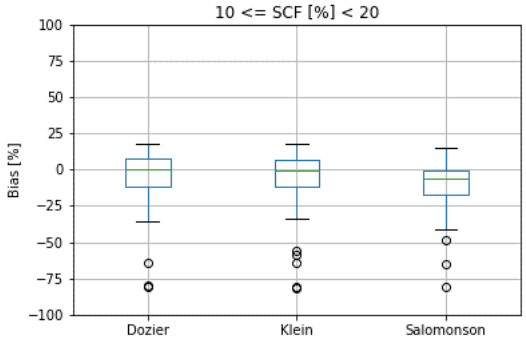	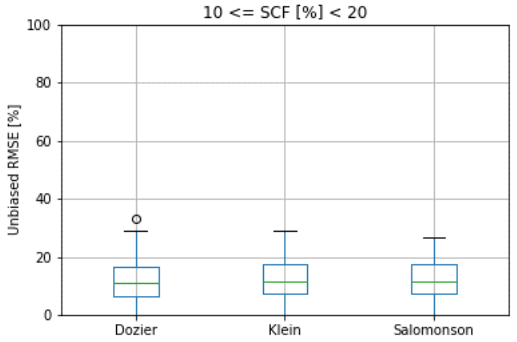
(c)	(n)
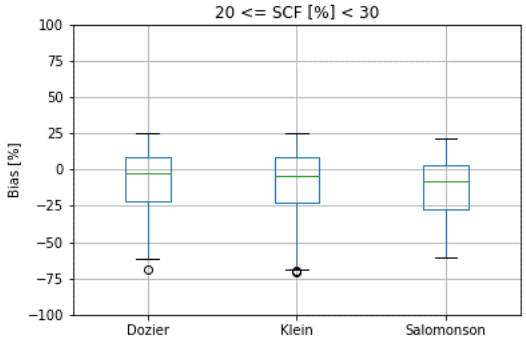	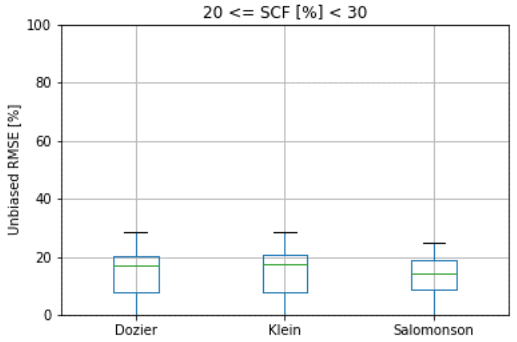
(d)	(o)

AATSR	
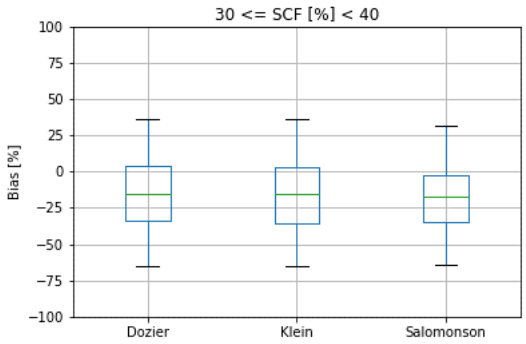	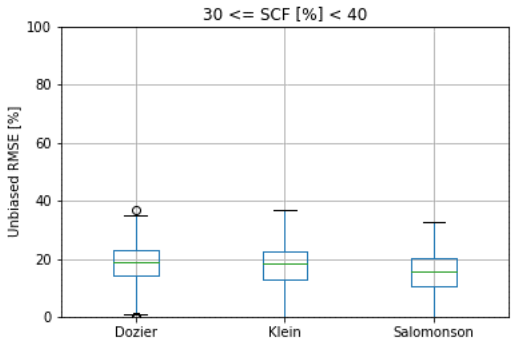
(e)	(p)
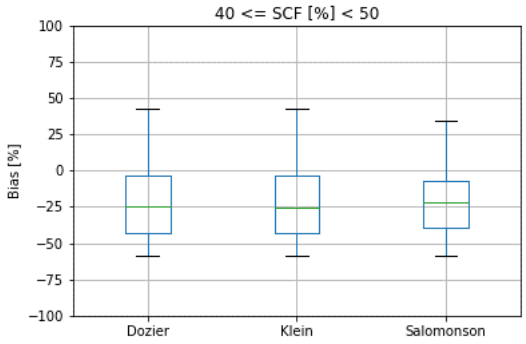	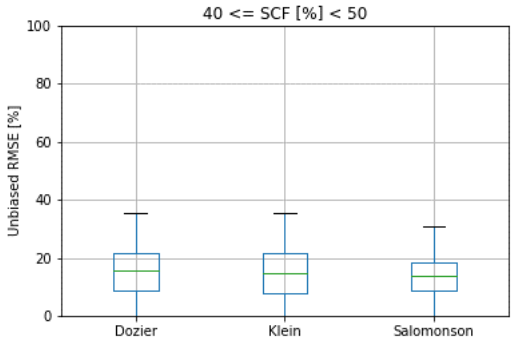
(f)	(q)
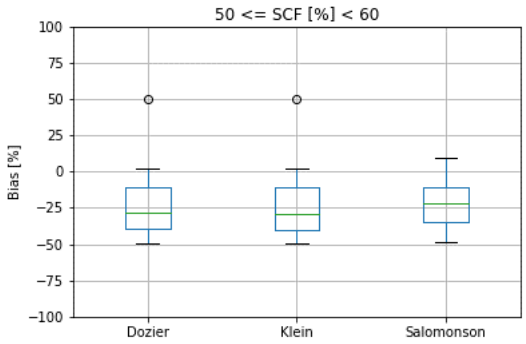	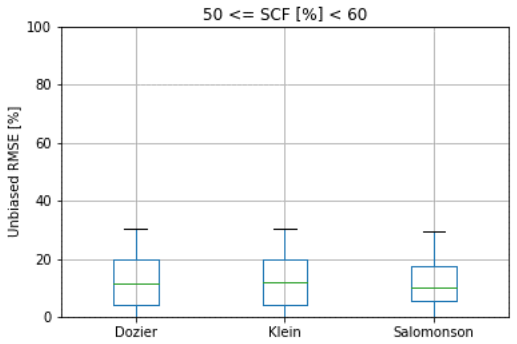
(g)	(r)
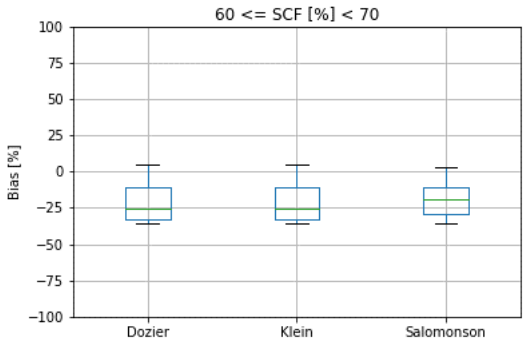	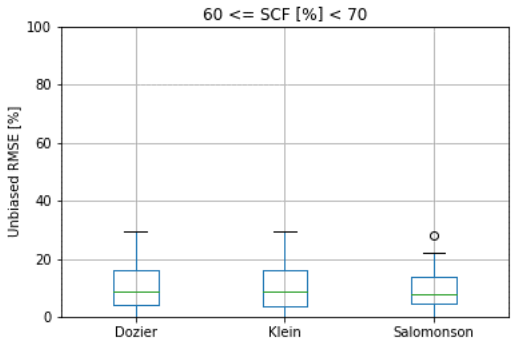
(h)	(s)

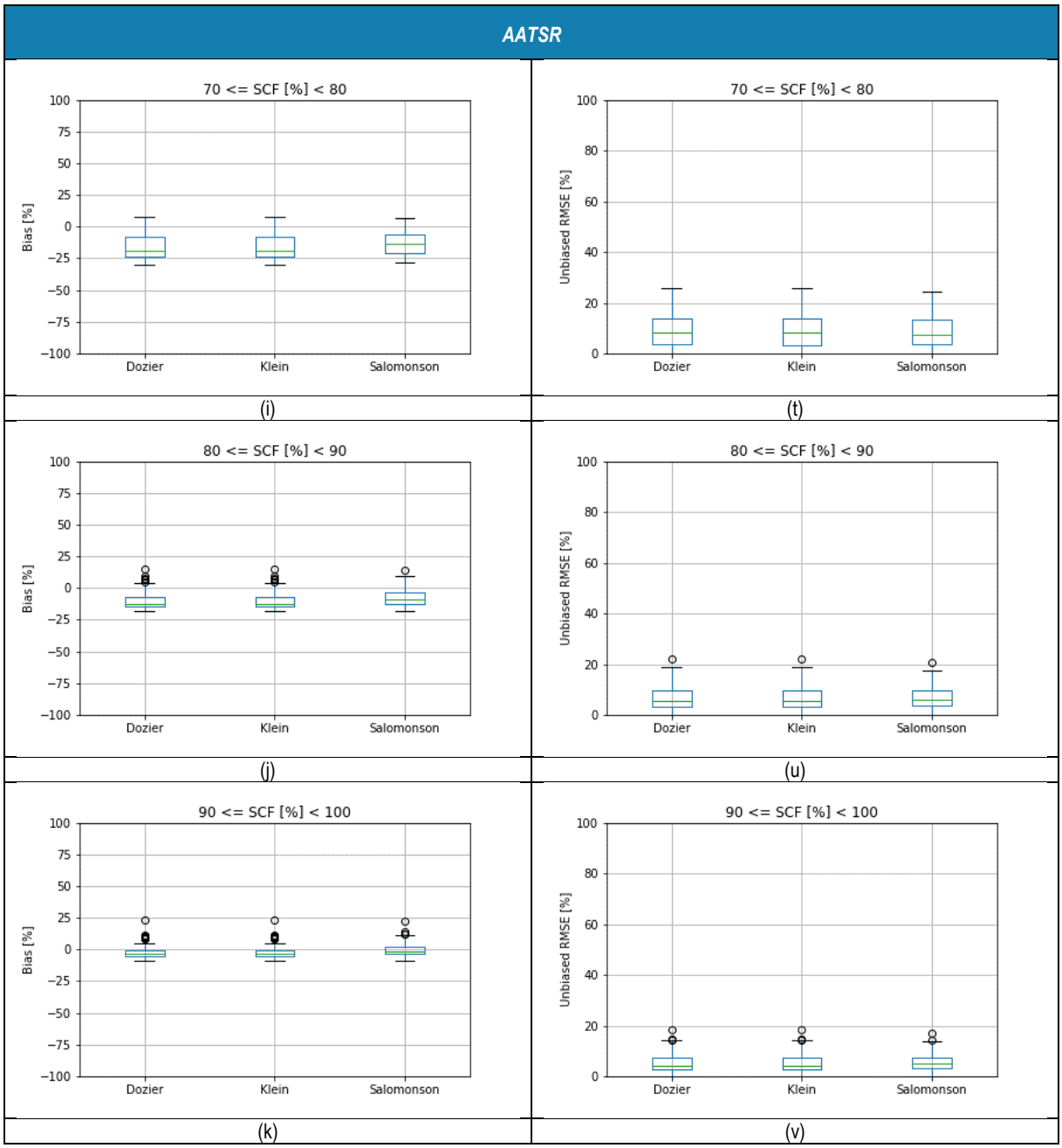

Figure 3.11: Bias (a)-(k) and unbiased RMSE (l)-(v) resulting from the validation of the **AATSR** based SCF products with SCF step of 10% in non-forested areas.

MODIS

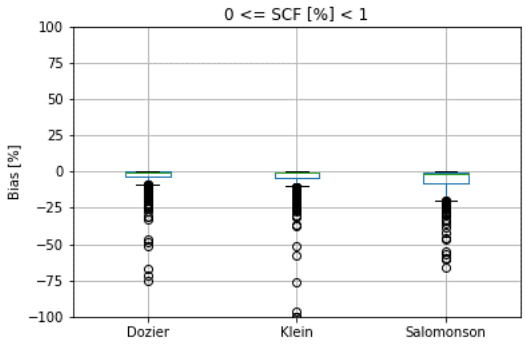

(a)

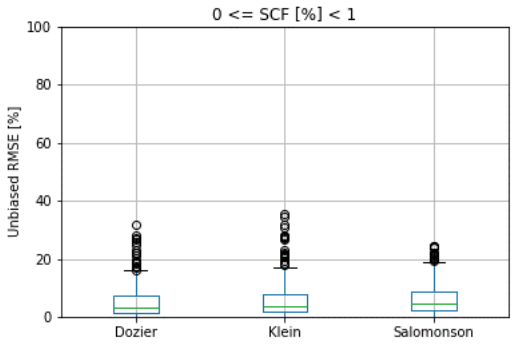

(l)

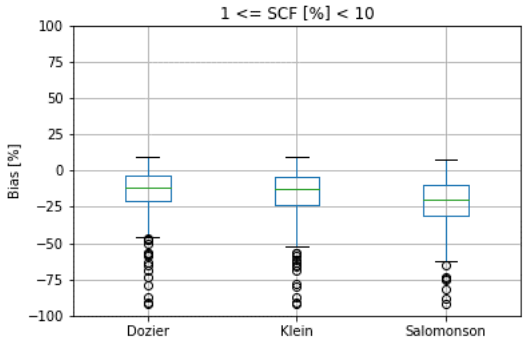

(b)

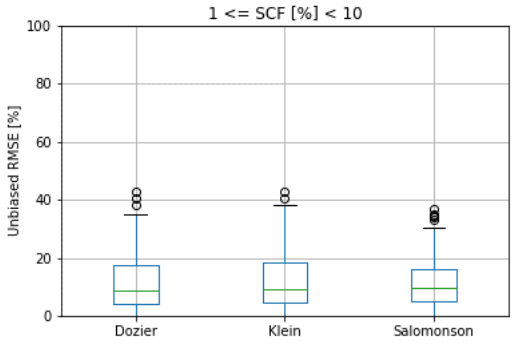

(m)

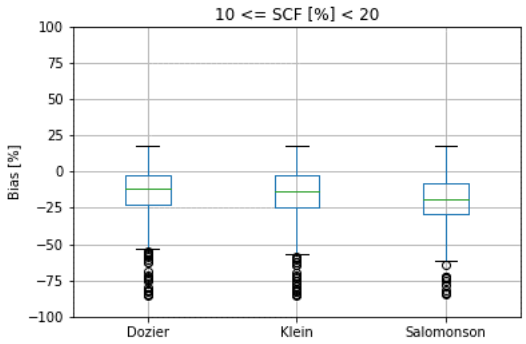

(c)

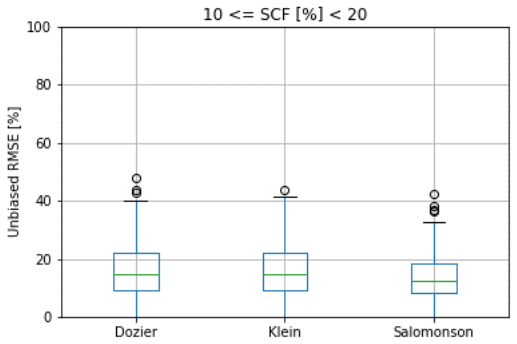

(n)

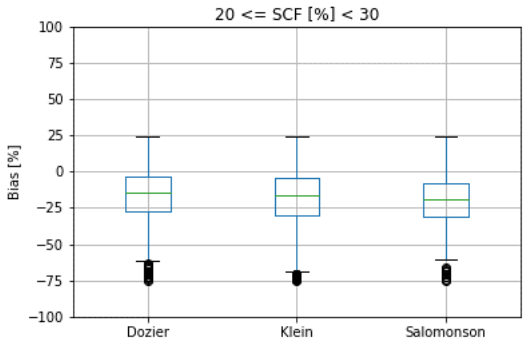

(d)

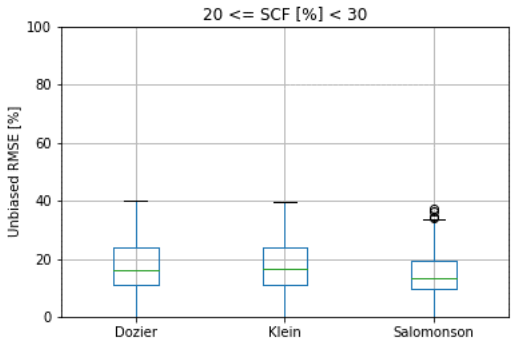

(o)

MODIS

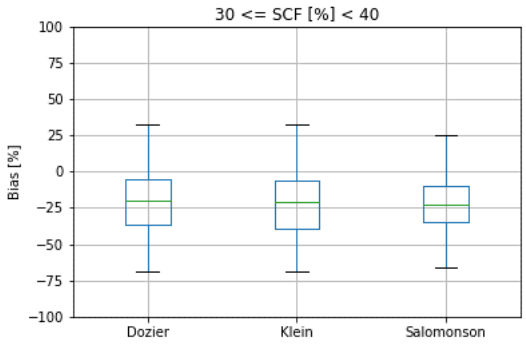

(e)

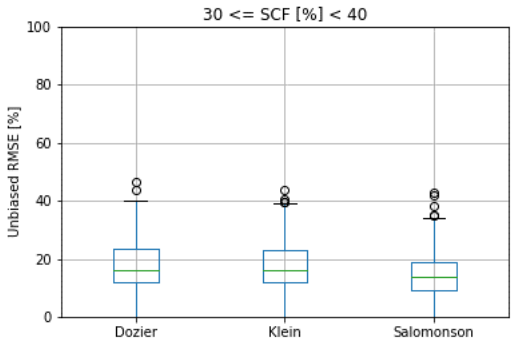

(p)

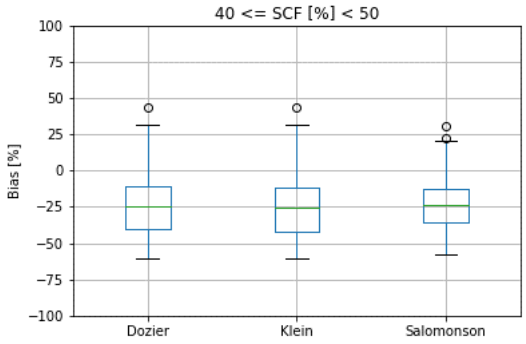

(f)

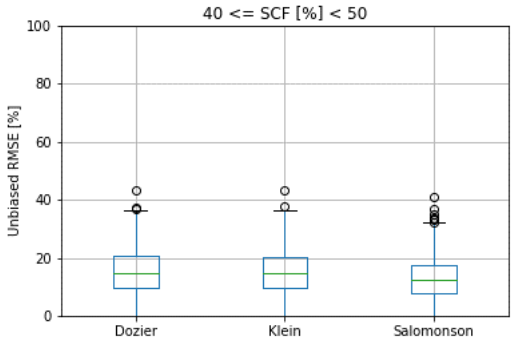

(q)

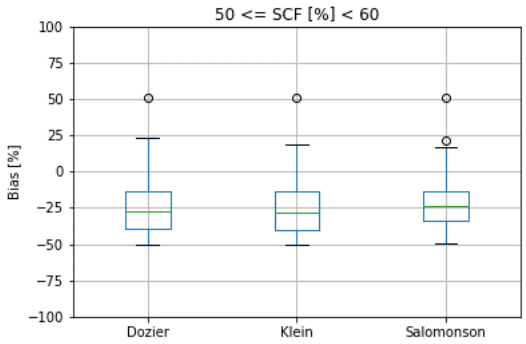

(g)

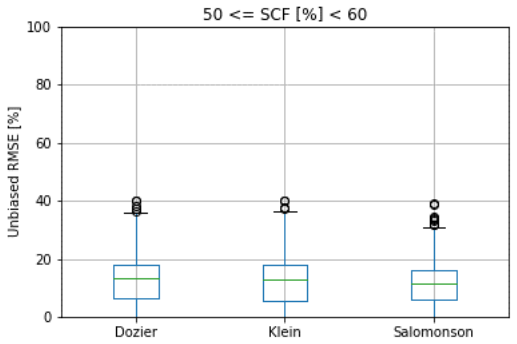

(r)

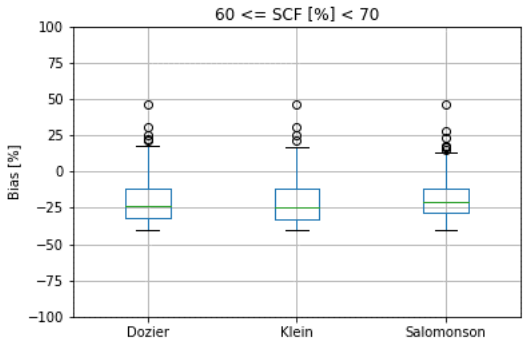

(h)

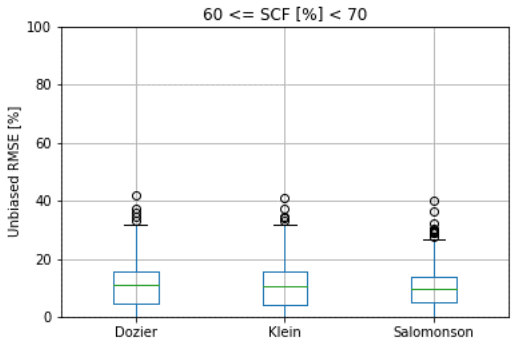

(s)

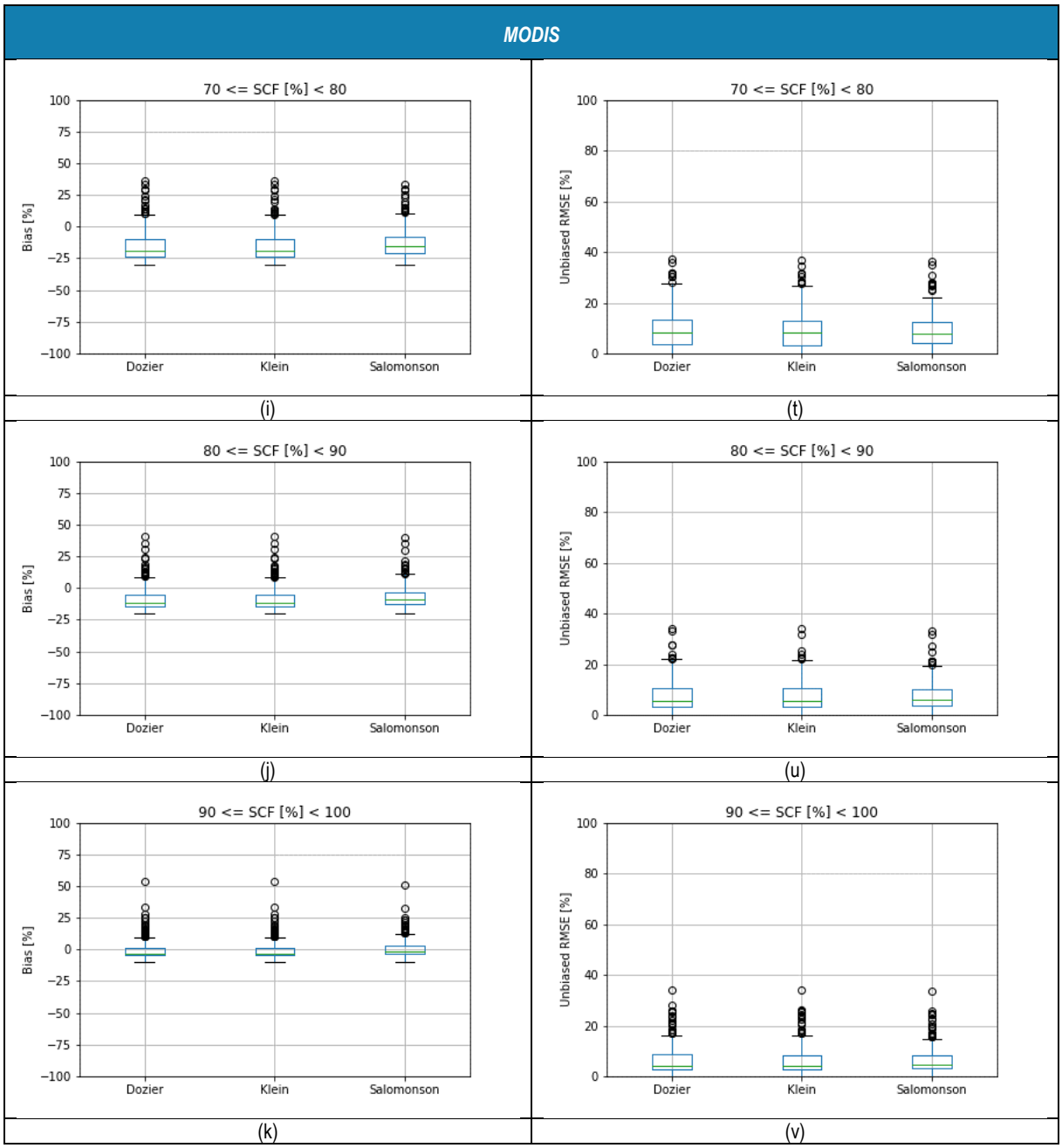

Figure 3.12: Bias (a)-(k) and unbiased RMSE (l)-(v) resulting from the validation of the **MODIS** based SCF products with SCF step of 10% in non-forested areas.

3.2.1. Comparison with high resolution snow maps from snow_cci Option 4

This section provides the detailed validation results derived from the pixel-by-pixel comparison of the *snow_cci* CRDP v3.0 SCF products with snow maps derived from high-resolution (HR) optical satellite data classified with the algorithm generated in the *snow_cci* Option 4 – High resolution snow mapping from Sentinel-2 and Landsat data. This reference data set of 65 images is composed of Landsat-5, Landsat-8, Landsat-9 and Sentinel-2 scenes, manually selected for their representativeness.

Figure 3.13: High-resolution images selected for *snow_cci* CRDP v3.0 SCF product validation using the Option 4 snow maps as reference.

The HR reference snow maps are obtained by merging the products obtained with the two different algorithms developed in the Option 4:

1) Multi-Spectral Unmixing with Locally Adaptive end-member selection (LAMSU) and

2) Snow extent applying a Flexible Learning Algorithm using KErnel-based Spectral unmixing (SnowFLAKES).

These two algorithms proved good capabilities in the identification of snow in challenging situations, such as cast shadowed areas with significantly reduced illumination conditions and in case of atmospheric disturbance. For the generation of the final reference snow maps, the results from both algorithms are combined. The technical details of the employed algorithms and the combination of the resulting products into one map per scene are described in the *snow_cci* Option 4 ATBD [RD-7]. The algorithms proved to have better performances than the state-of-the-art algorithms employed in the validation of the baseline product. Details on the accuracy of both new algorithms and of the combined reference snow product are provided in the *snow_cci* Option 4 PVIR [RD-8]. All validation results presented in the following and linked to *snow_cci* Option 4 refer to the combined reference snow products.

As in the previous cases, the reference snow maps are re-projected in the geographic map projection on WGS84 ellipsoid and aggregated to a fractional snow cover extent at the resolution of the *snow_cci*

SCE products (i.e., 0.01 degrees and 0.05 degrees). For describing the results of the pixel-by-pixel inter-comparison, the same statistical measures as before are used.

Table 3.22: Summary of the validation of the *snow_cci* products derived from **MODIS** considering the total areas of the 65 images of the validation dataset classified also with the *snow_cci* Option 4 algorithms. Results obtained for: a) SCFV and b) SCFG.

a) SCFV	*Salomonson*	*Klein*	*Dozier*	*Option 4*
RMSE	14.43	14.11	13.54	13.13
Unbiased RMSE	14.20	13.97	13.46	13.10
Bias	-2.57	-2.02	-1.46	0.97
Correlation Coefficient	0.95	0.95	0.96	0.97

b) ->SCFG	*Salomonson*	*Klein*	*Dozier*	*Option 4*
RMSE	12.11	12.33	12.51	17.92
Unbiased RMSE	12.04	12.30	12.45	17.54
Bias	-1.24	-0.94	-1.23	3.63
Correlation Coefficient	0.96	0.96	0.96	0.92

From the results reported in the Table 3.22, one can observe that overall if we compare the products of the *snow_cci* CRDP v3 to the *snow_cci* Option 4 reference snow maps, the results for the viewable snow outperform the other state of the art methods. Compared to the results with other reference snow products, the validation of the *snow_cci* CRDP v3 products with *snow_cci* Option 4 reference snow maps results in a lower bias in absolute value, but with a positive instead of a negative sign. This implies an overestimation of the snow in the *snow_cci* CRDP v3 products with respect to the *snow_cci* Option 4 reference snow maps. This may be due to the fact that the *snow_cci* Option 4 reference snow product show a high sensitivity to fractional snow, while the state-of-the-art methods tend to overestimate the snow coverage in such cases.

As the algorithm of Salomonson and Appel (2006), referred to as Salomonson in the following, the *snow_cci* Option 4 algorithm provides only information on the viewable snow. Table 3.23 presents thus only the comparison with the SCFV products. In forested areas, it is possible to notice how the RMSE and bias are reduced if compared with the Salomonson based reference snow maps in forest. The big negative bias of Salomonson (-7.38) is symptom of an overestimation of snow in forest. This method in fact is based on NDSI, which is very sensitive on the snow presence, and tend to overestimate the viewable snow in forest. On the other hand, the Option 4 reference snow maps show a better agreement with the *snow_cci* CRDP v3 SCFV product, with metrics aligned with the global case. Taking a look instead at the values in open areas, the metrics of all the methods are aligned to the same values, with the Option 4 method still presenting a positive bias in opposition to the others.

Table 3.23: Summary of the validation of the *snow_cci* products derived from **MODIS** considering the 65 images of the validation dataset classified also with the Option 4 algorithm separating forest from open areas. Results obtained for SCV.

SCFV	*Salomonson forested*	*Salomonson open areas*	*Dozier open areas*	*Klein open areas*	*Option 4 forested*	*Option 4 open areas*
RMSE	20.76	12.10	12.33	12.50	14.184	12.73
Unbiased RMSE	19.40	12.04	12.30	12.45	14.183	12.67
Bias	-7.38	-1.24	-0.94	-1.23	0.20	1.25
Correlation Coefficient	0.89	0.96	0.97	0.96	0.92	0.96

3.3. Comparison with other SCE products

We compared the *snow_cci* maps with the MOD10C1 v5 (Hall and Riggs, 2021). This global data set provides the percentage of snow-covered land and cloud-covered land observed daily, within 0.05° (approx. 5 km) MODIS Climate Modeling Grid (CMG) cells. Percentages are computed from snow cover observations in the MODIS/Terra Snow Cover Daily L3 Global 500m data set. According to the PVP [RD-1] the *snow_cci* dataset are aggregated at the resolution of MOD10C1 and intercompared. The results obtained in terms of bias and unbiased RMSE for MODIS, AVHRR and AATSR stratified for global, open, forested areas, unforested areas, mountains areas, plain areas, Northern and Southern hemisphere are reported in Figure 3.14 to Figure 3.19.

MODIS- and AATSR-based *snow_cci* products present low bias and unbiased RMSE for all the selected categories when compared to MOD10C1, indicating a general good agreement between the products. Interestingly, the comparison is better for SCFG than for SCFV *snow_cci* products.

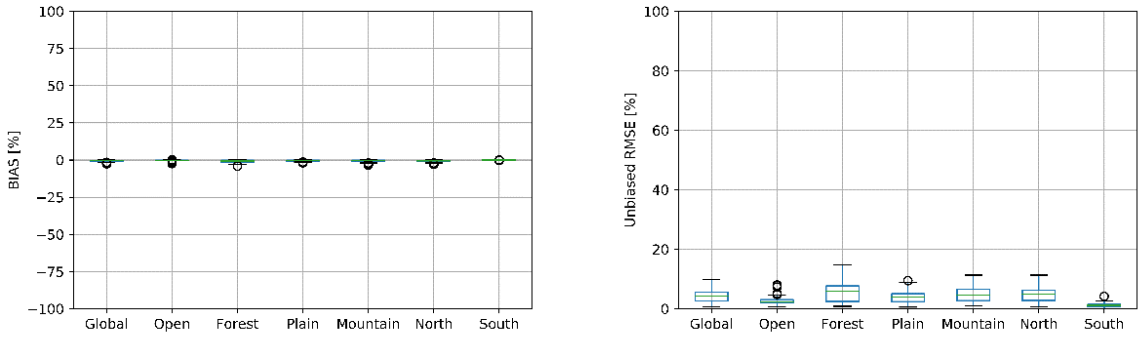

(a) (b)

Figure 3.14: Intercomparison between **MOD10C1** and ***snow_cci* MODIS**-based SCFG. (a) bias; and (b) Unbiased RMSE.

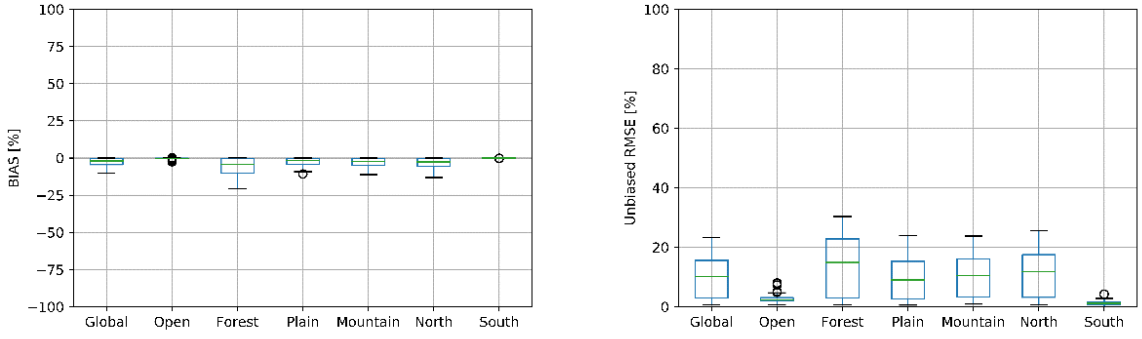

(a) (b)

Figure 3.15: Intercomparison between **MOD10C1** and ***snow_cci*** **MODIS**-based SCFV. (a) bias; and (b) Unbiased RMSE.

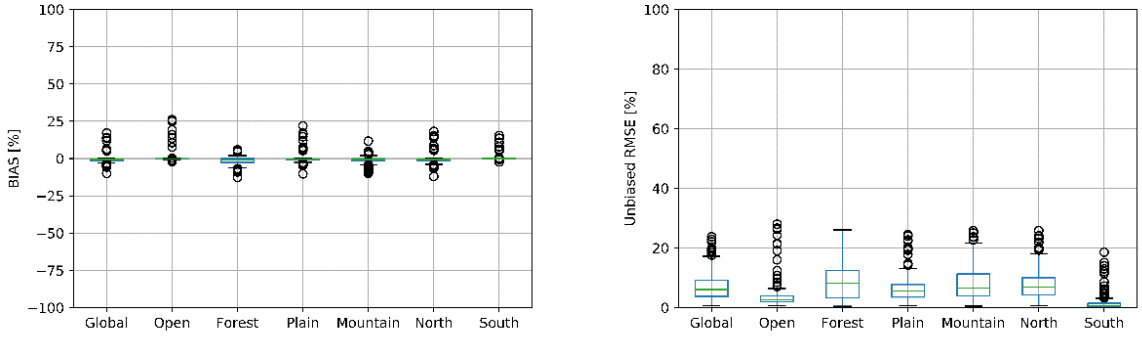

(a) (b)

Figure 3.16: Intercomparison between **MOD10C1** and ***snow_cci*** **AATSR**-based SCFG. (a) bias; and (b) Unbiased RMSE.

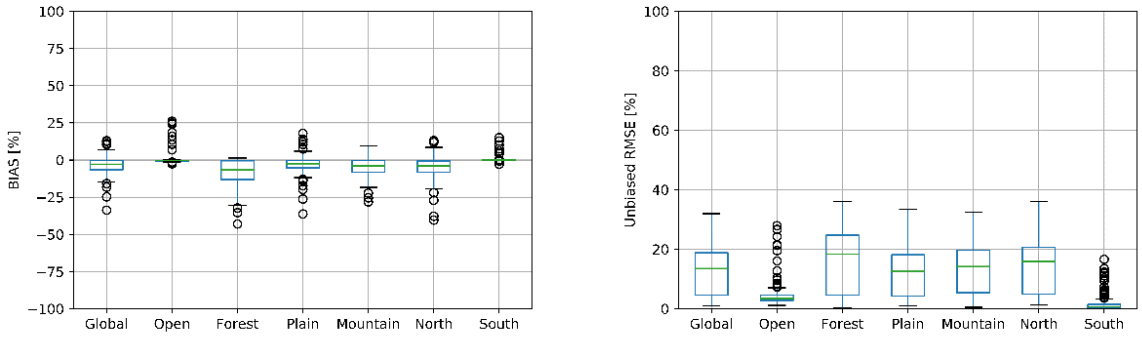

(a) (b)

Figure 3.17: Intercomparison between **MOD10C1** and ***snow_cci*** **AATSR**-based SCFV. (a) bias; and (b) Unbiased RMSE.

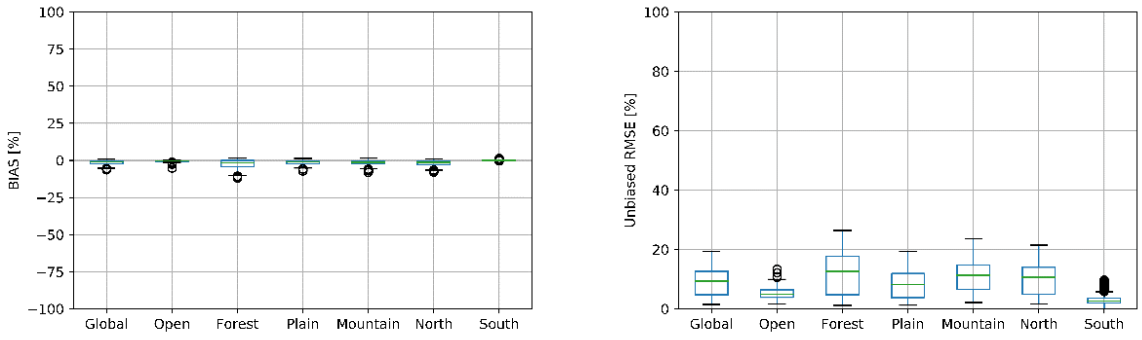

(a) (b)

Figure 3.18: Intercomparison between **MOD10C1** and ***snow_cci* AVHRR**-based SCFG. (a) bias; and (b) Unbiased RMSE.

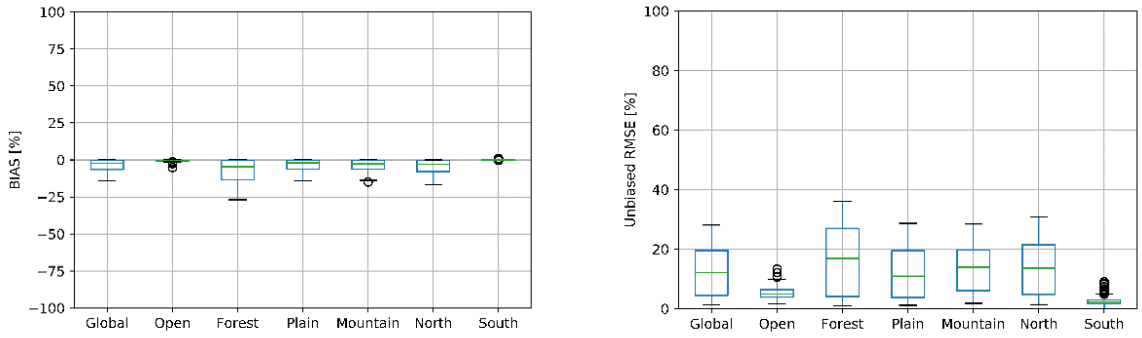

(a) (b)

Figure 3.19: Intercomparison between **MOD10C1** and ***snow_cci AVHRR***-based SCFV. (a) bias; and (b) Unbiased RMSE.

In order to better analyse the agreement among the products we consider the bias and unbiased RMSE calculated for SCF steps of 10% in open areas in Figure 3.20, Figure 3.21 and Figure 3.22. The agreement is high for low and high SCF values, whereas the products tend to disagree more on the intermediate values of SCF.

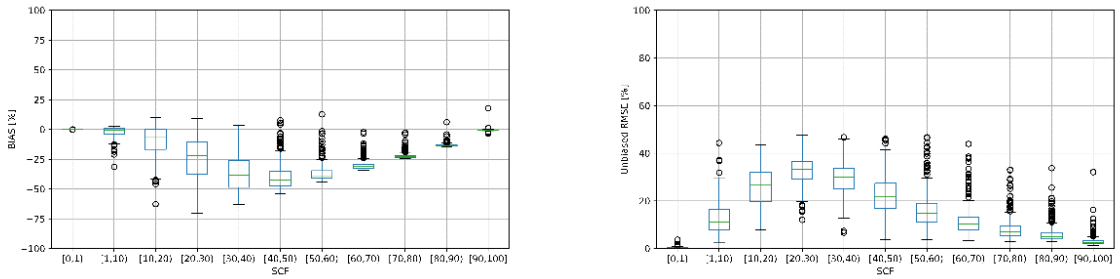

(a) (b)

Figure 3.20: Intercomparison between **MOD10C1** and ***snow_cci* MODIS**-based in open areas. (a) bias; and (b) Unbiased RMSE.

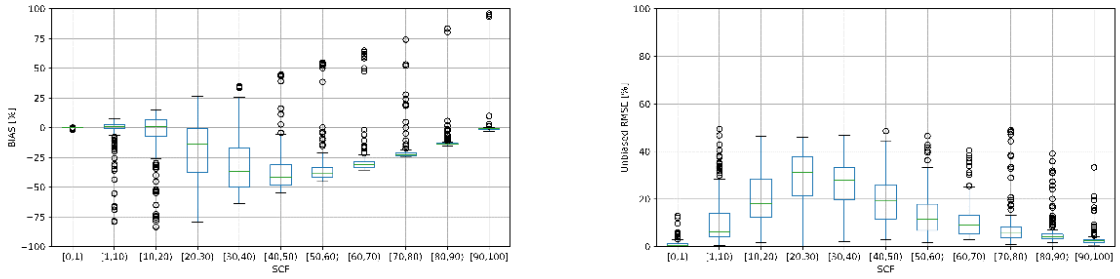

(a) (b)

Figure 3.21: Intercomparison between **MOD10C1** and ***snow_cci*** **AATSR**-based in open areas. (a) bias; and (b) Unbiased RMSE.

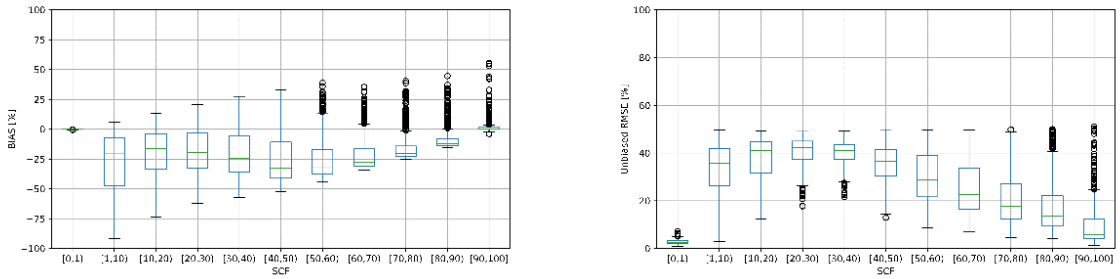

(a) (b)

Figure 3.22: Intercomparison between **MOD10C1** and ***snow_cci*** **AVHRR**-based in open areas. (a) bias; and (b) Unbiased RMSE.

3.4. Validation of the uncertainty

The validation activity for the uncertainty have been started by comparing the estimation provided at the pixel level with the absolute error identified by comparing the reference HR snow maps with the *snow_cci* products for both, SCFG and SCFV. This has been done for all the non-forested areas and considering global and discretised SCF with a step of 10% SCF. The results of the validation reflect the ability of the provided uncertainty layer to estimate the quality of the detection of the *snow_cci* products. The metrics used for evaluating how close is the uncertainty to the absolute error are the bias and the RMSE.

Table 3.24: Summary of the validation of the uncertainty of the *snow_cci* products derived from **MODIS** considering 705 Landsat images of the validation dataset (non-forested areas only).

	Salomonson	***Klein***	***Dozier***
RMSE	11.03	11.76	11.41
Bias	1.37	1.67	1.80

Table 3.25: Summary of the validation of the uncertainty of the *snow_cci* products derived from **AATSR** considering 192 Landsat images of the validation dataset (non-forested areas only).

	Salomonson	*Klein*	*Dozier*
RMSE	9.98	10.27	10.26
Bias	0.75	1.45	1.47

Table 3.26: Summary of the validation of the uncertainty of the *snow_cci* products derived from **AVHRR** considering 1050 Landsat images of the validation dataset (non-forested areas only).

	Salomonson	*Klein*	*Dozier*
RMSE	12.48	12.50	12.50
Bias	-0.25	-0.32	-0.32

The statistical measures unbiased RMSE and bias resulting from the validation of the *snow_cci* SCF uncertainty with snow maps generated by Dozier, Klein and Salomonson approaches from Landsat scenes are illustrated in the plots of Figure 3.23, Figure 3.24 and Figure 3.25 for MODIS, AATSR and AVHRR, respectively. No temporal trends are visible (for AVHRR, the series has several snow free images acquired from 1991 to 2000). However, it heralds the considerations drawn in the next paragraph by considering steps of SCF.

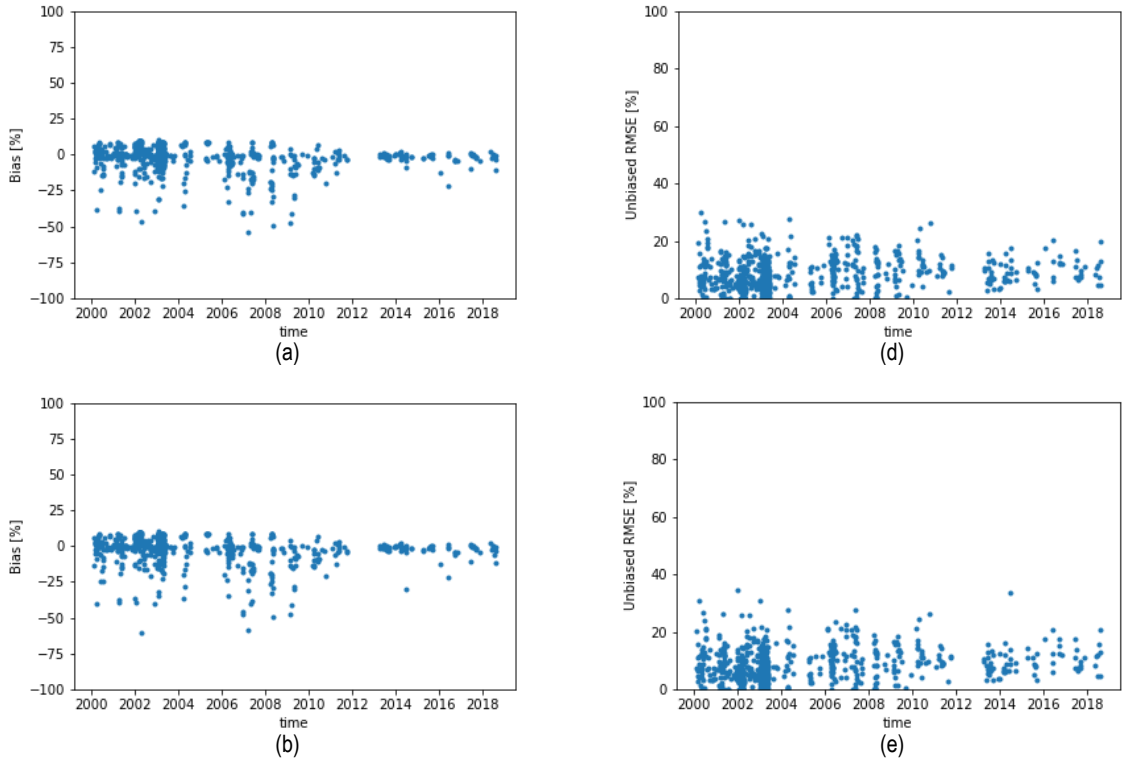

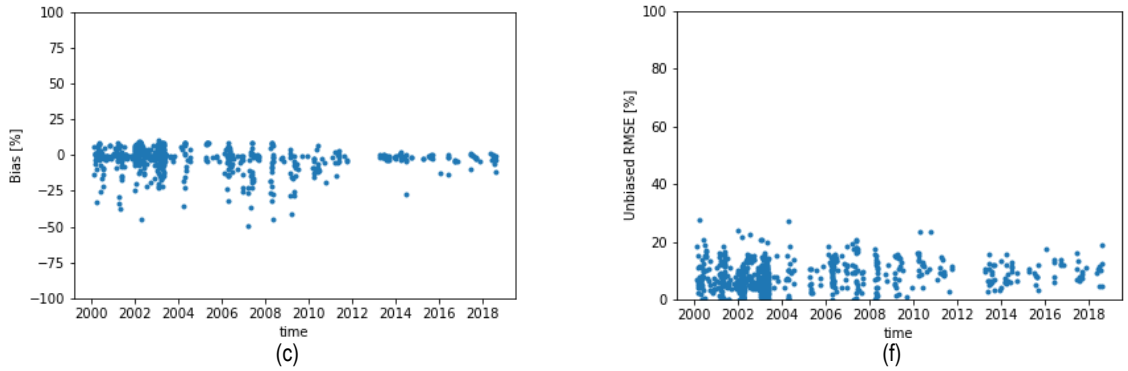

Figure 3.23: (a)-(c) Bias and (d)-(f) unbiased RMSE resulting from the validation of the *snow_cci* SCF product uncertainties derived from **MODIS** with snow maps generated by Dozier, Klein and Salomonson.

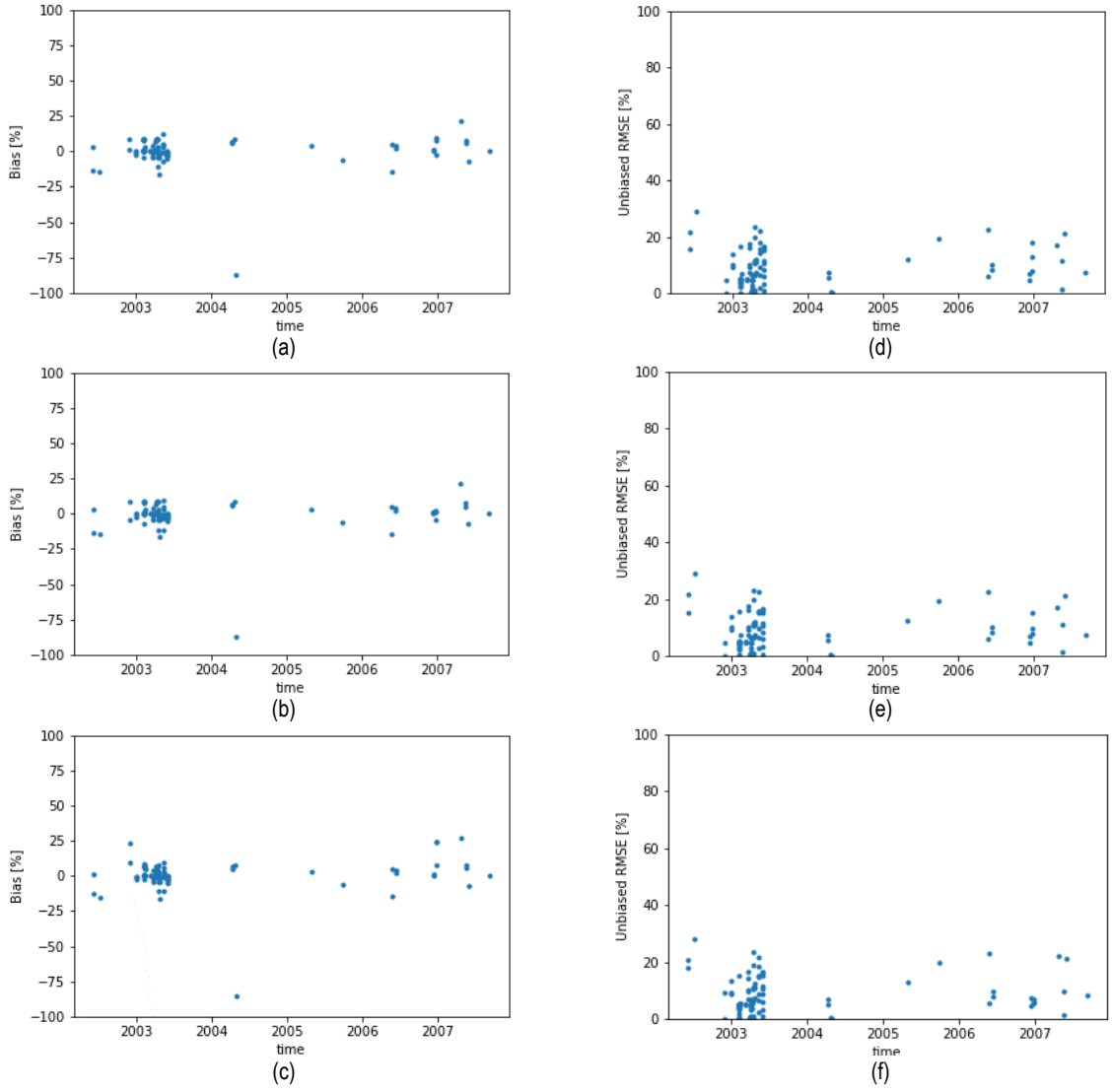

Figure 3.24: (a)-(c) Bias and (d)-(f) unbiased RMSE resulting from the validation of the *snow_cci* SCF product uncertainties derived from **AATSR** with snow maps generated by Dozier, Klein and Salomonson.

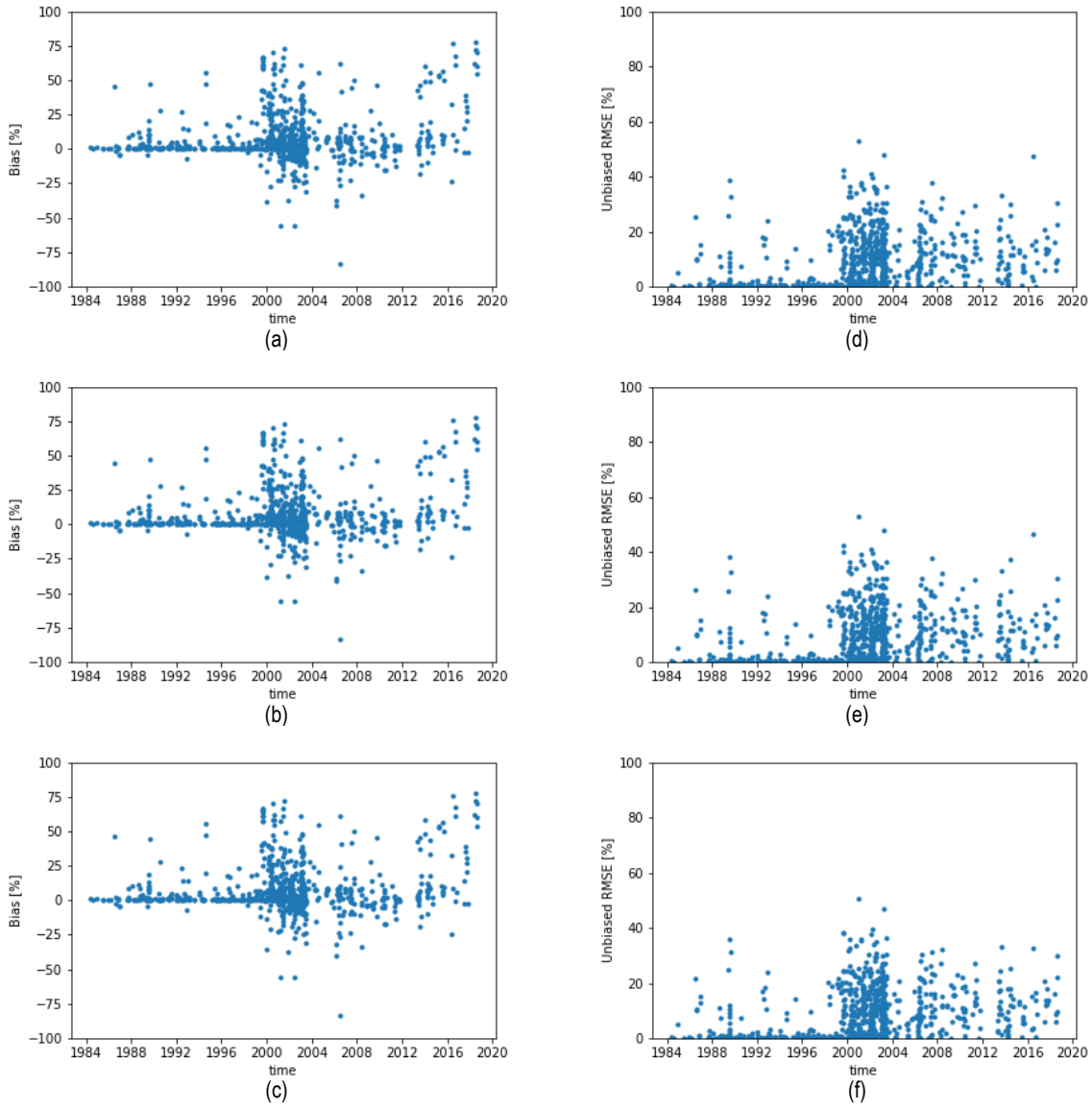

Figure 3.25: (a)-(c) Bias and (d)-(f) unbiased RMSE resulting from the validation of the *snow_cci* SCF product uncertainties derived from **AVHRR** with snow maps generated by Dozier, Klein and Salomonson.

By quantizing the *snow_cci* SCF with steps of 10%, a negative bias is still visible for MODIS- and AVHRR derived maps whereas a positive for AASTR-based maps for intermediate vales. Figure 3.26, Figure 3.27 and Figure 3.28 show also that the uncertainty estimation for higher and low SCF values is more accurate than intermediate values. The lowest errors are identifiable for snow free i.e., SCF equal to 0% and complete snow covered i.e., SCF equal to 100%. The high presence of outliers needs to be further investigated especially in snow free and 100% snow cover.

MODIS	
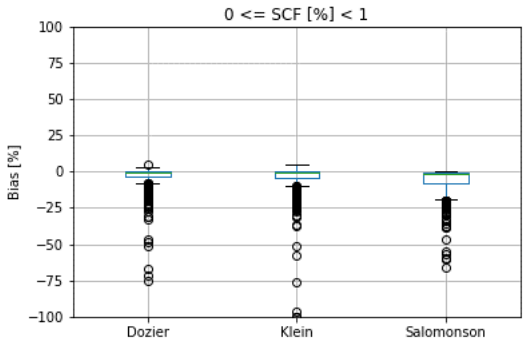	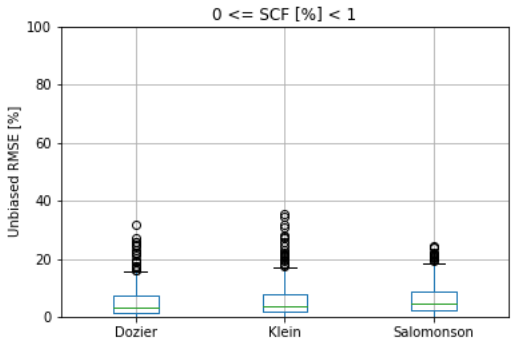
(a)	(l)
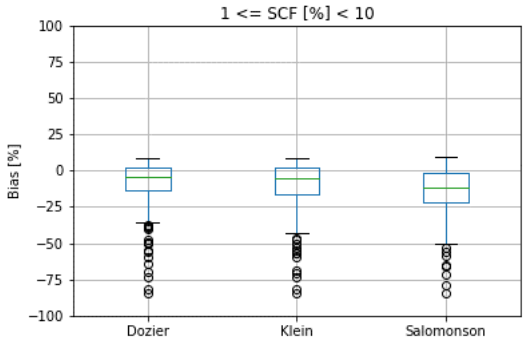	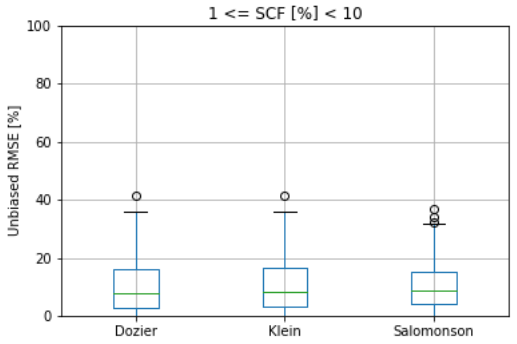
(b)	(m)
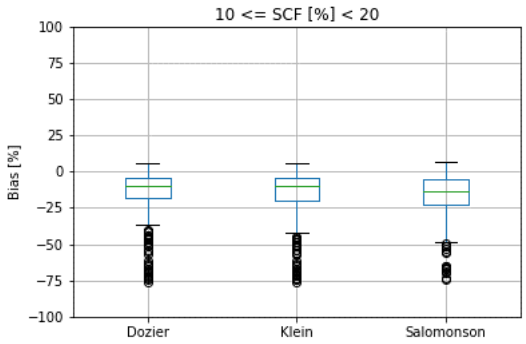	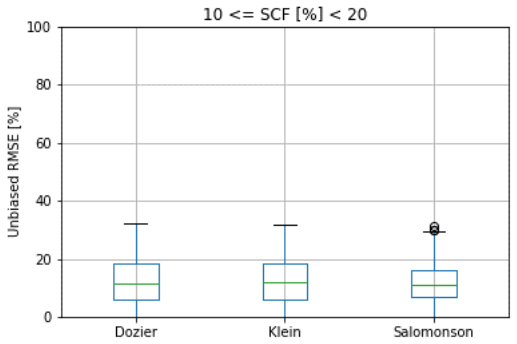
(c)	(n)
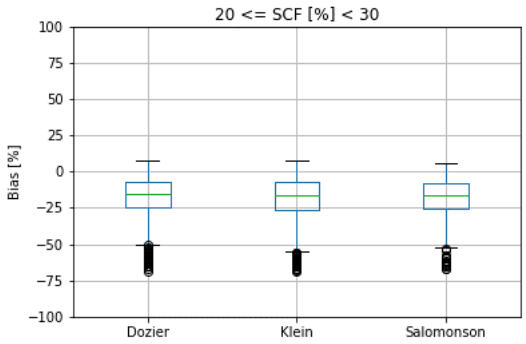	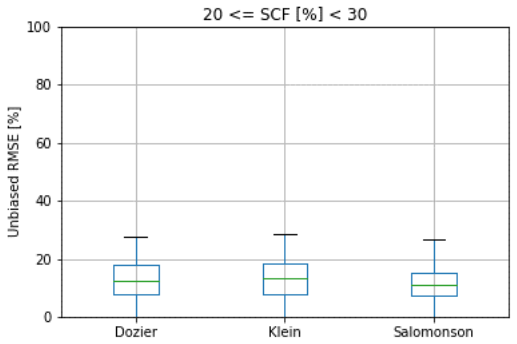
(d)	(o)

MODIS	
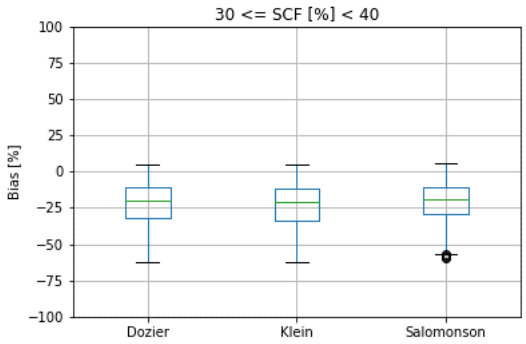	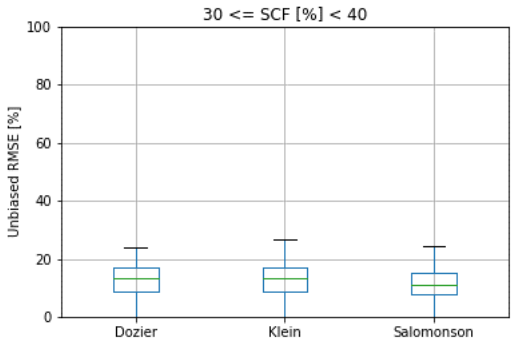
(e)	(p)
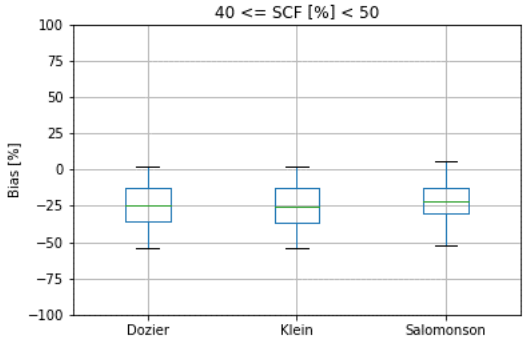	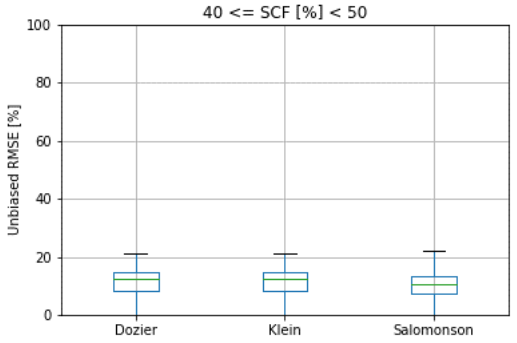
(f)	(q)
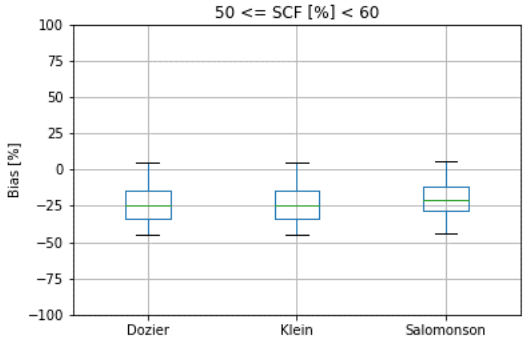	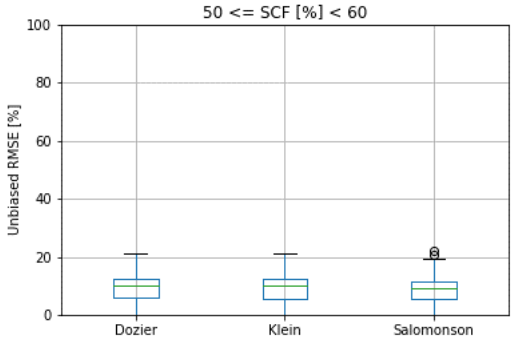
(g)	(r)
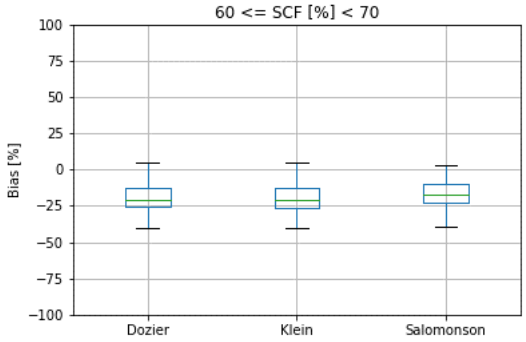	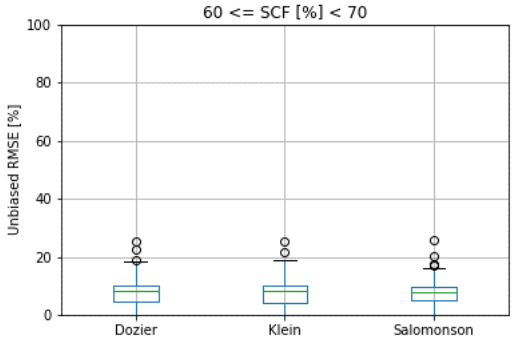
(h)	(s)

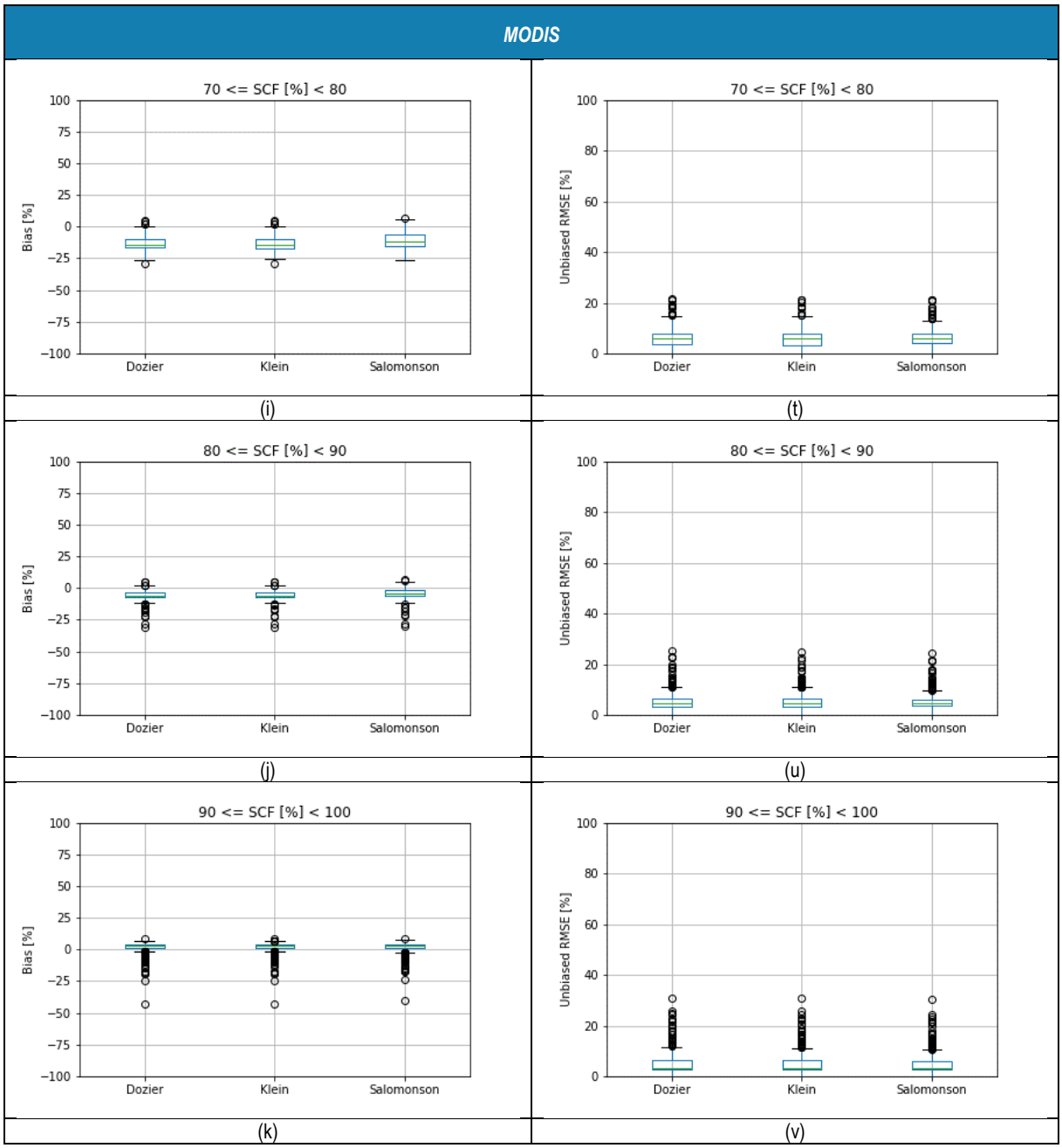

Figure 3.26: Bias (a)-(k) and unbiased RMSE (l)-(v) resulting from the validation of the **MODIS uncertainties** with SCF step of 10% in non-forested areas.

AATSR	
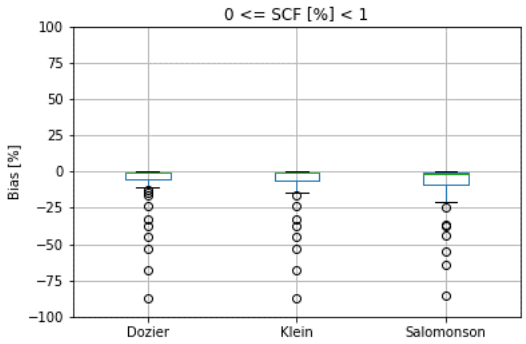	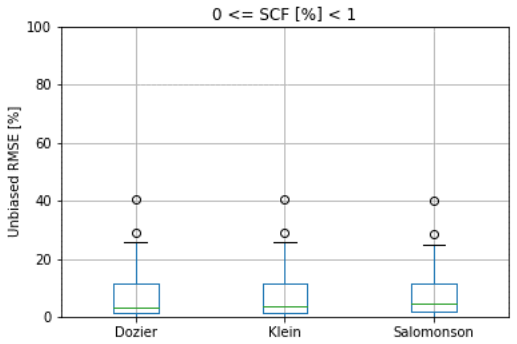
(a)	(l)
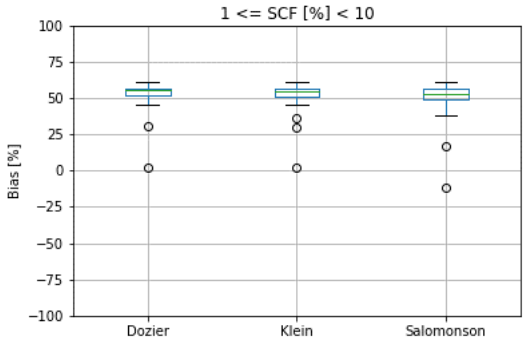	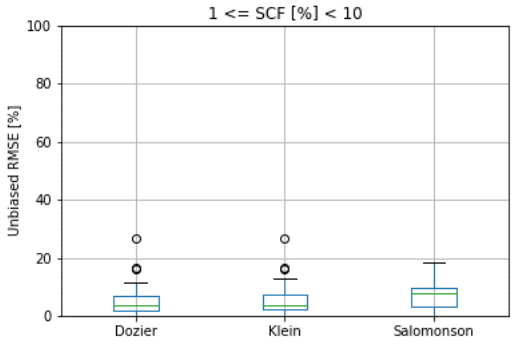
(b)	(m)
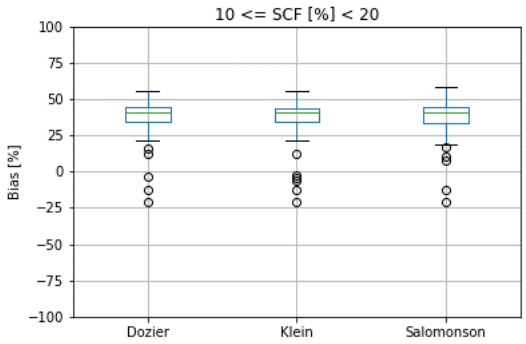	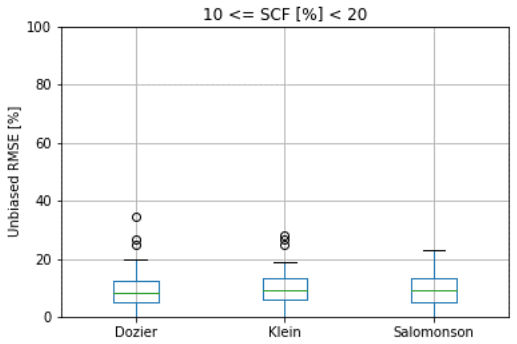
(c)	(n)
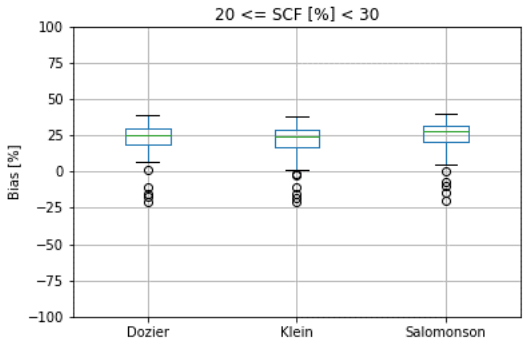	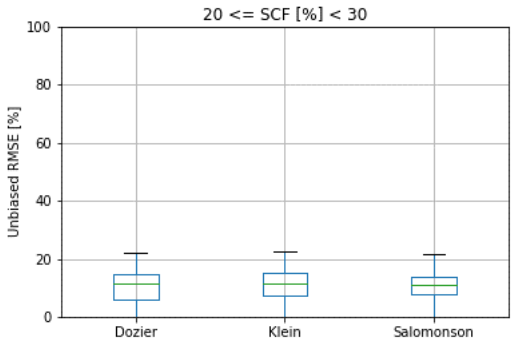
(d)	(o)

AATSR	
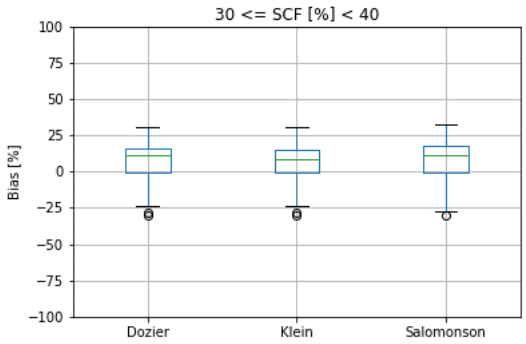	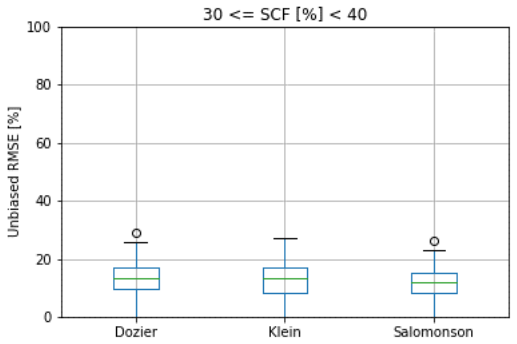
(e)	(p)
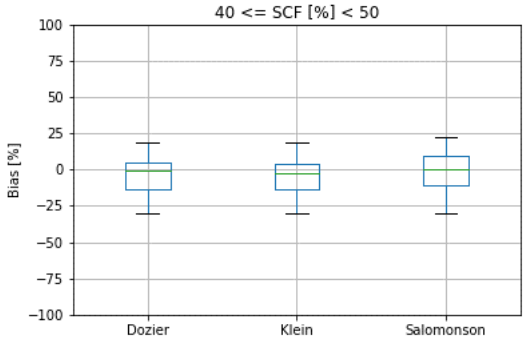	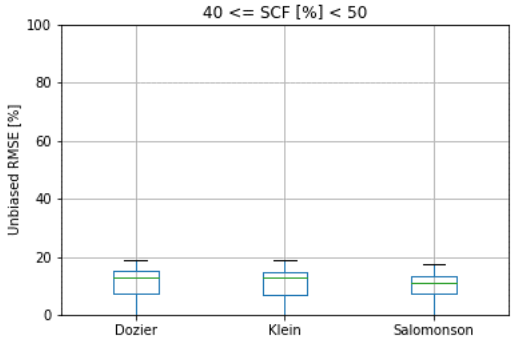
(f)	(q)
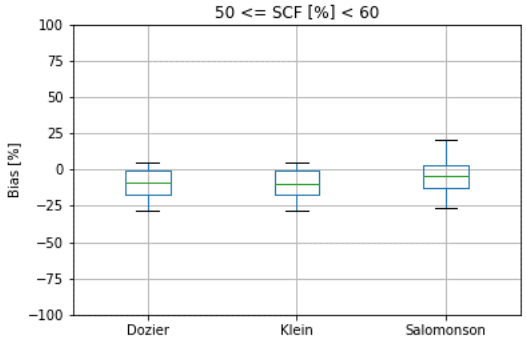	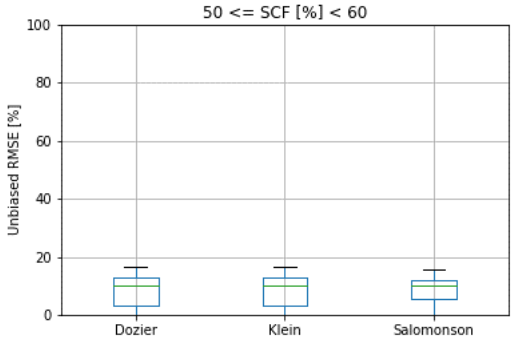
(g)	(r)
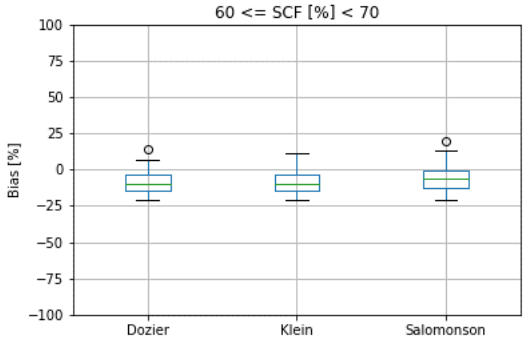	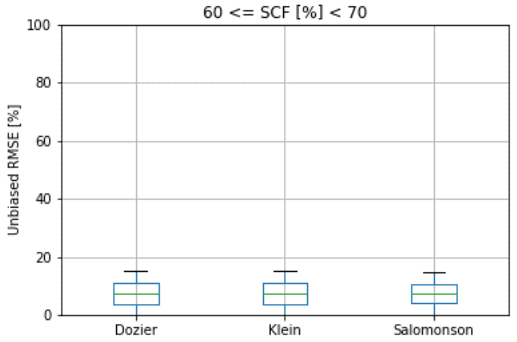
(h)	(s)

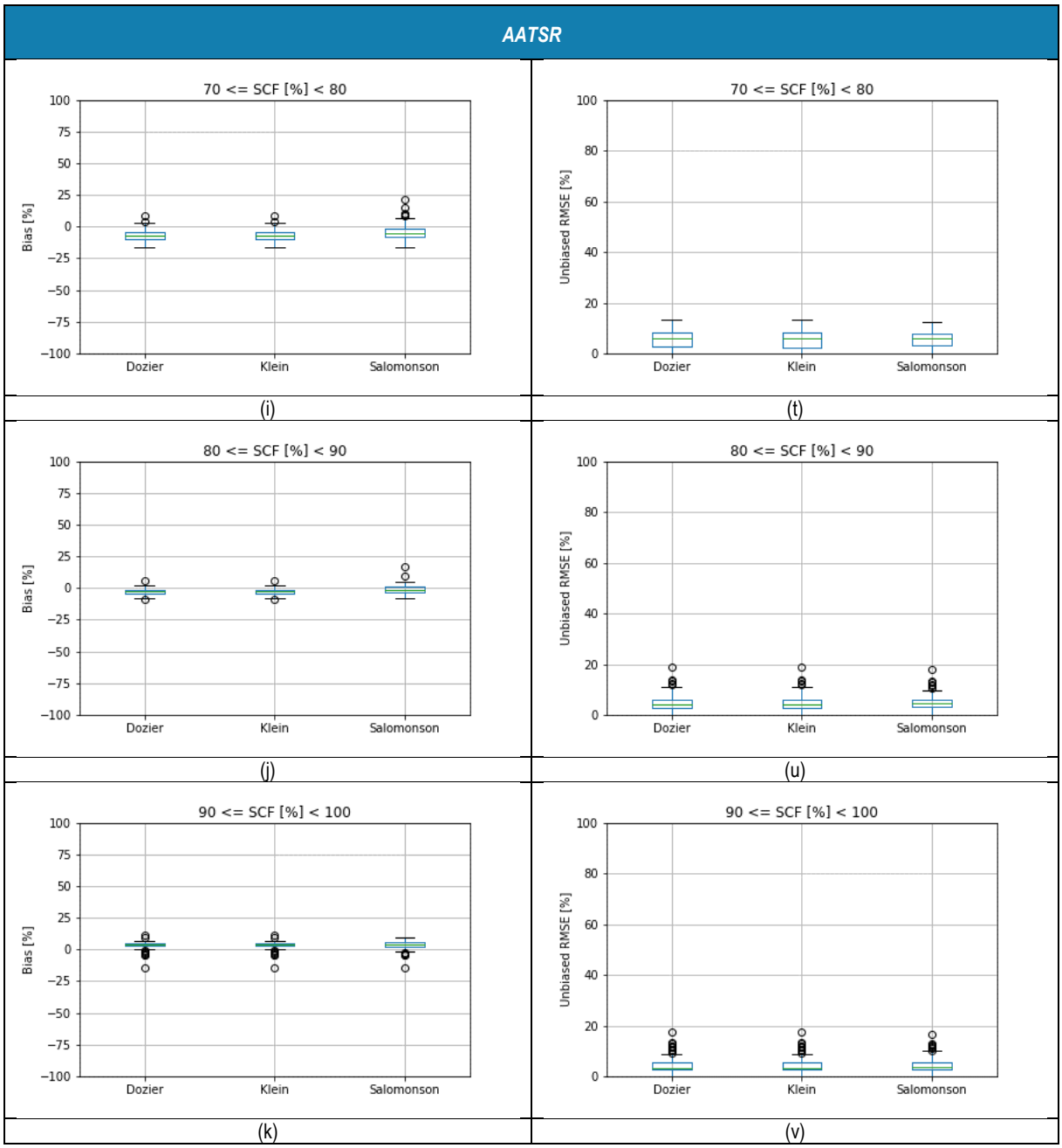

Figure 3.27: Bias (a)-(k) and unbiased RMSE (l)-(v) resulting from the validation of the **AATSR uncertainties** with SCF step of 10% in non-forested areas.

AVHRR	
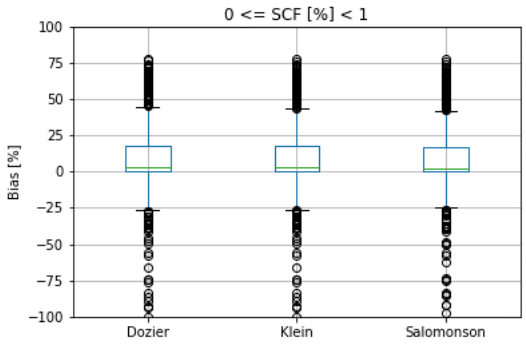	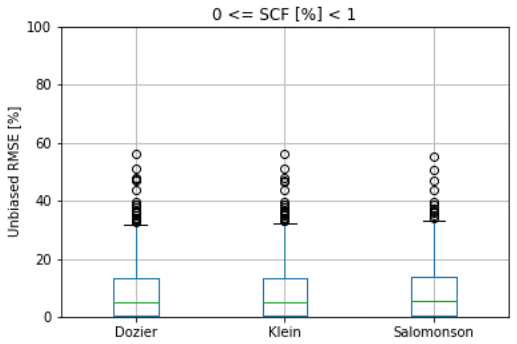
(a)	(l)
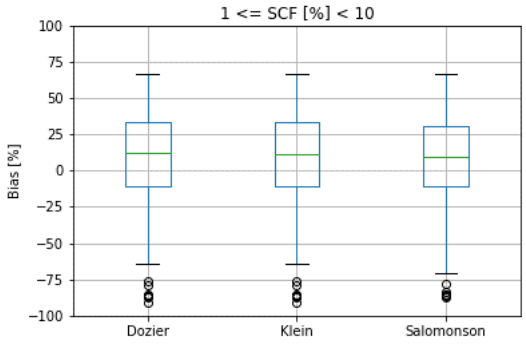	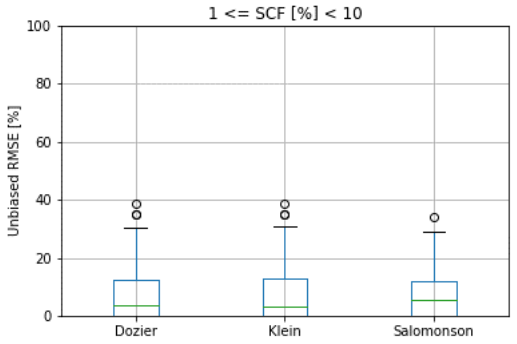
(b)	(m)
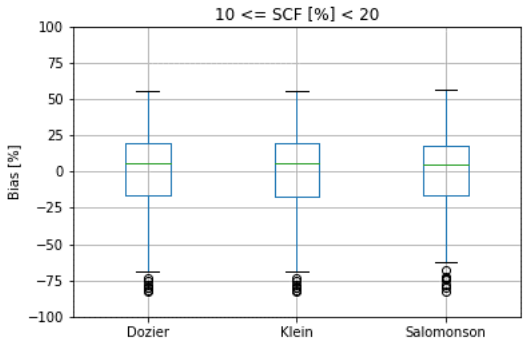	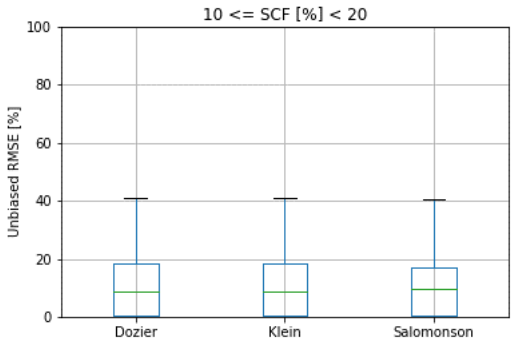
(c)	(n)
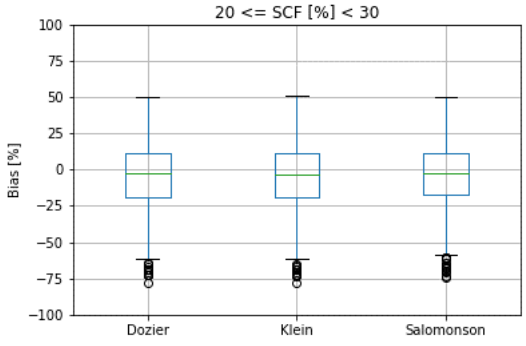	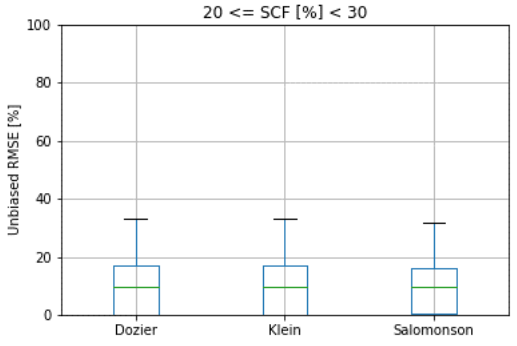
(d)	(o)

AVHRR	
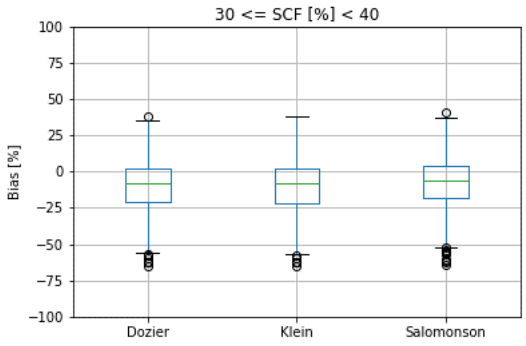	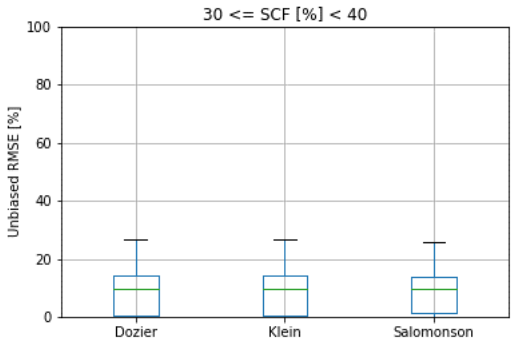
(e)	(p)
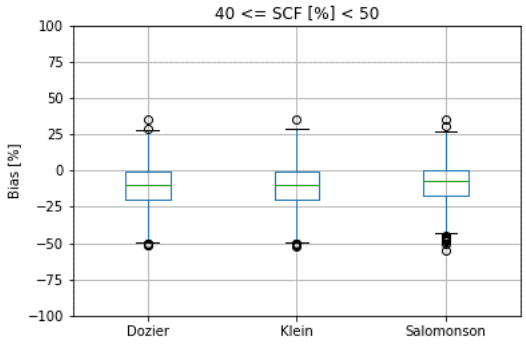	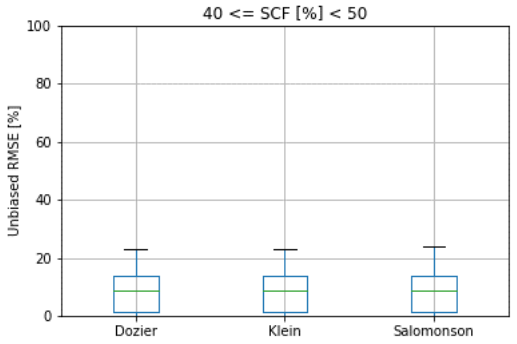
(f)	(q)
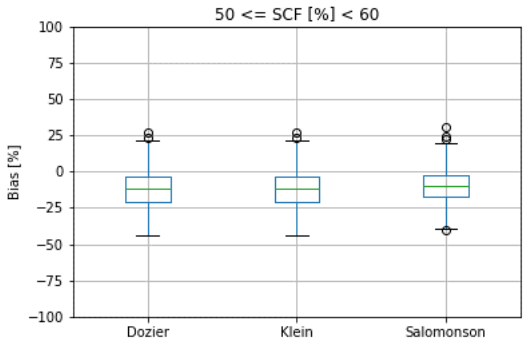	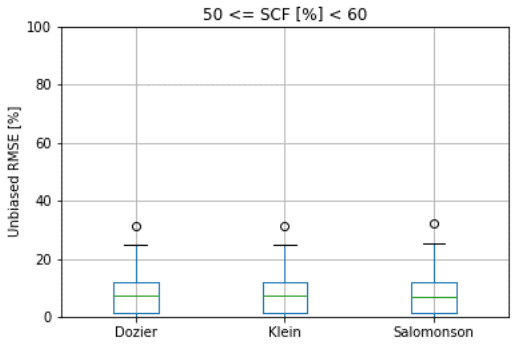
(g)	(r)
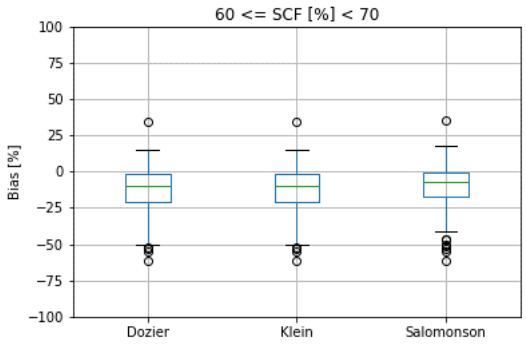	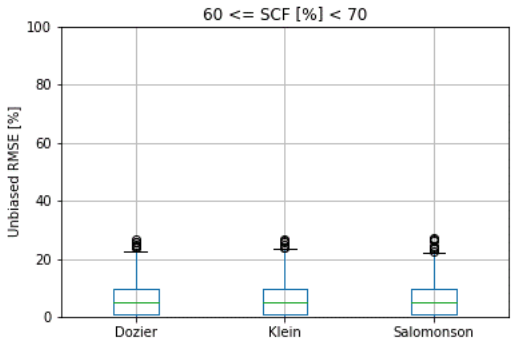
(h)	(s)

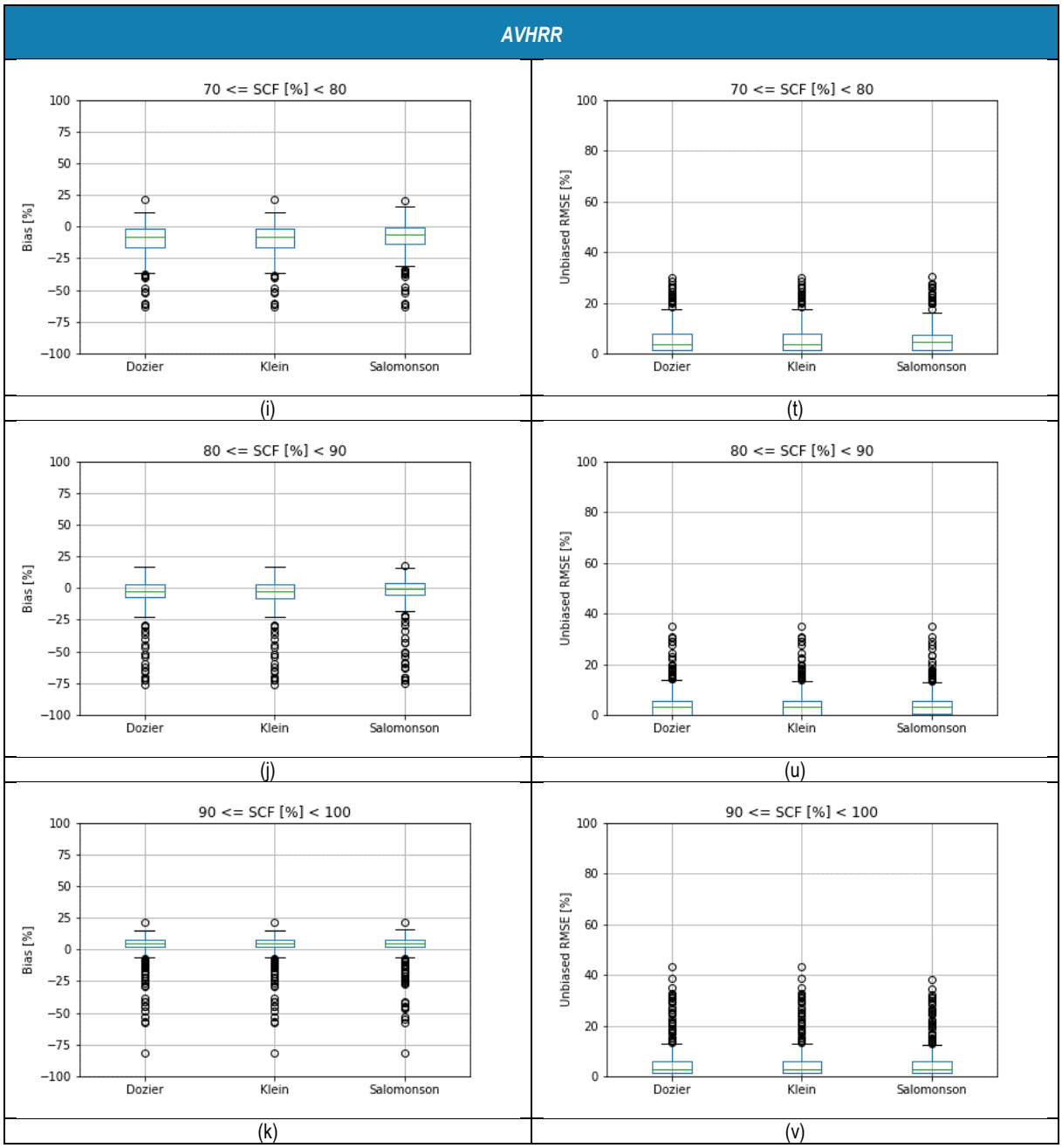

Figure 3.28: Bias (a)-(k) and unbiased RMSE (l)-(v) resulting from the validation of the **AVHHR uncertainties** with SCF step of 10% in non-forested areas.

4. VALIDATION RESULTS FOR SNOW WATER EQUIVALENT

4.1. Overview of algorithm modifications and validation procedure

The *snow_cci* SWE CRDP v3 was assessed according to the product validation plan [RD-2], key parts of which are detailed below. The evaluation consists of validation based on in situ snow courses (Figure 4.1), and intercomparison of the monthly Northern Hemisphere climatological snow mass with other products from land surface and snow models driven by reanalysis.

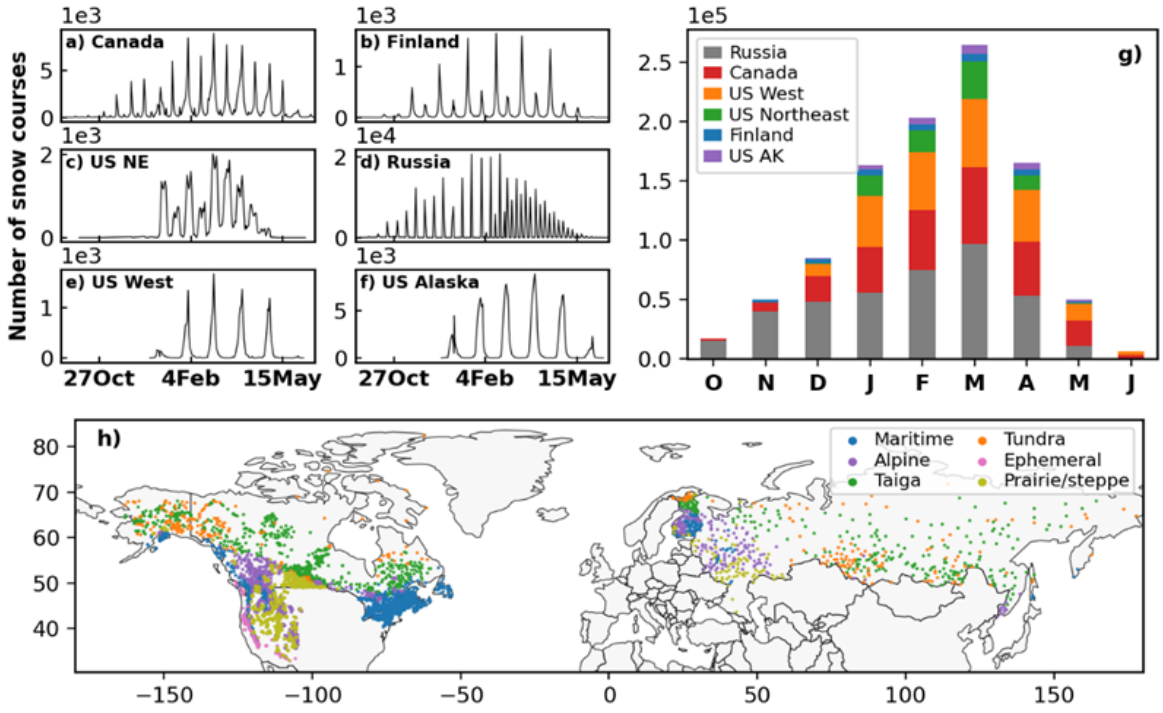

Figure 4.1: Reference snow course data distribution in time (panels a through g) and space (panel h). (From Mortimer et al. 2022).

Validation: For quality assurance purposes, records with bulk snow density outside the range 0.025–0.700 kg m-3 were removed (Brown et al., 2019; Vionnet et al., 2021). Measurement values of zero were excluded from both the snow course dataset and the *snow_cci* SWE retrievals because zero values are not reported in a consistent manner across the snow course datasets. A temporally consistent subset of data is used when assessing the stability of the validation statistics over the full time period where grid cells must have reference measurements from (1) at least two years during each decade (defined as: 1979–1988, 1989–1998, 1999–2008 and 2009–2018) and (2) at least twenty years during the entire 1979–2018 period. This temporal subset was not used for analysis of the development products which were only produced for 10yr test periods (2000-2009). Evaluations were conducted separately for SWE up to 150 mm and SWE up to 500 mm for the months November through May. When comparing multiple products only dates and locations common to all products are included in the calculations.

Intercomparison: Daily SWE fields were produced during the 1981–1987 SMMR period by linearly interpolating missing fields between days with available SWE (every other day during SMMR period). Monthly SWE climatologies were then calculated across the 1980/81–2017/18 snow seasons (September–June) and re-gridded to a common regular 0.5° x 0.5° grid. Climatological daily snow mass was aggregated from the daily SWE fields on the respective product grids over the same period.

The effect of algorithm modifications outlined in [RD-2] and [RD-3] on SWE estimates was assessed as systematically as possible using a series of developmental products where, ideally, only one element is altered at a time. The production plan is provided in the PVP is reproduced here (Table 4.1). *snow_cci* SWE CRDP v2 is the baseline product. Compared to *snow_cci* SWE CRDP v1, it includes a correction for snow density in post processing (Venäläinen et al. 2021), is produced at a higher spatial resolution (0.1° vs 0.25°) and uses updated PMW data from the NADA MEaSUREs Calibrated Passive Microwave Science Data Record enhanced resolution rSIR (Brodzik et al., 2016). The impact of algorithm changes from *snow_cci* SWE CRDP v1 to CRDv2 is described in [RD-1] and Mortimer et al. (2022).

The development of *snow_cci* SWE CRDP v3 included several prototype products focused on identifying the optimal configurations for changes to the dynamic density implementation and the snow masking. Since the production of *snow_cci* SWE CRDP v2, additional in situ data sources have been obtained over North America and have been added to the pool of data used to derive the density fields. We first evaluate the impact of these additional data by comparing *snow_cci* CRDP v2 (old density fields) with a development product '3X' over North America for a ten-year period (2000-2009) (Table 4.1, test 1). Both products use the same approach to derive the density fields but *v3X* includes the additional data. Next, the shift of dynamic snow density implementation from post-processing to inside the SWE processor is evaluated in Test 2 (see also Venäläinen et al. 2023) by comparing product *3x* with *Test product 2a*. These two products use the same density field but *2a* applies it within the processor and *3x* in post-processing. Once the impact of moving the dynamic snow density implementation has been ascertained we also test the impact (on the SWE retrieval) of changing the way in which the snow density fields are calculated. Specifically, two additional development datasets (Test *2b* & *2c*), each with different snow density fields obtained using different combinations of spatial and temporal interpolations, were evaluated. Again, these snow density fields were applied inside the processor. Comparisons of test products *2a*, *2b* and *2c* were used to determine the optimal dynamic density field to be used inside the processor. Finally, the impact of a new snow mask (CryoClim instead of JASMES data), applied in post processing, is evaluated in Test 3. In this test only the snow mask is altered. We are unable to separate the impact of a revised dry snow detection parameterization applied inside the processor from the impact of applying the final dynamic density field, which uses 10yr moving averages instead of sequential 10yr periods, inside the processor as both changes were applied simultaneously in production.

This section is organized as follows: Section 4.2 presents evaluations related to snow density field implementation using various developmental products. This includes i) the addition of new data over North America, ii) moving the dynamic density inside the processor, iii) evaluation of different interpolation methods to generate the snow density fields. Section 4.3 presents evaluations related to changing the snow masking. Section 4 provides a summary evaluation of the CRDP3 product.

Table 4.1: Phase 2 SWE proposed evaluation strategy. Product order and design subject to change. Green shading denotes modification being evaluated. All development products are in EASE 2 12.5 km grid while final *snow_cci* SWE products are in lat/lon 0.1°.

	Test1: Updated density field, post-processing		**Test 2: Density implementations inside processor**			**Test 3: Snow masking (post-processing)**	
Product	**CCI CDRv2 (baseline)**	**3x: updated density field**	**2a: Density decadal kriging**	**2b: Density annual kriging**	**2c: Density annual IDWR**	**CCI CDR3 old snow mask**	**CCI CDRv3**
Temporal frequency	2 day SMMR, daily SSM/I-SSMIS	2 day SMMR, daily SSM/I-SSMIS	2 day SMMR, daily SSM/I-SSMIS	2 day SMMR, daily SSM/I-SSMIS	2 day SMMR, daily SSM/I-SSMIS	2 day SMMR, daily SSM/I-SSMIS	2 day SMMR, daily SSM/I-SSMIS
SYNOP SD	CCIv1/GS	CCIv1/GS	CCIv1/GS	CCIv1/GS	CCIv1/GS	CCIv1/GS	CCIv1/GS
PMW data	12.5 km EASE2 rSIR	12.5 km EASE2 rSIR	12.5 km EASE2 rSIR	12.5 km EASE2 rSIR	12.5 km EASE2 rSIR	12.5 km EASE2 rSIR	12.5 km EASE2 rSIR
Snow density	Venäläinen et al. 2021 (post-processing)	Updated 10 yr DD field in post-processing	Updated 10 yr DD field inside processor; kriging	Updated annual DD field inside processor; kriging	Updated annual DD field inside processor; Inverse wieghted regression (IDWR)	Updated 40 yr DD field inside processor, kriging, 10yr moving average	Updated 40 yr DD field inside processor, kriging, 10yr moving average
Autumn snow accumulation mask	Hall et al. 2002	Hall et al. 2002	Hall et al. 2002	Hall et al. 2002	Hall et al. 2002	Updated mask based on Zschenderlein et al. (2023)	Updated mask based on Zschenderlein et al. (2023)
Spring snow melt mask	Takala et al. 2009 (PMW & optical (JASMES))	Takala et al. 2009 (PMW & optical (JASMES))	Takala et al. 2009 (PMW & optical (JASMES))	Takala et al. 2009 (PMW & optical (JASMES))	Takala et al. 2009 (PMW & optical (JASMES))	Takala et al. 2009 (PMW & optical (JASMES))	Takala et al. 2009 (PMW & optical (CryoClim))
Topo mask	CCIv1/GS	CCIv1/GS	CCIv1/GS	CCIv1/GS	CCIv1/GS	CCIv1/GS	CCIv1/GS
Uncertainty field	CCIv1/GS	CCIv1/GS	CCIv1/GS	CCIv1/GS	CCIv1/GS	CCIv1/GS	CCIv1/GS
Time period	1979-2020	2000-2009	2000-2009	2000-2009	2000-2009	1979-2022	1979-2019

4.2. CCI Phase 2 prototyping - snow density implementation

4.2.1. Additional in situ data in North America

The updated density field produced negligible changes in product performance (Figure 4.2). The seasonal evolution of product performance is similar and aggregate validation metrics computed over the full 2000-2009 evaluation period are within 1.5 mm (bias and uRMSE) and 0.02 (correlation). This comparison was based on CRDP v2 (0.1°) and *CP3X* (EASE2 12.5km, updated density fields based on new density data). New data was only added over North America, so this comparison is restricted to that domain. These products are in different grids so are not directly comparable. Nonetheless, this comparison provides a general sense of the impact of this change.

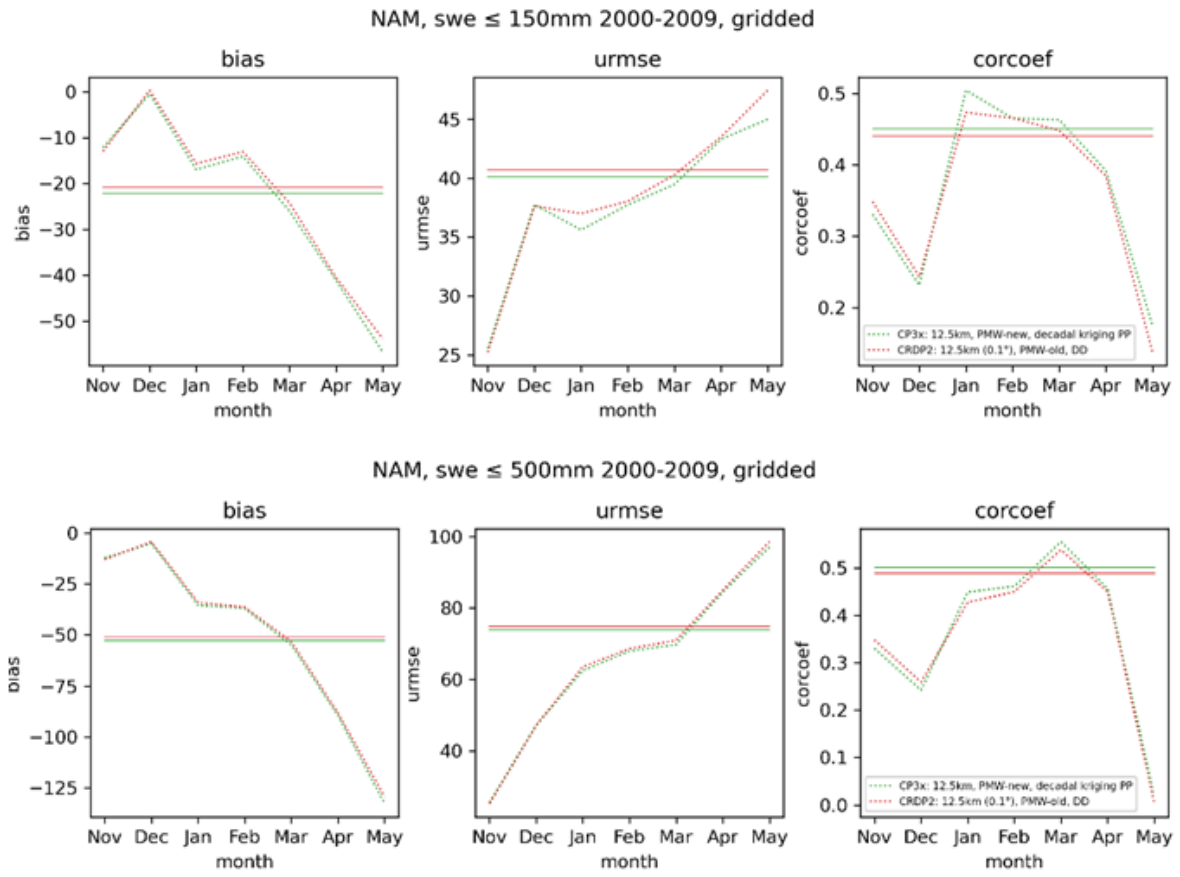

Figure 4.2: Evaluation statistics against snow courses over North America 2000-2009 for CDRv2 (CRDP2) and a similar product but with updated density fields that include new data (CP3x) for SWE ≤ 150 mm (top) and SWE ≤ 500 mm (bottom).

4.2.2. Dynamic density inside the processor

Implementing the dynamic density inside the retrieval as opposed to in post-processing did not result in any measurable change in overall accuracy when compared to the in situ reference data (Figure 4.3); however, there are improvements in the overall snow mass (Figure 4.4). Adding the dynamic density correction in post processing ([RD-1], Mortimer et al. 2022) shifted the timing of peak SWE approximately two weeks later brining it more in line with other reanalysis products, however, it also reduced the snow mass near peak (Figure 4.4, yellow line), resulting in larger biases compared to the in situ reference data and also putting it at the lower range of the reanalysis product suite (Figure 4.11). Moving the dynamic density correction inside the processor (Figure 4.3, green line) increased the snow mass near peak, closer to that of the static density product (v1, Figure 4.4, black line), while retaining the shift in peak SWE. We consider this development to be an improvement.

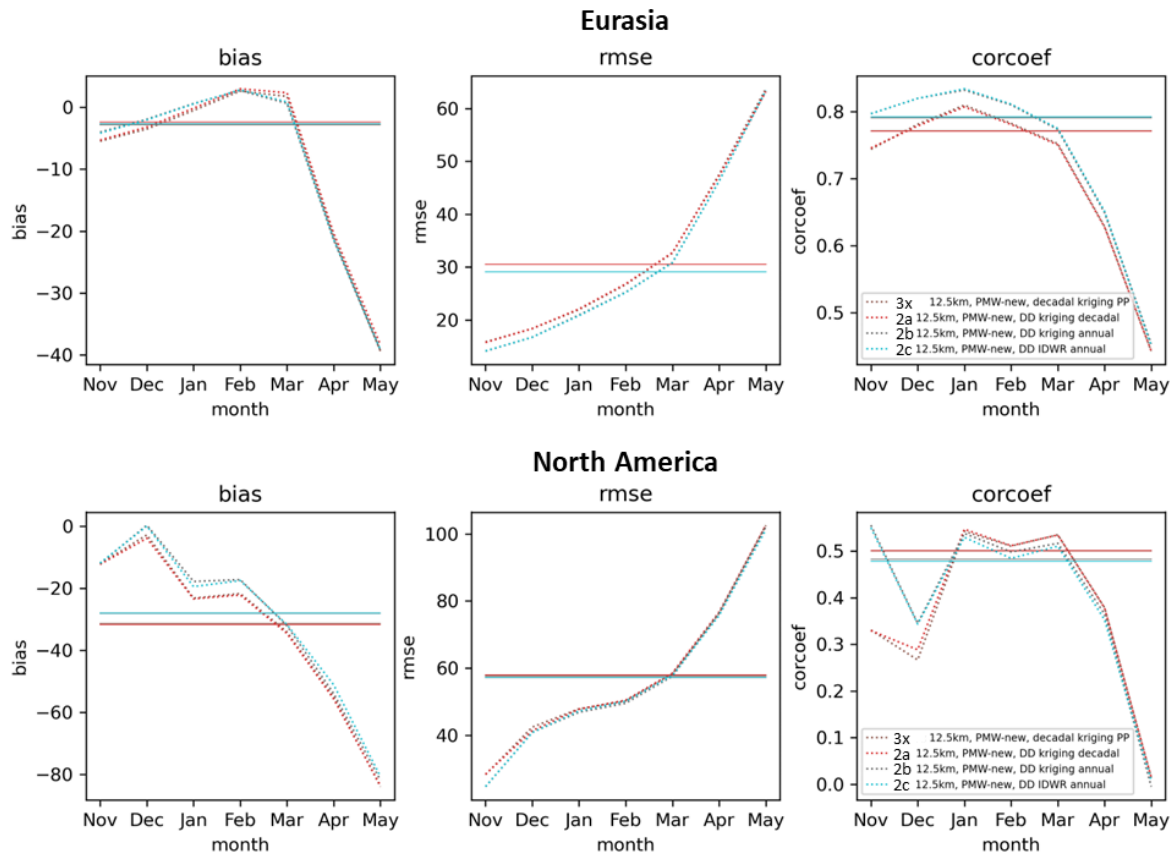

Figure 4.3: Comparison of various dynamic density implementations for SWE ≤ 200mm. CP3X and *2a* use the same density field but *3x* is implemented in post processing while *2a* is used inside the processor. *2a* through *2c* use different snow density fields, all produced with the same initial dataset but using different spatial and temporal interpolation methods.

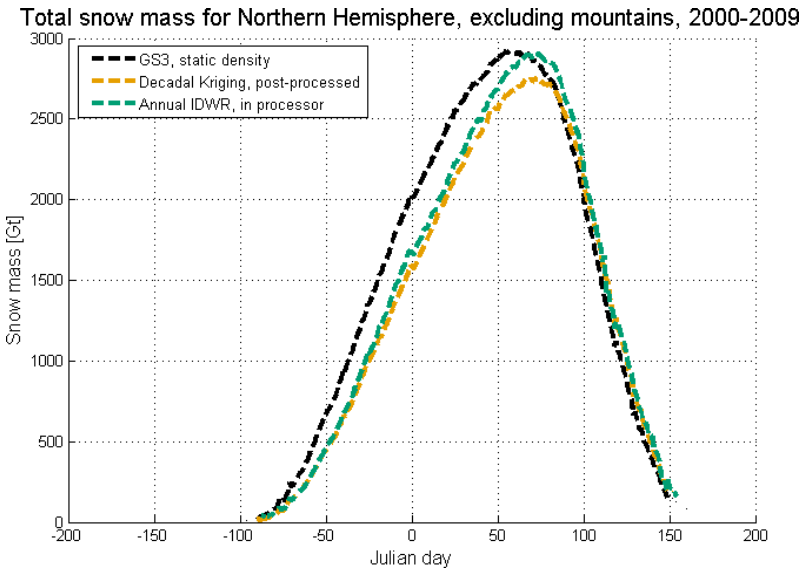

Figure 4.4: Impact of snow density implementations on the Northern Hemisphere snow mass excluding mountains for 2000-2009. GS3 (black line) is the GlobSnow v3 product which uses a static snow density. The yellow line shows CRDP v2 which implemented dynamic snow densities in post processing while the green line is a developmental product where the dynamic density step is implemented inside the retrieval.

4.2.3. Dynamic density fields

Three different dynamic density fields (*2a*,*2b*,*2c*), each produced using different combinations of spatial and temporal interpolation methods, were implemented inside the processor for a ten-year test period (2000-2009). Detailed description and analysis is provided in Venäläinen et al. (2023). The differences in validation statistics of the various implementations are negligible (Figure 4.3). However, presented in Venäläinen et al. (2023) there are notable differences in the SWE fields that are not captured by the sparse in situ reference data. Venäläinen et al. (2023) found the inverse distance weighted regression (IDWR) spatial interpolation produced physically unrealistic boundaries in the density field in North America (Figure 4.5) so kriging was selected as the method of choice for spatial interpolation. Comparing temporal interpolations based on annual data (Figure 4.6, green lines) versus pooled sequential decadal averages (Figure 4.6, yellow lines) found the decadal case to have a more realistic seasonal evolution of snow density. This is likely due to the larger pool of data available to draw from in the decadal case. There is an unrealistic drop is snow density at the end of the snow season in the annual case (Figure 4.6, green lines). For the production run, the density fields were further modified to use a moving 10-year window instead of sequential 10-year periods to avoid adding any potential breaks in the time series when moving from one decade to the next. Since the prototype products were only produced for a 10-year period we were unable to evaluate the impact of the change from sequential to moving 10-year periods.

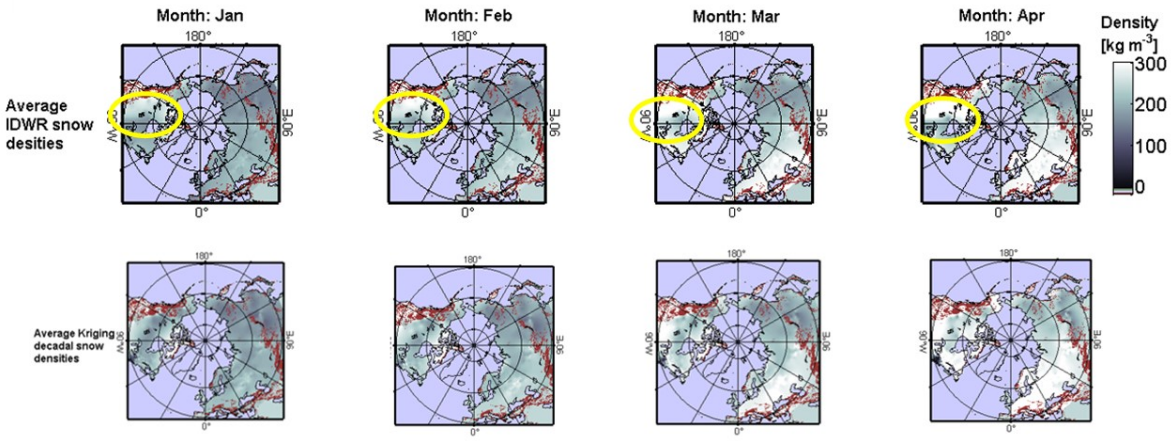

Figure 4.5: Monthly snow density fields resulting from two different spatial interpolation methods (same temporal interpolation). Image courtesy of P. Venäläinen.

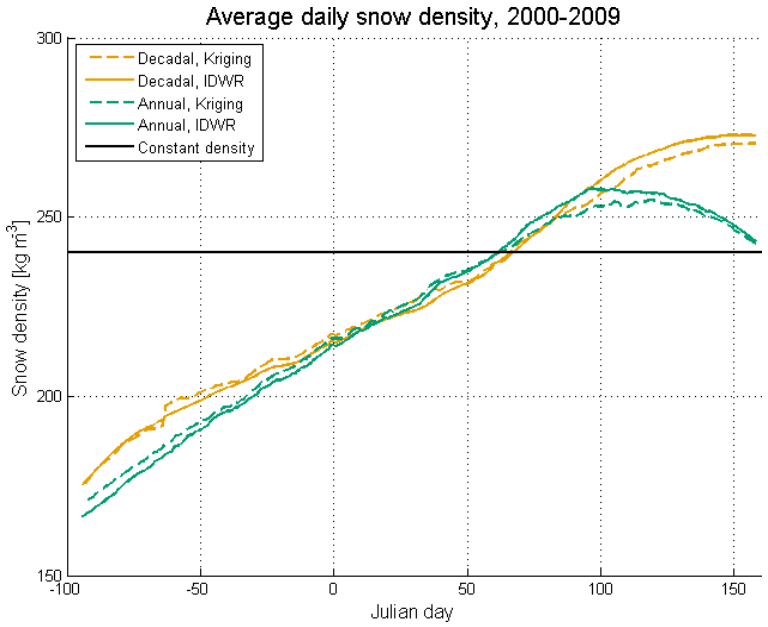

Figure 4.6: Average Northern Hemisphere snow density evolution for various interpolation approaches. (figure from Venäläinen et al. 2023).

4.3. 3. CCI Phase 2 prototyping – cumulative snow mask

snow_cci SWE CRDP v3 implements new snow masking procedures. There is a new dry snow detection adapted from Zschenderlein et al. (2023) and the JASMES data has been replaced by CryoClim. The dry snow detection is expected to have the most impact during the accumulation season while the CryoClim mask is most important during the melt season. Changes to the snow masking and implementation of dynamic snow density (10yr moving averages) inside the processor were implemented simultaneously. A developmental dataset that applied the old post-processing snow masking was provided. However, this product only allows us to assess the impact of the external snow masking, not the internal dry snow detection.

To evaluate the impact of changes in post-processing snow masks we modified the validation approach. Instead of only using locations and dates present in all products under consideration, we used all dates and locations. This modification is important because changes due to snow masking should result in one product having snow at a given site and date but it being cleared in the other product. Since all other aspects of the retrieval are kept constant the traditional validation approach would produce the same statistics for both products. We extended the monthly analysis to include September, October and June but the bulk statistics are still calculated for Nov-May 1979-2018. Due to the temporally discontinuous nature of the reference data, it is difficult to capture all impacts of the changes in snow masking from comparisons with the reference data alone. Therefore, we also rely on intercomparisons of the various *snow_cci* products (e.g. Figure 4.10).

The new CryoClim snow mask provides modest improvements in validation metrics (Figure 4.7). The revised snow masks retain more snow especially during the accumulation season (Figure 4.8). This is evident from Figure 4.8 which shows the number of times a reference site has corresponding SWE retrievals in a given month when the new CryoClim snow masks are applied but does not have snow using the old JASMES data. These differences seem to track the snowline especially over Eurasia where the coverage of snow courses is more spatially representative and where measurements are conducted earlier in the snow season (see Figure 4.1 for spatial and temporal distribution of the reference data). Product accuracies at these sites produce the differences in monthly statistics [between the two products] shown in Figure 4.9. There were only 6 instances where a location had SWE with the old masks but not with the new masks so we are fairly confident in attributing the changes to additional snow mass rather than the removal of snow. Comparing the monthly SWE fields of *snow_cci* CRDP v2 and v3 (Figure 4.10), v3 has more snow during onset and melt and across north and eastern North America compared to *snow_cci* SWE CRDP v2. Although this comparison also includes changes in the snow density implementation these differences are small (4.2.2). We conclude that moving from the JASMES to CryoClim based snow mask led to positive changes in the Snow CCI SWE product.

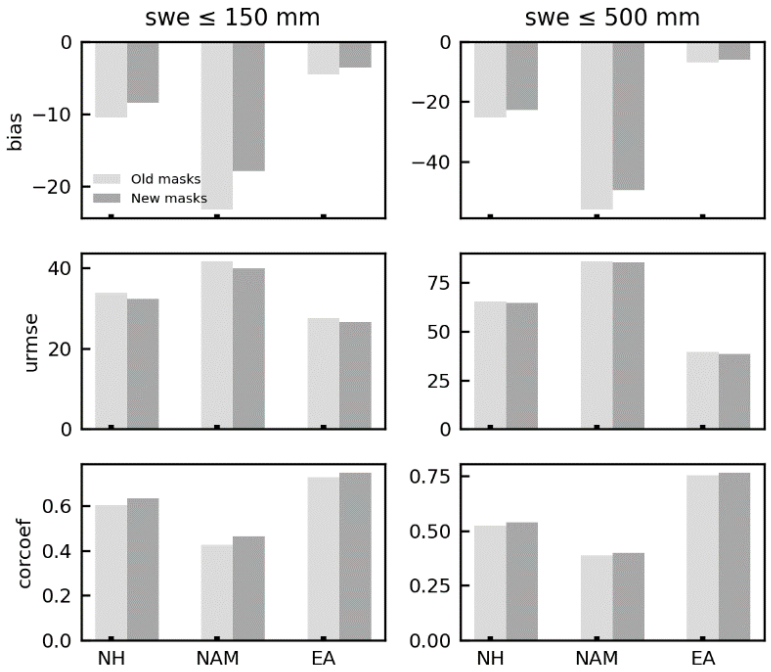

Figure 4.7: November-May 1979-2018 validation statistics calculated against snow courses (Figure 4.1) for SWE retrievals using the new (dark grey) and old(light grey) snow mask separately for North America (NAM) and Eurasia (EA) and the full Northern Hemisphere (NH) domain.

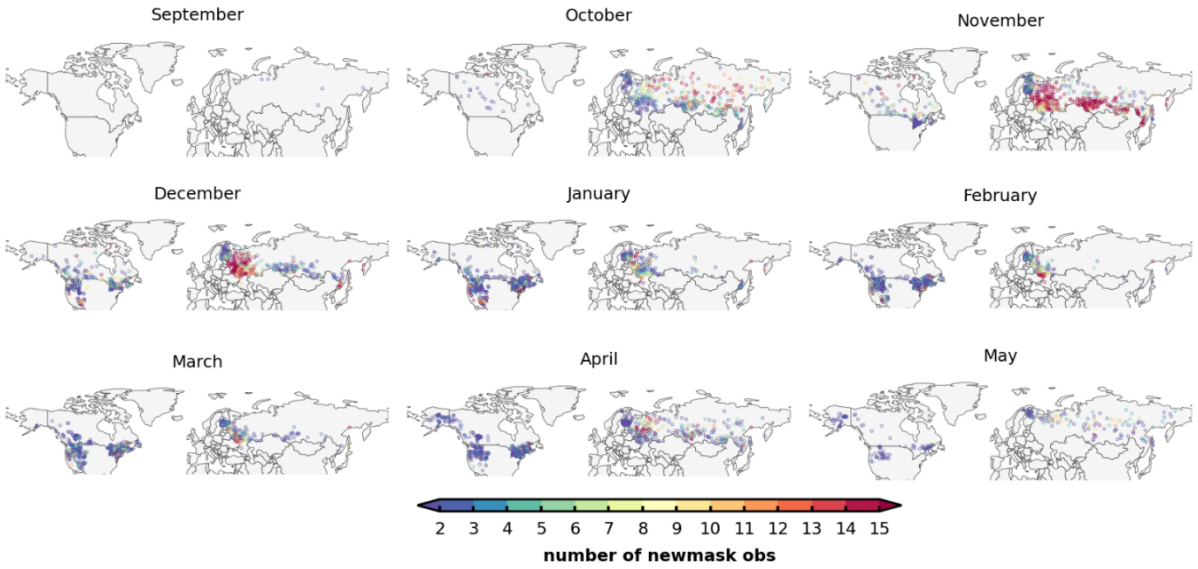

Figure 4.8: Number of instances per month over the time period (1979-2018) where there is a SWE retrieval matching with a reference observation when the new (CryoClim) snow mask are applied but not when the old (JASMES) snow mask are applied. Note that the reference data are not continuous in space or time (see Figure 4.1).

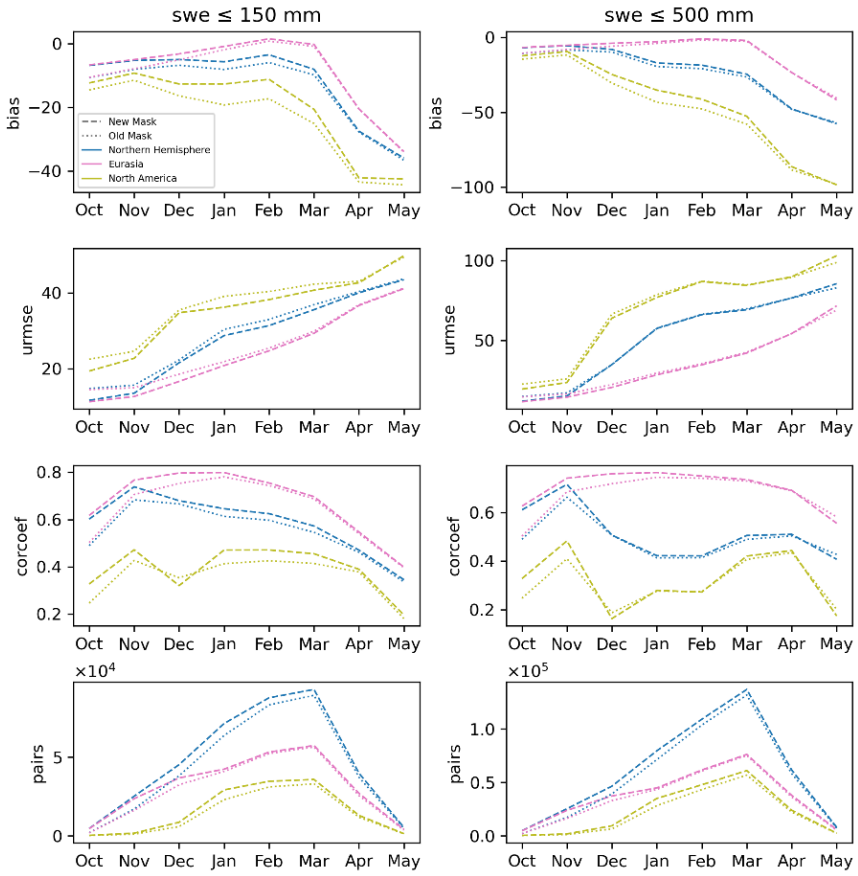

Figure 4.9: Monthly validation statistics for product using the old (JASMES, dotted line) and new (CRYOCLIM, dashed line) snow masks for the full Northern Hemisphere (blue) and separately for North America (yellow) and Eurasia (pink); 1979-2018. The last row shows the number of grid cells with corresponding reference data in each month.

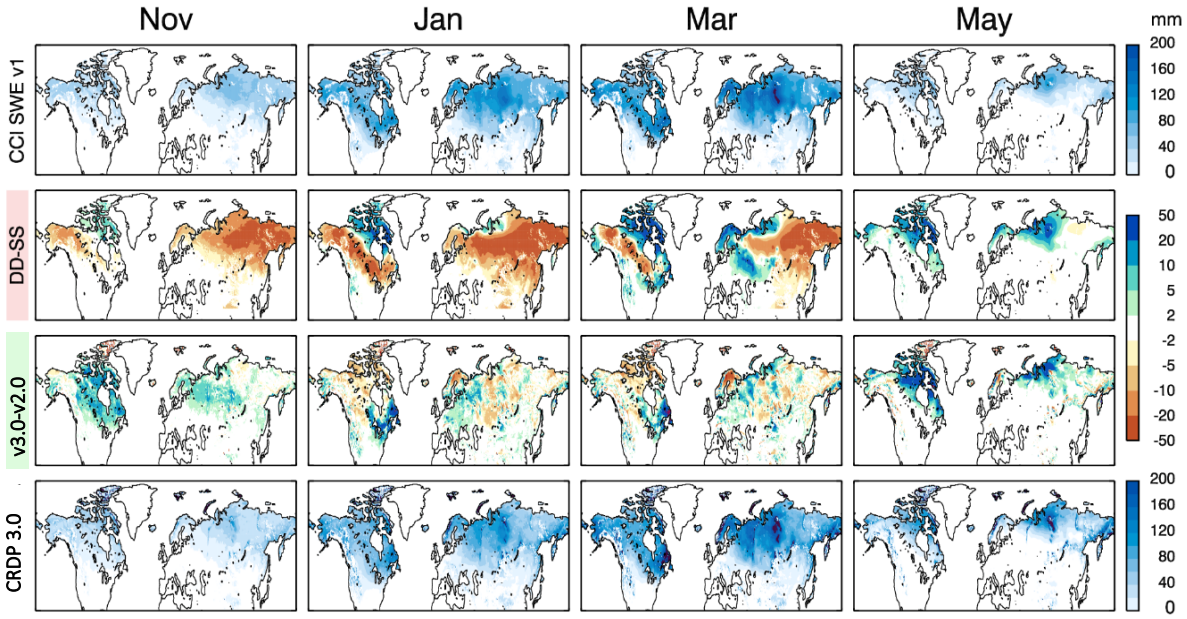

Figure 4.10: November, January, March and May climatological SWE of CCI CDR v1 (top) and CDR v3 (bottom row). The difference attributed to the move from static to dynamic snow density in post processing is shown in the second row and the difference in snow mass between v2 and v3 is shown in the third row.

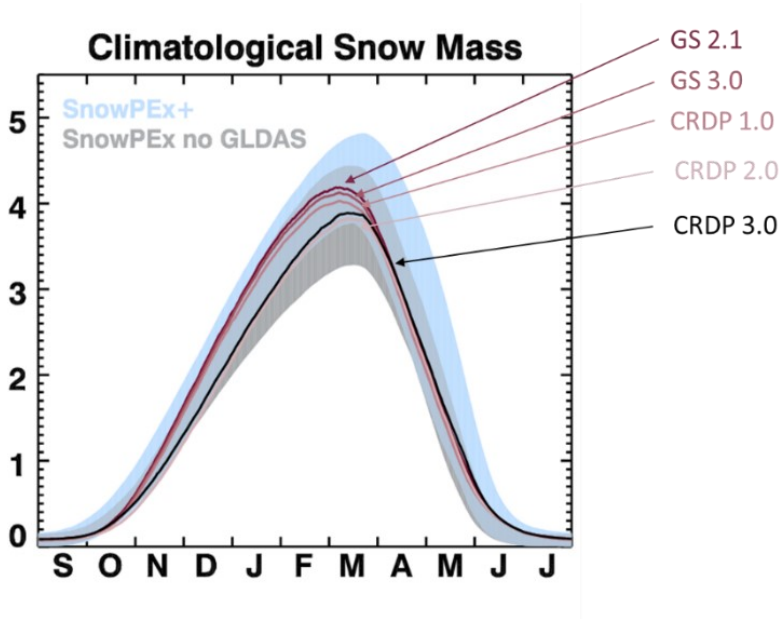

Figure 4.11: Northern Hemisphere climatological snow mass for the three Snow CCI CDRs (v1, v2, v3) and GlobSnow v2.1 (GS 2.1) and v3 (GS 3.0). The range of the suite of reanalysis products included in SnowPEx and SnowPEx+ is shown in the grey and blue shading, respectively.

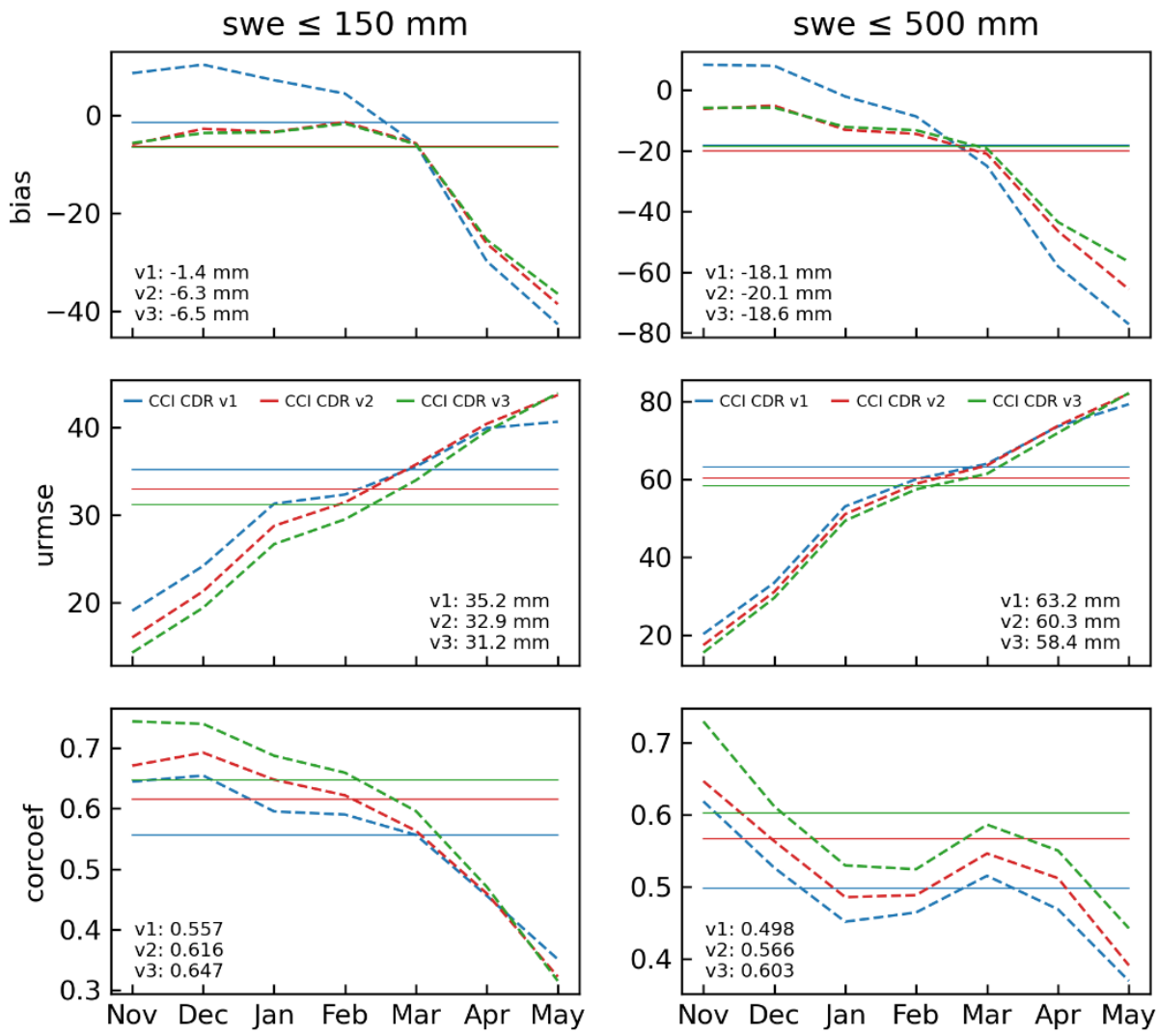

Figure 4.12: Monthly validation statistics for the Northern Hemisphere 1979-2018 computed on the full reference dataset (Figure 4.1) for the three *snow_cci* SWE CDRs. Solid horizontal lines show the metric when calculated over the full time period for Nov-May (values are also printed on each plot) and are equivalent to the light grey bars for the Northern Hemisphere on Figure 4.14.

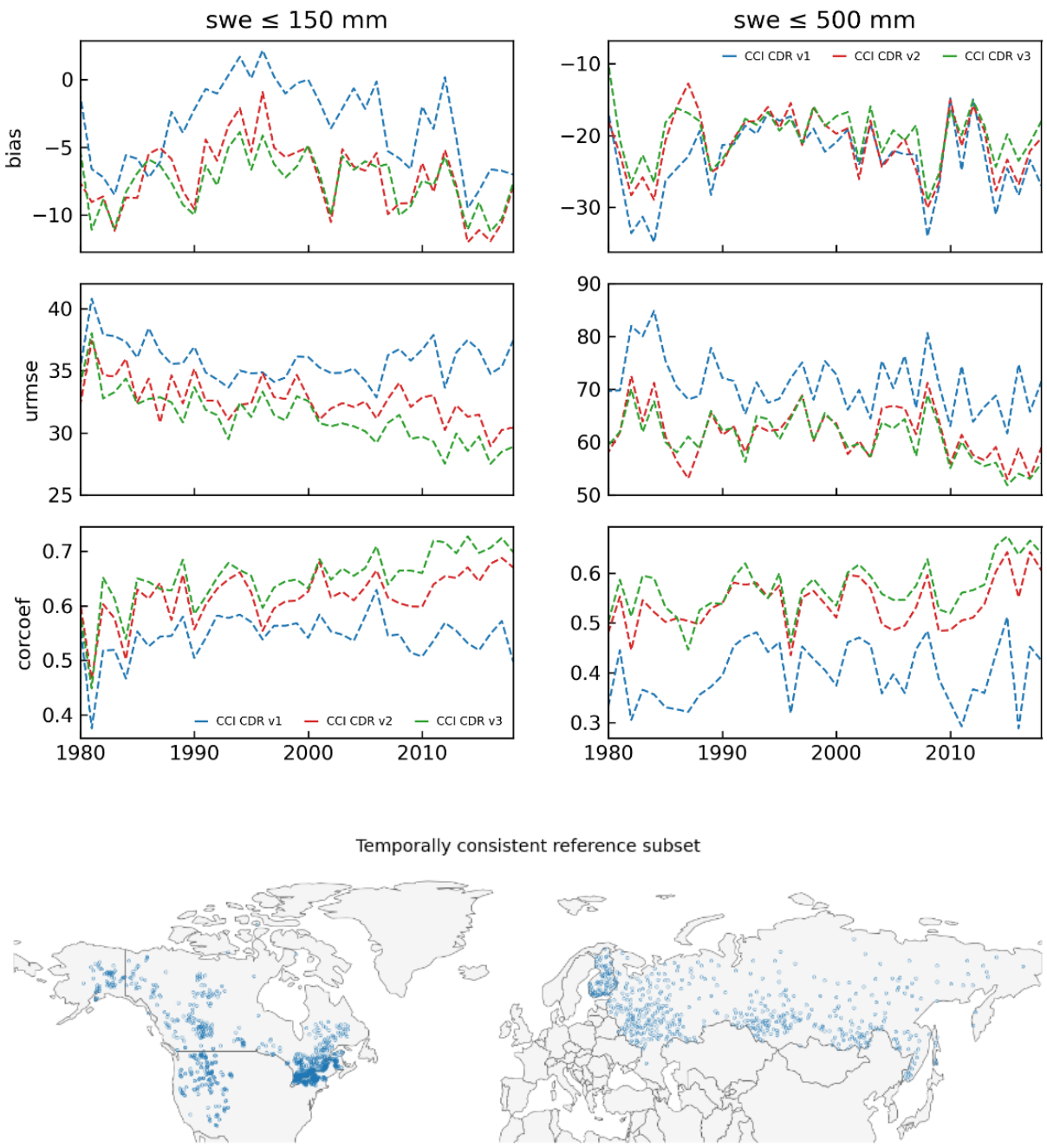

Figure 4.13: Annual metrics (months Nov-May) calculated using the temporally consistent reference subset shown in the bottom row for the Northern Hemisphere. The temporally consistent subset consists of grid cells with corresponding reference data in at least 20 of the 40yrs and in at least 2 years in each decade starting in 1979.

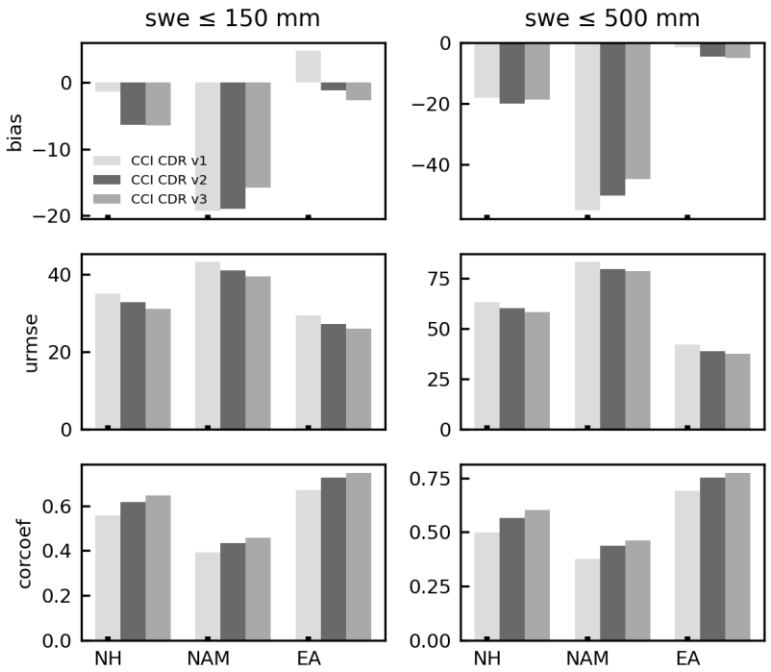

Figure 4.14: Summary validation statistics of the three Snow CCI CDRs for Nov-May 1979-2018. Metrics are calculated separately for North America (NAM) and Eurasia (EA) as well as for the full Northern Hemisphere domain.

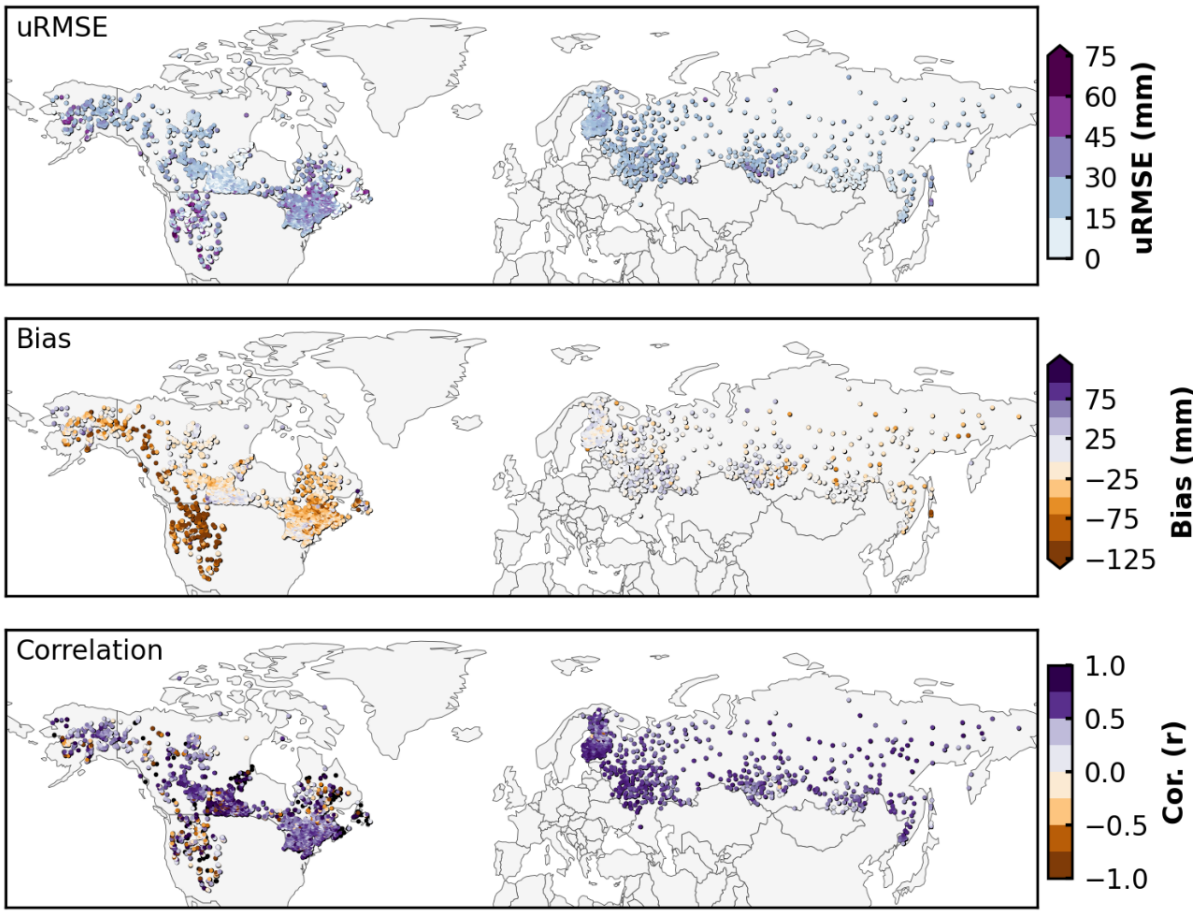

Figure 4.15: March CCI CDR v3 validation statistics for SWE ≤ 200 mm, 1979-2018.

5. RECOMMENDATIONS FOR FIXING ERRORS AND IMPROVING THE PRODUCT QUALITY

In this chapter, some recommendations to fix and improve the overall product quality are provided for both SCF and SWE *snow_cci* products.

5.1. Summary of the validation for Snow Cover Fraction products

The *snow_cci* SCF products have been validated with more than 3.6 million, 250 thousand, and 2.5 million in-situ measurements and 1050, 192 and 705 high resolution SCE maps for AVHRR (CRDP v3.0), AATSR (CRDP v1.0) and MODIS (CRDP v3.0), respectively. The validation followed the PVP [RD-2]. By considering the validation with in-situ data the reported accuracy (hit rate and F-score) for both the sensors is high. Based on the analysis at the different thresholds, the *snow_cci* SCF products identify shallow snowpack or patchy situations with good accuracy. We found that for the in-situ validation, the same considerations done for global statistics are valid considering both mountainous and plain areas. In forested areas, SCFG products show a better agreement with the snow information from in-situ measurements than the SCFV products, as expected. SCFV and SCFG show an identical behaviour in unforested areas proving the consistency between the products in open land.

The overall unbiased RMSE calculated from the high-resolution snow maps is below 13%. These values are compliant with the user requirements [RD-6]. The overall bias is below -5%, showing a general underestimation of the SCF compared to the reference snow maps from HR reference snow maps. The correlation coefficient is always above 0.95 reflecting a good overall performance of the *snow_cci* products.

The performance was assessed also considering different topography conditions i.e., plains vs mountains and forested and non-forested conditions and temporal variability. As expected, the *snow_cci* SCFV products are performing better in the open fields than in forested areas, whereas no substantial differences are present in the case of plains or mountainous areas. SCFG presents similar performance in forest and non-forested areas indicating a robustness of the method. However, the SCFG must be further validated considering also very high-resolution images and advanced snow classification methods able to identify the snow on ground from these kinds of images. The *snow_cci* products show a good temporal stability being sensible more on the number of mixed pixels. Additionally, the *snow_cci* SCF products were validated in steps of 10% of SCF showing that the algorithm is performing slightly different at different snow conditions.

The comparison between *snow_cci* SCF products and MOD10v5 has also been performed showing a high correlation between the two products.

The validation of the uncertainty estimation shows how the *snow_cci* products provide in average an accurate information about the uncertainty. However, the uncertainties have a relative high variance in the representation of the error (RMSE of about 13-14% for the provided uncertainties).

An added value consists of the introduction of a selected set of scenes classified using the snow maps from *snow_cci* Option-4 [RD-7]. The comparison with these maps confirmed the satisfaction of user requirements. The main difference that can be appreciated is the change of the bias sign. In fact, for all the state-of-the-art methods used for the validation of the *snow_cci* CRDP v3 products the bias was negative, meaning that the CRDP v3 snow maps are underestimating the snow coverage. Comparing instead the *snow_cci* CRDP v3 products with the new reference snow maps generated in *snow_cci* Option-4 results in a lower absolute bias value with a positive sign. The reason may be that the new reference maps have been corrected for snow overestimation, which results typically from NDSI based methods.

5.2. Recommendation for Snow Cover Fraction products

All the cases in which the unbiased RMSE is above the user requirement threshold of 20% and the bias is high should be carefully checked. These are scenes that generally present peculiar snow conditions that must explicitly be considered. For this reason, a collaboration of the validation and science teams is recommended also in the future to decrease the variance of the performance.

During the validation we noticed that several validation samples were excluded since they were identified as cloud covered in the *snow_cci* products but not in the reference Landsat scenes or in the MOD10C1 products. That problem was present in the previous versions of the *snow_cci* product and are still present in CRDP v3. An accurate checking on the performance of cloud detection also collaborating with other ESA initiatives for cloud detection (that are designed for snow covered areas) are recommended.

5.3. Summary of the validation for Snow Water Equivalent products

snow_cci SWE CRDP v3 has a native grid spacing of 12.5 km in EASE-Grid 2.0 (re-gridded to 0.1°). PMW data are from the enhanced resolution (rSIR) NASA MEaSUREs Calibrated Passive Microwave Daily EASE-Grid 2.0 (CETB) Earth Science Data Record (ESDR), and spatially and temporally varying snow densities are used within the processor. A new dry snow masking, adapted from Zschenderlein et al. (2023), is applied inside the processor and the JASMES-based optical snow mask, applied in post-processing, is replaced with CryoClim.

Validated against snow course observations, *snow_cci* CRDP v3 has an unbiased RMSE of 31.2 mm (58.4 mm), bias of -6.5 mm (-18.6 mm) and correlation of 0.647 (0.603) for SWE ≤150 mm (≤500 mm). All but the bias for SWE ≤ 150 mm are improved compared to CRDP v2. As discussed in 4.2.2, peak

snow mass in v3 is marginally higher than in v2 and the timing of peak snow mass is shifted compared to v1 and is more in line with that of a suite of reanalysis products (blue and grey shading in Figure 4.11). The decrease in snow mass associated with the move to dynamic snow densities is discussed in [RD-1] and Mortimer et al. 2022. As expected, errors increase over the course of the snow season (Figure 4.12). The annual time series computed using a temporally consistent reference subset (Figure 4.13), shows decreasing unbiased RMSE and increasing correlation. More work is needed to determine if there are trends in the reference data itself are affecting these apparent trends.

Performance is worse in North America compared to Eurasia. On aggregate, the magnitude of improvement from v2 to v3 is fairly consistent between these two domains (Figure 4.14). From Figure 4.15, errors are larger in the mountain regions of western North America and in northern Quebec where the boreal forest and high SWE makes accurate SWE retrievals difficult. Overall, the *snow_cci* SWE CRDP v3 represents an improvement compared to CRDP v2, largely owing to the changes in snow masking.

5.4. Recommendation for Snow Water Equivalent products

The end users should understand the limitations of estimating SWE using coarse resolution passive microwave radiometer measurements coupled with surface snow depth observations. Deep snow and dense forest cover pose known challenges. Complex terrain is masked in the SWE product, but future versions could explore various approaches to filling this gap. Nonetheless, *snow_cci* SWE products are suitable for long term continental-scale snow analyses. The following lists specific areas that should be considered in future versions of *snow_cci*.

Complex topography mask: The current implementation masks out complex terrain defined as a 25 km EASE grid 1.0 grid cell with an elevation standard deviation > 200 mm (Luojus et al., 2021) based on the ETOP05 elevation model. High elevation mountain plateaus are not removed, and their inclusion significantly degrades product accuracy. The appropriateness of the *snow_cci* algorithm in non-complex mountain regions should be re-visited and a more conservative mountain mask, or one that also considers slope and elevation, should be explored. Research and development activities should be developed to explore the feasibility of addressing user requirements for mountain SWE estimates (which necessitates much finer grid spacing than the 0.1 deg. of CRDP v2).

Bias correction: The implications of the re-gridded (0.1° lat/lon versus 12.5 km EASE2) on the bias-correction procedure applied in Pulliainen et al. (2020) needs to be examined if a bias-corrected version is to be produced as part of *snow_cci*. If bias corrected products are to be provided as part of *snow_cci*, new bias correction fields may need to be computed in 0.1° lat/lon grid and not simply re-gridded from EASE2 12.5 km dataset.

PMW-related discontinuity: *snow_cci* SWE CRDP v2 no longer has the SSM/I to SSMIS discontinuity in CRDP v1 but retains the discontinuity in the monthly Northern Hemisphere snow mass time series in 1987 related to the change from SSMR to SSM/I (Section 4.3; Mortimer et al., 2022). Future versions of *snow_cci* should explore the feasibility of addressing this issue, perhaps at the monthly scale.

High SWE areas: A key limitation of *snow_cci* SWE (and any PMW-based SD or SWE algorithm) is a systematic low bias under high SWE (>150 mm) conditions. Although assimilation of SD data in Snow *snow_cci* SWE and GlobSnow results in much better retrieval skill compared to PMW-only algorithms (e.g., Mortimer et al. 2020), the fundamental physics upon which the algorithm is based essentially limits SWE estimates to below about 200 mm. Pulliainen et al. (2020) addressed this issue by applying a post-processing bias correction to monthly SWE estimates. Alternatively, it may be possible to further exploit the synoptic SD data, and screen for regions and times where SD is above the sensitivity of PMW Tb differencing techniques. The PMW uncertainty term used in the data assimilation is related to the sensitivity of the ΔTb to SD magnitude, with larger uncertainties corresponding to deeper snow (higher SWE). Future iterations of *snow_cci* SWE could explore whether a PMW uncertainty threshold can be identified above which the PMW ΔTb signal is saturated. In such circumstances, SD (SWE) could be applied solely from the background SD field interpolated from synoptic SD data. This proposed approach is consistent with other aspects already employed within the *snow_cci* SWE algorithm; for example, in cases of wet snow SD (SWE) is already obtained only from the background SD field.

Updated uncertainty layer: The current uncertainty estimation was developed for *snow_cci* CRDP v1's precursor, GlobSnow v2. Advancements in the *snow_cci* SWE algorithm, availability of new in situ data, and developments in the field of uncertainty characterization for CDRs warrants a revisit of the approach and data used to derive the SWE uncertainty layer.

6. REFERENCES

Armstrong, R. L., Knowles, K.W., Brodzik, M. J. and Hardman, M. A.: DMSP SSM/I Pathfinder daily EASE-Grid brightness temperatures, Version 2, 1987-2019. Boulder, Colorado USA: National Snow and Ice Data Center, https://doi.org/10.5067/3EX2U1DV3434, 1994, updated 2019.

Brodzik, M. J. and Knowles, K. W.: "EASE-Grid: a versatile set of equal-area projections and grids" in M. Goodchild (Ed.) Discrete Global Grids. Santa Barbara, CA, USA: National Center for Geographic Information & Analysis. http://escholarship.org/uc/item/9492q6sm, 2002.

Brodzik, M. J., Long, D.G., Hardman, M.A., Paget, A., and Armstrong, R.: MEaSUREs Calibrated Enhanced-Resolution Passive Microwave Daily EASE-Grid 2.0 Brightness Temperature ESDR, Version 1. Boulder, Colorado USA. NASA National Snow and Ice Data Center Distributed Active Archive Center. https://doi.org/10.5067/MEASURES/CRYOSPHERE/NSIDC-0630.001, 2016, updated 2020.

Brown, R. D., Brasnett, B., and Robinson, D.: Gridded North American monthly snow depth and snow water equivalent for GCM evaluation, Atmos.-Ocean, 41(1): 1–14, https://doi.org/10.3137/ao.410101, 2003.

Brown, R.D., Fang, B., and Mudryk, L.: Update of Canadian historical snow survey data and analysis of snow water equivalent trends, 1967–2016, Atmos.-Ocean, 57: 1–8, https://doi.org/10.1080/07055900.2019.1598843, 2019.

Brun, E., Vionnet, V., Boone, A., Decharme, B., Peings, Y., Vallette, R., Karbou, F. and S. Morin, S.: Simulation of northern Eurasian local snow depth, mass, and density using a detailed snowpack model and meteorological reanalyses, J. Hydrometeorol., 14, 203–219, https://doi.org/10.1175/JHM-D-12-012.1, 2013.

Cohen J, Lemmetyinen J, Pulliainen J, Heinilä K, Montomoli F, Seppänen J, Hallikainen M. The effect of boreal forest canopy in satellite snow mapping - A multisensor analysis, IEEE Trans. Geosci. Remote Sens., 53: 6593–6607, https://doi.org/10.1109/TGRS.2015.2444422, 2015.

Derksen, C., T. Nagler and G. Schwaizer (2020) ESA CCI+ Snow ECV: User Requirements Document, version 3.0, December 2020.

Dozier, J., & Painter, T. H. (2004). Multispectral and Hyperspectral Remote Sensing of Alpine Snow Properties. *Annual Review of Earth and Planetary Sciences*, *32*(1), 465–494. doi:10.1146/annurev.earth.32.101802.120404

Hall, D. K. and G. A. Riggs. 2021. *MODIS/Terra Snow Cover Daily L3 Global 0.05Deg CMG, Version 61*. [Indicate subset used]. Boulder, Colorado USA. NASA National Snow and Ice Data Center Distributed Active Archive Center. doi: https://doi.org/10.5067/MODIS/MOD10C1.061.

Gelaro, R., McCarty, W., Suárez, M.J., Todling, R., Molod, A., Takacs, L., Randles, C.A., Darmenov, A., Bosilovich, M.G., Reichle, R. and Wargan, K., Coy, L., Cullather, R., Draper, C., Akella, S., Buchard, V., Conaty, A., da Silva, A. M., Gu, W., Kim, G., Koster, R., Lucchesi, R., Merkova, D., Nielsen, J. E., Partyka, G., Pawson, S., Putman, W., Rienecker, M., Schubert, S., Sienkiewicz, M., and Zhao, B.: The modern-era retrospective analysis for research and applications, version 2 (MERRA-2), Journal of climate, 30(14): 5419–5454, https://doi.org/10.1175/JCLI-D-16-0758.1, 2017

Hersbach, H., Bell, B., Berrisford, P., Hirahara, S., Horányi, A., Muñoz-Sabater, J., Julien Nicolas, J. et al.: The ERA5 global reanalysis, Quarterly Journal of the Royal Meteorological Society, 146(730): 1999–2049, https://doi.org/10.1002/qj.3803, 2020.

Hori, M., Sugiura, K., Kobayashi, K., Aoki, T., Tanikawa, T., Kuchiki, K., Niwano, M., and Enomoto, H.: Northern Hemisphere daily snow cover extent product derived using consistent objective criteria from satellite-borne optical sensors. Remote Sens. Environ., 191: 402–418, https://doi.org/10.1016/j.rse.2017.01.023, 2017.

Klein, A. G., Hall, D. K., & Riggs, G. A. (1998). Improving snow cover mapping in forests through the use of a canopy reflectance model. *Hydrological Processes*, *12*, 1723–1744.

Knowles, K., Njoku, E.G., Armstrong, R., and Brodzik, M.J.: Nimbus-7 SMMR Pathfinder Daily EASE-Grid Brightness Temperatures, Version 1. Boulder, Colorado USA. NASA National Snow and Ice Data Center Distributed Active Archive Center, https://doi.org/10.5067/36SLCSCZU7N6, 2000.

Kobayashi, S., Ota, Y., Harada, Y., Ebita, A., Moriya, M., Onoda, H., Onogi, K., Kamahori, H., Kobayashi, C., Endo, H., Miyaoka, K., and Takahashi, K.: The JRA-55 reanalysis: General specifications and basic characteristics, Journal of the Meteorological Society of Japan. Ser. II, 93(1): 5–48, https://doi.org/10.2151/jmsj.2015-001, 2015.

Lemmetyinen, J., Kontu, A., Kärnä, J.-P., Vehviläinen, J., Takala, M., and Pulliainen, J.: Correcting for the influence of frozen lakes in satellite microwave radiometer observations through application of a microwave emission model, Remote Sens. Environ., 115: 3695–3706, https://doi.org/10.1016/j.rse.2011.09.008, 2011.

Luojus, K., Pulliainen, J., Takala, M., Lemmetyinen, J., Mortimer, C., Derksen, C., Mudryk, L., Moisander, M., Venäläinen, P., Hiltunen, M., Ikonen, J., Smolander, T., Cohen, J., Salminen, M., Veijola, K., and Norberg, J.: GlobSnow v3.0 Northern Hemisphere snow water equivalent dataset. Scientific Data, 8(163), https://doi.org/10.1038/s41597-021-00939-2, 2021.

Moisander, M., Luojus, K., Lemmetyinen, J., Takala, M., and Venäläinen, P.: Snow Water Equivalent In: Schwaizer, G.S., Metsämäki, S., Moisander, M., Luojus, K., Wunderle, S., Naegeli, K., Nagler, T., Lemmetyinen, J., Pulliainen, J., Takala, M., Solberg, R., Keuris, L., and Venäläinen, P. 2020. ESA CCI+ Snow ECV: Algorithm Theoretical Basis Document, version 3.0, November 2021.

Mortimer, C., Mudryk, L., Derksen, C., Brady, M., Luojus, K., Venäläinen, P., Moisander, M., Lemmetyinen, J., Takala, M., Tanis, C., and Pulliainen, J.: Benchmarking algorithm changes to the Snow CCIC snow water equivalent product, Remote Sens. Environ., 274, 112988, https://doi.org/10.1016/j.rse.2022.112988, 2022.

Mortimer, C., Mudryk, L., Derksen, C., Brady, M., Luojus, K., Venäläinen, P., Moisander, M., Lemmetyinen, J., Takala, M., Tanis, C., and Pulliainen, J. : Benchmarking algorithm changes to the Snow CCI Snow Water Equivalent product, Remote Sens. Environ., under review.

Notarnicola, C., V. Premier, C. Marin, G. Schwaizer, T. Nagler, K. Luojus, C. Derksen, C. Mortimer, S. Wunderle, K. Naegeli (2020) ESA CCI+ Snow ECV: Product Validation and Intercomparison Report, version 2.0, November 2020.

Notarnicola, C., Marin, C., Schwaizer, G., Nagler, T., Luojus, K., Derksen, C., Mortimer, C., Wunderle, S., Naegeli, K. (2020) ESA CCI+ Snow ECV: Product Validation Plan, version 3.0, 2021.

Pulliainen, J., Luojus, K., Derksen, C., Mudryk, L., Lemmetyinen, J., Salminen, M., Ikonen, J., Takala, M., Cohen, J., Smolander, T., and Norberg, J.: Patterns and trends of Northern Hemisphere snow mass from 1980 to 2018, Nature, 581: 294–298, https://doi.org/10.1038/s41586-020-2258-0, 2020.

Salomonson, V. V., & Appel, I. (2006). Development of the Aqua MODIS NDSI fractional snow cover algorithm and validation results. *IEEE Transactions on Geoscience and Remote Sensing*, *44*(7), 1747–1756. doi:10.1109/TGRS.2006.876029

Sturm, M., J. Holmgren, and G. Liston. 1995. A seasonal snow cover classification system for local to global applications. Journal of Climate. 8: 1261-1283.

Sturm, M., Taras, B., Liston, G., Derksen, C., Jonas, T., and Lea, J.: Estimating snow water equivalent using snow depth data and climate classes, J. Hydrometeorol., 11: 1380–1394, https://doi.org/10.1175/2010JHM1202.1, 2010.

Takala, M., Luojus, K., Pulliainen, J., Derksen, C., Lemmetyinen, J., Kärnä, J.-P., and Koskinen, J.: Estimating northern hemisphere snow water equivalent for climate research through assimilation of space-borne radiometer data and ground-based measurements, Remote Sens. Environ., 115, 3517–3529, https://doi.org/10.1016/j.rse.2011.08.014, 2011.

Venäläinen, P., Luojus, K., Lemmetyinen, J., Pulliainen, J., Moisander, M., and Takala, M.: Impact of dynamic snow density on Globsnow snow water equivalent retrieval accuracy, The Cryosphere, 15: 2969–2981, https://doi.org/10.5194/tc-15-2969-2021, 2021.

Venäläinen, P., Luojus, K., Mortimer, C., Lemmetyinen, J., Pulliainen, J., Takala, M., Moisander, M., and Zschenderlein, L.: Implementing spatially and temporally varying snow densities into the GlobSnow snow water equivalent retrieval, The Cryosphere 17, 719–736, https://doi.org/10.5194/tc-17-719-2023, 2023.

Vionnet, V., Mortimer, C., Brady, M., Arnal, L., and Brown, R.: Canadian historical Snow Water Equivalent dataset (CanSWE, 1928–2020), Earth System Science Data, 13: 4603–4619 https://doi.org/10.5194/essd-13-4603-2021, 2021.

Wang, X. L.: Penalized maximal F-test for detecting undocumented mean-shifts without trend-change, J. Atmos. Oceanic Tech., 25(3): 368–384. https://doi.org/10.1175/JTECHA982.1, 2008.

Zschenderlein, L., Luojus, K., Takala, M., Venäläinen, P., and Pulliainen, J.: Evluation of passive microwave dry snow detection algorithms and application to SWE retrieval during seasonal snow accumulation, Remote Sens. Environ., 288, 113476, https://doi.org/10.1016/j.rse.2023.113476, 2023.